Thermo-physical property models for well-characterized hydrocarbon mixtures and fuels and effect of composition on fluid properties up to 4,500 bar

Houman B. Rokni

Thesis submitted for the fulfilment of the requirements for the Degree of Doctor of Philosophy

School of Mathematics, Computer Science & Engineering
Department of Aeronautical and Mechanical Engineering

June 2019

“Strategy without patience can be caustic. Patience without strategy can become anemic. Having both strategy and patience is a rare gift.”

(Brannon Marshal)

Present Contribution

Summary of Dissertation

- There are only a few fluid models in the literature which are commonly used to model the properties of fuels
    - The utility of these techniques has been limited by the need for expensive and time-consuming high pressure experimental measurements to fit multiple model parameters or require complex compositional characterization to define multiple pseudo-components
- This dissertation presents a novel framework for accurately predicting thermodynamic and dynamic thermophysical properties of hydrocarbon mixtures and fuels
    - Variations in mixture and fuel composition are captured using a molecular-based equation of state (PC-SAFT) in lieu of complex compositional characterization for every fuel and fitting empirical correlations to high temperature and pressure (HTHP) data
        - Hundreds of compounds within a fuel are modeled as one pseudo-component using two experimentally measured or calculated inputs:
            - Number averaged molecular weight
            - Hydrogen to carbon ratio
    - Predictions are validated for a wide range of hydrocarbon mixtures and fuels (e.g., gasoline, kerosene, jet, rocket propellant, and diesel) up to high temperature and high pressure (HTHP) conditions (550 K and 3,500 bar)
        - Density is predicted within 1 % mean absolute percent deviation (MAPD)
        - Viscosity is predicted within 4 % MAPD
        - Thermal conductivity is predicted within 3 % MAPD
        - Errors in predictions are generally within the uncertainty of the experimental measurement

Impact of Dissertation on Scientific Community

- This dissertation presents a unified framework to predict thermodynamic and dynamic fluid properties of hydrocarbon mixtures and fuels up to high temperature and pressure conditions

- The framework is based upon the PC-SAFT equation of state and residual entropy scaling
    - This dissertation is the first application of residual entropy scaling using pseudo-component based methodologies to predict dynamic properties
- Properties are accurately predicted and do not require detailed measurements of the molecular structure of the mixtures and fuels
    - Only two inexpensive and commonly measured or calculated mixture properties are required as inputs
        - Number average molecular weight
        - Hydrogen to carbon ratio

- The pseudo-component technique requiring only two inputs is shown to be less accurate when predicting dynamic properties (i.e. viscosity, thermal conductivity) for mixtures or fuels with high concentrations of branched alkanes, which can significantly impact these properties at high pressure
    - Two methodologies are proposed to overcome this limitation:
        - Fitting one model parameter to a low pressure reference data point (i.e. ambient pressure viscosity or thermal conductivity)
        - An empirical correlation is proposed to correct the predicted residual entropy required for calculating dynamic properties
    - Both methodologies significantly improve predictions with the empirical correlation improving viscosity to within 9% MAPD

Application of Models to Computational Fluid Dynamics

- The predictive framework in this dissertation has been implemented into the open-source CFD software OpenFOAM by Rodriguez, Rokni, et al. (Submitted to *Fuel*, 2019)
- Predictions are shown to be accurate at extreme pressures relevant to modern fuel injectors
    - The accuracy of the CFD simulations is improved using the predictive methods from this dissertation compared to previous empirically based state-of-the-art models which are generally correlated to low pressure measurements.
    - These techniques are able to capture compositional variations in fluid properties during a simulation, leading to more accurate representations of evaporation,

condensation, and mass transfer, which may not be properly accounted for in models parameterized at a fixed composition and low pressure.

- As the CFD community progresses toward modeling complex fuel surrogates, the predictive framework in this dissertation will lead to significant reductions in computational costs.
    - Only one pseudo-component is required compared to up to tens to hundreds of compounds in a fuel or fuel surrogate

Impacts on Overall Objectives of IPPAD Program:

- The thermophysical property framework described in this dissertation provides the link between experimentalists who are measuring fluid properties for selected fuels (ESR1), and researchers who are modeling injector hydrodynamics and spray performance (ESRs 6, 12, and 13) for a wide range of fuels and conditions.
- The models developed in this study are computationally efficient, as evidenced by the CFD study of ESR 6 of the IPPAD project.
- The models account for the compositional variations in fuel properties including density, compressibility, expansivity, viscosity, and thermal conductivity reported in literature or measured by ESR 1 of the IPPAD project.
- The objective of the IPPAD project was to investigate the effect of fuels and additives on diesel injection, spray and soot formation at pressures up to 4,500 bar. Accurate modeling of fluid properties is needed for accurate CFD simulations, though the state-of-the art experimental apparatus can only measure properties up to limited pressures (3,000 bar for ESR 1). Therefore, accurate, predictive equation of state approaches are required to predict fuel properties beyond experimental limitations and for fuels outside of IPPAD for which measurements may not be available. The models presented in this dissertation enable both of these objectives.
- ESR 6 of the IPPAD project has utilized the thermodynamic models in this dissertation in CFD to simulate diesel injections at high-load conditions. The one pseudo-component based EoS models provided accurate and computationally efficient predictions, compared to a state-of-the-art multi-component surrogate approach. A manuscript based on this study is in review for publication in the journal *Fuel*.

- ESR 1 of the IPPAD project has measured the properties of diesel fuels and kerosene up to high pressures and temperatures. A co-authored manuscript with ESR 1 is in preparation and demonstrates the ability to predict density and viscosity differences between fuels due to variations in composition.
- Researchers at Afton are utilizing the models presented in this dissertation to understand differences in diesel fuel composition on engine performance, particularly

Table of Contents

List of Tables

List of Figures

Nomenclature

List of abbreviations

BD	Benzene Derivative
BWR	Benedict-Webb-Rubin
CE	Chapman Enskog
CFD	Computational Fluid Dynamics
CN	Carbon Number
DA	Dymond-Assael
DDB	Dortmund Data Bank
DoU	Degree of Unsaturation
ECN	Effective Carbon Number
EFB	Expanded Fluid-Based
EFT	Expanded Fluid Theory
EoS	Equation of State
FIE	Fuel Injection Equipment
FT	Friction Theory
FVT	Free Volume Theory
GC	Group Contribution
HN	Hydrogen Number
HN/CN	Hydrogen to Carbon Ratio
HTHP	High Temperature and High Pressure
KV40	Kinematic Viscosity at 40 °C
MAPD	Mean Absolute Percent Deviation
Max	Maximum
MW	Molecular Weight
PC-SAFT	Perturbed-Chain Statistical Associating Fluid Theory
PNA	Poly-Nuclear Aromatic
SAFT	Statistical Associating Fluid Theory
SAFT-VR	Statistical Associating Fluid Theory Variable Range
SD	Standard Deviation

List of Symbols

A, B, C, and D	coefficients for the third order polynomial correlation reduced viscosity and thermal conductivity to reduced, dimensionless residual entropy
A_{s^*}, B_{s^*}, C_{s^*}, and D_{s^*}	coefficients in the Δs^* correlation
$\tilde{\alpha}$	reduced Helmholtz free energy
α, l, and B_i	FVT parameters
α_p	volumetric thermal expansion coefficient
d	temperature dependent segment diameter
Δs^*	the difference between the predicted (using the two-parameter model) and fitted reduced dimensionless residual entropies
ε/k	depth of the potential well (K)
η	packing fraction or viscosity
η^*	reduced viscosity
η_o	viscosity data point at the lowest reported temperature and pressure
g	radial distribution function
I_1 and I_2	integrals in perturbation theory
k	Boltzmann's constant
κ_T	isothermal compressibility
λ	reduced well width or thermal conductivity
λ^*	reduced thermal conductivity
λ_o	thermal conductivity data point at the lowest reported temperature and pressure
m	number of segments
N	number of data points
N_A	Avogadro's number
$\Omega^{(2,2)*}$	reduced collision integral
P	pressure
π	mathematical constant, approximately equal to 3.14159
r	radial distance between two segments
R	gas constant

ρ	mass density or number density
ρ_0	density at the reference pressure of 0.1 MPa
$\tilde{s}$	reduced entropy
$\bar{s}$	molar entropy
s^*	reduced dimensionless residual entropy
σ	segment diameter (Å)
T	temperature
$u(r)$	pair potential
V	volume
X	mole fraction
y	property considered in the calculation (density, isothermal compressibility, volumetric thermal expansion coefficient, viscosity, or thermal conductivity)
Z	averaging parameter

List of Superscripts/Subscripts

disp	dispersion
exp	experimental data
fitted	fitted parameter
hc	hard chain
hs	hard sphere
predict	prediction
res	residual

Acknowledgments

I would like to thank Professor Manolis Gavaises (City University London), Professor Mark M^{c}Hugh (Virginia Commonwealth University), Dr. Joseph Roos (Afton Chemical), Dr. Joseph Remias (Afton Chemical), Dr. Mark Devlin (Afton Chemical), Dr. Joshua Moore (Afton Chemical), Dr. Ashutosh Gupta (Afton Chemical), and Dr. Rajendar Mallepally (Honeywell International) for their helpful, technical discussions and continuous encouragement throughout this project.

I acknowledge the European Union for providing the financial support through the European Union Horizon 2020 Research and Innovation program, Grant Agreement No 675528.

I express my deepest gratitude to my family and dear wife for their continual support, prayers, and advice, and finally wish everyone good health and happiness.

London, June 2019

Houman B. Rokni

Declaration

I hereby declare that the presented work in this thesis is my own or was developed in a joint effort with other members of the research group as it is stated and referenced in the text accordingly!

I grant powers of discretion to the University Librarian to allow this thesis to be copied in whole or in part without further reference to me. This permission covers only single copies made for study purposes, subject to normal conditions of acknowledgement.

London_____

_____

(Houman B. Rokni)

Abstract

Knowledge of fluid properties (e.g., density, viscosity, thermal conductivity) is critical for the design, testing, and development of fuel injection equipment (FIE) in academia and industry, especially at extreme temperature and pressure conditions where better spray performance leads to less soot emission. Currently, there is a lack of experimental data for fuels up to these conditions, and predictive approaches are required to model fuel properties. The objective of this research is to develop molecular-based techniques to predict transport and thermodynamic properties for well-characterized hydrocarbon mixtures and fuels up to high temperature and high pressure (HTHP) conditions.

This PhD focuses on the development of pseudo-component techniques using the Perturbed-Chain Statistical Associating Fluid Theory (PC-SAFT) equation of state (EoS) for several well-characterized hydrocarbon mixtures and various fuels (e.g., rocket propellant, jet, kerosene, and diesel) with varying composition. The predictive techniques, which treat mixtures as a single pseudo-component, do not require binary interaction parameters. The methodology is first used to predict density, isothermal compressibility, and volumetric thermal expansion coefficient up to HTHP conditions for six hydrocarbon mixtures, two jet fuels, and four diesel fuels using two calculated or measured mixture properties as inputs (i.e., the number averaged molecular weight (MW) and the hydrogen to carbon (HN/CN) ratio). Density, isothermal compressibility, and volumetric thermal expansion coefficient are predicted up to 470 K and 3,500 bar for the hydrocarbon mixtures with 1, 4, and 7% mean absolute percent deviations (MAPDs), respectively. For fuels, density, isothermal compressibility, and volumetric thermal expansion coefficient are predicted with MAPDs of 1, 9, and 13 %, respectively.

Entropy scaling based, pseudo-component techniques are also developed to predict viscosity and thermal conductivity up to HTHP conditions for mixtures and fuels using the number averaged MW and the HN/CN ratio. Viscosity and thermal conductivity are predicted less accurately when the mixture contains high concentrations of iso-alkanes. However, predictions for mixtures in this study are improved when a third input, a single data point at a chosen reference state, is used to fit one model parameter. For six hydrocarbon mixtures with varying concentrations, viscosity is predicted with MAPDs of 12 and 7% using the two-parameter and three-parameter models, respectively, from 293 to 353 K and up to 1,000 bar. For two different diesel fuels, viscosity is predicted with an MAPD of 21% using the two-parameter model and 9% using the three-parameter model from 323 to 423 K and up to 3,500 bar. For six different mixtures at conditions from 288 to 360 K and up to 4,500 bar, thermal conductivities are predicted with MAPDs of 16 and 3% using the two-parameter and three-parameter models, respectively. Thermal conductivities are predicted for three RP fuels and three jet fuels at conditions from 293 to 598 K and up to 700 bar with MAPDs of 14 and 2% using the two-parameter and three-parameter models, respectively. Finally, the viscosity pseudo-component technique is further analyzed, and a correlation is proposed to improve residual entropy predictions when using the two-parameter model. This correlation, fit to ~700 hydrocarbon mixture data points, significantly improves viscosity predictions, reducing the two-parameter model MAPD from 12.0% to 9.2% for ~1,500 hydrocarbon mixture and fuel data points. The successful completion of this thesis expands the current field of hydrocarbon mixture and fuel property prediction up to the extreme operating conditions encountered by engineers in the petroleum industry. The developed techniques enable simple and accurate predictions without requiring expensive and time-consuming experimental HTHP measurements for the design, testing, and development of fuel injection equipment (FIE).

1. Chapter 1: Introduction

1.1 Motivation

Diesel engines produce ~30 wt% of soot emissions in the world [1] but remain the predominant combustion technologies for the heavy duty, automotive, and aviation sectors, due to their performance and fuel economy [2, 3]. A recent study, Graham et al. [4] reported that increasing pressure to 3,000 bar significantly reduced soot. Fuel is introduced in an engine through fuel injectors, the operation and performance of which are sensitive to fluid properties, including density, viscosity, volatility, and composition. Emission regulations and the need for improved fuel economy have motivated diesel engine manufacturers to increase fuel injector operating pressures up to 4,500 bar [5]. Therefore, fuel injectors not only have to perform at extreme operating conditions but also need to be robust and ensure performance for diesel and jet fuels that vary in composition in different markets, leading to resource and time intensive experimental development, testing, and validation of these technologies.

1.2 Computational fluid dynamics as an alternative and need of property as inputs

To accelerate this process and reduce costs, computational fluid dynamics (CFD) simulations are routinely used by manufacturers to evaluate, understand, and optimize fuel injection equipment (FIE) design and operation. Many numerical methods and approaches have been developed to simulate the performance of fuel injectors and provide insight into the physical processes taking place inside these systems [6-20]. CFD has been used to demonstrate temperature and pressure effects on nozzle flow [21] and cavitation [22], fuel vaporization [23], and spray distribution [24]. Temperature and pressure dependence of thermophysical properties can be incorporated in CFD through empirical correlations, look-up tables, or equations of state (EoS).

These approaches most often require fitting or measurement of experimental data, which is rarely available for fuels up to high temperature and high pressure (HTHP) operating conditions.

At high pressures, compositional variance between fuels can lead to significant differences in properties. For example, the viscosity of two different diesel fuels reported by Aquing et al. [25] and Schaschke et al. [26] at 323 K differ by more than 120% at 1,800 bar and 200% at 2,400 bar. Models fit to viscosity data for one diesel fuel sample cannot be expected to accurately represent the viscosity of another diesel fuel with a different composition. Therefore, predictive models are needed that account for temperature, pressure, and composition. Ideally, the models should require no or minimal input of experimental data to reduce characterization expense.

1.3 Methodologies to predict properties of hydrocarbon mixtures and fuels

Approaches available to model the thermodynamic properties of complex mixtures (e.g., crude oils, bitumens, heavy oils, and diesel and biodiesel fuels) include general classes of equations of state (EoS) such as cubic EoS (e.g., van der Waals [27, 28], Peng-Robinson [29-31], Soave-Redlich-Kwong [30, 32, 33], Elliott-Suresh-Donohue [34]), Statistical Associating Fluid Theory (SAFT) based EoS (e.g., Soft-SAFT [35], Perturbed Chain SAFT (PC-SAFT) [36-38], SAFT Variable Range (SAFT-VR) [39], SAFT-γ Mie [40]), and EoS based upon virial expansion (e.g., Virial EoS [41, 42], Benedict-Webb-Rubin (BWR) [43, 44]). Cubic and virial expansion based EoS involve fitting multiple pure-component parameters to experimental data for every compound present in fuels. SAFT-based approaches also require fitting parameters for the compounds present in fuels, but are generally shown to have superior accuracy compared to cubic EoS [45-49]. Many modifications to the original SAFT EoS, which will be discussed in Chapter 2, have been proposed, with perhaps the most widely and currently used in industry being the Perturbed-Chain SAFT (PC-

SAFT) EoS of Gross and Sadowski [38]. Group contribution (GC) approaches have been devised for SAFT-based EoS [40, 50-61], including PC-SAFT [40, 52-55, 58], and can be used to calculate parameters for every compound in a given fuel, if the molecular structures of the molecules are known.

Amongst approaches to model the thermodynamic properties of complex mixtures, only a few composition-based approaches have been utilized to model properties for diesel fuels and their surrogates, a small number of components chosen as a mixture to closely match the thermophysical properties of the fuel [25, 62-68]. In a recent study, Vidal et al. [69] utilized the PC-SAFT EoS to predict density for four surrogates containing four to nine compounds, calculating the PC-SAFT parameters using a GC method [61] and previously fit molecular weight (MW) dependent PC-SAFT parameter correlations [70, 71]. Despite the relative simplicity surrogates may offer, selection of the individual components and their concentrations is difficult and involves a significant amount of manual effort. Furthermore, since the surrogate mixture is optimized for a specific fuel, this mixture cannot be expected to predict the properties of another fuel with a different composition.

Another approach is to represent a complex mixture (e.g., fuels, crude oils) through one or more pseudo-components [37, 72-88]. Burgess et al. [76] used PC-SAFT to model the density of two crude oils using three pseudo-components representing saturates (e.g., alkanes and naphthenes), aromatics, and asphaltenes. In another study, Abutaqiya et al. [37] defined a pseudo-component to predict density and phase behavior for several crude oils. Their approach required fitting of a model parameter to the saturated liquid density and bubble-point pressure. These techniques for predicting properties for complex mixtures have been limited by the need for experimental measurements to fit the EoS parameters or requiring complex compositional

characterization to define multiple pseudo-components. These limitations can be overcome using predictive, pseudo-component techniques which do not require fitting to experimental data.

1.4 Objectives of this study

The main focus of this PhD study is to develop molecular-based, pseudo-component techniques based upon the PC-SAFT EoS to predict transport and thermodynamic properties for well-characterized hydrocarbon mixtures and fuels up to high temperature and high pressure (HTHP) conditions without need for fitting individual fuel model parameters to expensive HTHP experimental measurements. Mixtures are treated as a single pseudo-component; therefore, binary interaction parameters are not needed. The pseudo-component techniques require only two calculated or measured mixture properties as inputs: the number averaged molecular weight (MW) and the hydrogen-to-carbon (HN/CN) ratio. In Chapter 2, we describe a purely predictive, pseudo-component technique used to predict density, isothermal compressibility, and volumetric thermal expansion coefficient up to HTHP for mixtures and fuels. In Chapters 3 and 4, the technique presented in Chapter 2 is extended to transport properties and used to develop residual entropy scaling based, pseudo-component techniques to predict viscosity and thermal conductivity for well-characterized mixtures and fuels. Less accurate predictions are achieved when the mixtures contain significant amounts of branched alkanes. Predictions for viscosity and thermal conductivity of these mixtures are improved when a third input, a single data point at a chosen reference state, is used to fit one model parameter. In Chapter 5, the viscosity pseudo-component technique is further analyzed, and a correlation is proposed to improve viscosity and thermal conductivity predictions without the third input.

2. Chapter 2: Pseudo-Component Technique: Density and Its Derivatives[1]

Among the general classes of equations of state (EoS) used in modeling fluid properties are those based upon the van der Waals equation (1873) [28]. The most famous of these modifications include the Redlich-Kwong (RK) EoS (1949) [89] and it's modification by Soave (1972) [33] and the Peng Robinson (PR) (1976) [31] EoS. Another class of EoS includes those based on the Statistical Associating Fluid Theory (SAFT) [90-93], generally acknowledged as superior in predictive ability [45-49]. The SAFT EoS, based upon Wertheim's thermodynamic perturbation theory of first order (TPT1) [94, 95], was developed in the late 1980s by Gubbins and coworkers [90, 91, 96] and successfully describes the effects of molecular association and chain formation on thermodynamic properties. SAFT is derived as a summation of the reduced, Helmholtz free energies that account for dispersion and repulsive interactions between monomer segments, formation of chains from monomer segments, and association due to hydrogen bonding-like interactions. Repulsive interactions are determined from the expressions of Carnahan and Starling [97] with monomer segments treated as hard spheres, and a corresponding hard-sphere radial distribution function is used for the chain and association terms as originally proposed by Chapman et al. [90]. Huang and Radosz [93, 98] modified the original dispersion interaction term by using the perturbed hard chain theory of Beret and Prausnitz [99] fit to argon data of Chen and Kreglewski [100]. This version of SAFT, commonly denoted as SAFT-HR, was the most widely used variant until PC-SAFT (described below) became prevalent in the 2000s and has three adjustable parameters: m, the number of segments per chain; σ, the segment diameter; and ε/k, the depth of the potential well, along with two additional parameters, ϵ_{AB} and κ_{AB}, to describe association.

[1]Adapted from Ref. [36] Rokni HB, Gupta A, Moore JD, McHugh MA, Bamgbade BA, Gavaises M. Purely predictive method for density, compressibility, and expansivity for hydrocarbon mixtures and diesel and jet fuels up to high temperatures and pressures. Fuel **2019**;236:1377-90. doi.org/10.1016/j.fuel.2018.09.041

Huang and Radosz tabulated and fit SAFT parameters to saturated liquid vapor pressures and densities for over 100 pure components [93] and their mixtures [98] and found successful agreement with experimental data.

Later variants of SAFT [39, 40, 93, 101-107] modified the hard-sphere reference used to describe monomer segment and chain repulsion and attraction interactions. Soft-SAFT [108-110] utilizes a Lennard-Jones (LJ) potential in lieu of the hard-sphere reference and has been widely used by Vega and coworkers to accurately describe associating fluids and mixtures [111-113]. SAFT-VR [39] utilizes variable-range potentials using square-well, Yukawa, Lennard-Jones, or Mie fluids (SAFT-VR Mie [114]). SAFT-VR has more recently been cast within a group-contribution framework (SAFT-γ [40]), with the most recent variant for molecules formed from Mie heteronuclear segments (SAFT-γ Mie [56]).

The most widely used SAFT variant in industry today is the PC-SAFT EoS of Gross and Sadowski [38] and is the variant used in this work. In contrast to other variants of SAFT which use a hard-sphere as the reference system, PC-SAFT uses a chain of hard-spheres as the reference system and has had success in modeling industrial fluids, particularly hydrocarbons [115-120] and polymers [121]. Several researchers have also applied PC-SAFT to model complex mixtures (e.g., crude oils) through one or more pseudo-components [37, 72-76]. Ting [75] modeled the phase behavior of crude oil using three pseudo-components representing saturates (e.g., alkanes and naphthenes), aromatics, and asphaltenes. Ting correlated the PC-SAFT parameters to MW and calculated the parameters for the three pseudo-components using a weighted averaging term, defined as aromaticity. Ting [75] fit aromaticity to the bubble-point pressure and defined it to vary from 0 for poly-nuclear aromatics (PNAs) to 1 for benzene derivatives (BDs). Gonzalez [73] modified the PC-SAFT correlations reported by Ting [75] and redefined the range of aromaticity

from 0 for BDs to 1 for PNAs. Punnapala and Vargas [74] fit aromaticity to the saturated liquid density and bubble-point pressure and redefined the range of it from 0 for normal alkanes (n-alkanes) to 1 for PNAs, which provided better phase behavior predictions for crude oils.

Abutaqiya et al. [37] studied several crude oils and predicted density and phase behavior using a single pseudo-component. They used the PC-SAFT correlations proposed by Gonzalez and fit aromaticity to experimental saturated liquid density and bubble-point pressure. Burgess et al. [76] fit correlations for the PC-SAFT parameters to HTHP experimental data [122] and predicted density for two crude oils. To make the approach predictive, they calculated aromaticity from the HN/CN ratio of the fuel obtained from elemental analysis using a definition proposed by Huang and Radosz [93].

Previous techniques for predicting density and derivative properties for complex mixtures have been limited by the need for experimental measurements to fit the EoS parameters or requiring complex compositional characterization to define multiple pseudo-components. This chapter describes the development of a pseudo-component technique using the PC-SAFT EoS to predict density, isothermal compressibility, and the volumetric thermal expansion coefficient for hydrocarbon mixtures without the need for fitted binary interaction parameters. Two mixture properties are required for the predictions: the number averaged molecular weight (MW) and the hydrogen to carbon (HN/CN) ratio, both of which are either calculated when working with well-defined, simple mixtures or are measured when working with multicomponent fuel mixtures. The technique proposed in this study utilizes the HTHP group contribution (GC) parameters developed by Burgess et al. [53] to correlate the PC-SAFT parameters with respect to MW. The PC-SAFT parameters of the pseudo-component are then determined using the mixture HN/CN ratio in a modified averaging equation previously used by other researchers [123-127]. Fluid property

predictions are compared to experimental data for six well-characterized hydrocarbon mixtures with varying composition to demonstrate the technique. Further predictions are then presented for four diesel fuels and two jet fuels over a wide range of temperatures and pressures to more fully explore the capabilities of the pseudo-component technique with a focus on HTHP fluid properties.

2.1 PC-SAFT equation of state

The PC-SAFT EoS, developed by Gross and Sadowski [38], is molecularly-based and accounts for the effects of molecular size, molecular shape, dispersion forces, and association of molecules. In the present study, association is neglected since the compounds in the fuels and hydrocarbon mixtures do not exhibit association, such as hydrogen bonding. Therefore, the PC-SAFT EoS requires three parameters: m, the number of segments per chain; σ, the segment diameter; and ε/k, the depth of the potential well. The schematic representation of PC-SAFT is shown in Figure 2.1.

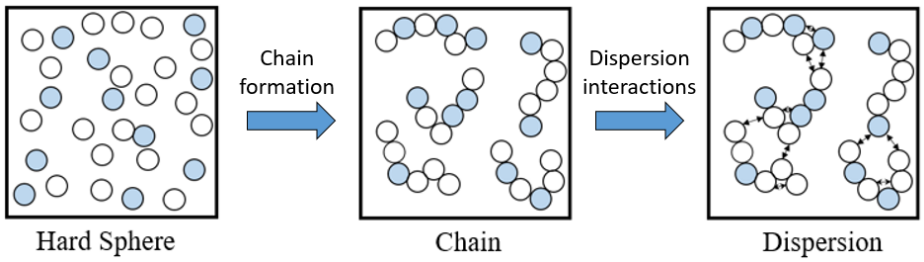

Figure 2.1. Schematic representation of PC-SAFT EoS; adapted from [128]. Hard chains are formed from hard spheres and attractive (dispersion) forces are added between chains. Association (not shown) is also possible within PC-SAFT to allow for hydrogen bonding-like interactions.

In PC-SAFT, the residual, reduced Helmholtz free energy ($\tilde{a}^{res}$) of the fluid without association is defined by Eq. 2.1:

$$\tilde{a}^{res} = \tilde{a}^{hc} + \tilde{a}^{disp} \qquad 2.1$$

where $\tilde{a}^{hc}$ and $\tilde{a}^{disp}$ are the contributions of the hard chain and dispersion reduced Helmholtz free energies, respectively. The hard chain contribution, defined by the hard sphere contribution and the average radial distribution function, g^{hs}, is expressed as:

$$\tilde{a}^{hc} = m\tilde{a}^{hs} - (\mathrm{m} - 1)\, ln\, g^{hs} \qquad 2.2$$

The Helmholtz free energy of the hard-sphere fluid is given by

$$\tilde{a}^{hs} = \frac{1}{\zeta_0}\left(\frac{3\zeta_1\zeta_2}{(1-\zeta_3)} + \frac{\zeta_2^3}{\zeta_3(1-\zeta_3)^2} + \left(\frac{\zeta_2^3}{\zeta_3^2} - \zeta_0\right) ln\,(1-\zeta_3)\right) \qquad 2.3$$

and the radial distribution function of the hard sphere fluid is given by

$$g^{hs} = \frac{1}{(1-\zeta_3)} + \left(\frac{d}{2}\right)\frac{3\zeta_2}{(1-\zeta_3)^2} + \left(\frac{d}{2}\right)^2 \frac{2\zeta_2^2}{(1-\zeta_3)^3} \qquad 2.4$$

with ζ_n defined as

$$\zeta_n = \frac{\pi}{6}\rho \mathrm{m} d^n \qquad n \in \{0,1,2,3\} \tag{2.5}$$

where ρ is the total number density of molecules, which can be calculated by Eq. 2.6.

$$\rho = \frac{6}{\pi}\eta (md(T)^3)^{-1} \tag{2.6}$$

where $d(T)$ is the temperature dependent segment diameter and η is the packing fraction (equal to ζ_3, representing the reduced segment density). Gross and Sadowski utilized a modified square-well potential, proposed by Chen and Kreglewski [100], to model the pair potential for the segments in the chain, as shown in Eq. 2.7.

$$u(r) = \begin{cases} \infty, & r < (\sigma - s_1) \\ 3\varepsilon, & (\sigma - s_1) \le r < \sigma \\ -\varepsilon, & \sigma \le r < \lambda\sigma \\ 0, & \lambda\sigma \le r \end{cases} \tag{2.7}$$

where $u(r)$, r, and λ denote the pair potential, the radial distance between two segments, and the reduced well width, respectively. As suggested by Chen and Kreglewski [100], a ratio of $s_1/\sigma = 0.12$ is assumed. The temperature dependent segment diameter can be calculated in the framework of Barker and Henderson's perturbation theory [129] for the pair potential in Eq. 2.7 as:

$$d(T) = \int_0^\sigma \left(1 - e^{\frac{-u(r)}{kT}}\right) dr = \sigma\left(1 - 0.12\, exp\left(-\frac{3\varepsilon}{kT}\right)\right) \tag{2.8}$$

The dispersion contribution reduced Helmholtz free energy is given by:

$$\tilde{a}^{disp} = -2\pi\rho I_1(\eta, m)m^2\varepsilon\sigma^3 - \pi\rho \mathrm{m} C_1 I_2(\eta, m)m^2\varepsilon^2\sigma^3 \quad 2.9$$

where the abbreviation C_1 is a compressibility expression defined as

$$C_1 = \left(1 + \mathrm{m}\frac{8\eta - 2\eta^2}{(1-\eta)^4} + (1-\mathrm{m})\frac{20\eta - 27\eta^2 + 12\eta^3 - 2\eta^4}{((1-\eta)(2-\eta))^2}\right) \quad 2.10$$

where I_1 and I_2 are integrals[2] approximated by a power series as a function of chain length and packing fraction Gross and Sadowski [38] . Eq. 2.11 is used to calculate pressure.

$$P = kT\rho\left[1 + \eta\left(\frac{\partial\tilde{a}^{res}}{\partial\eta}\right)\right] \quad 2.11$$

Pure-component PC-SAFT parameters are generally fit to vapor pressure and saturated liquid density data [38] and can also be calculated using group contribution (GC) methods [58-60].

2.2 Pseudo-component technique

The GC parameters from most methods are not fit to high pressure data and generally lead to property predictions which deviate at high pressures [51, 57, 59-61, 130]. Since Burgess et al. [53] fit their GC parameters to HTHP density data, their parameters are used here to calculate the

[2] I_1 and I_2 can be found in Ref. [38]: Gross J, Sadowski G. Perturbed-chain SAFT: An equation of state based on a perturbation theory for chain molecules. Industrial & Engineering Chemistry Research **2001**;40(4):1244-60. Eqs. (A.16) and (A.17).

PC-SAFT parameters of the 140 compounds reportedly found in two different diesel fuels [25]. Figure 2.2 shows the variation of m with respect to MW for this range of compounds, although only selected compounds from the different chemical families in the diesel fuel are shown to avoid a cluttered graph. For a given MW, m appears to be a function of molecular structure with n-alkanes and PNAs bounding the distribution. Similar trends are observed for the other PC-SAFT parameters, $m\sigma$ and ε/k. These observations are consistent with those reported by Huang and Radosz [93] and Gonzalez [73] who developed PC-SAFT parameter correlations based on pure component parameters fit to vapor pressure and saturated liquid density.

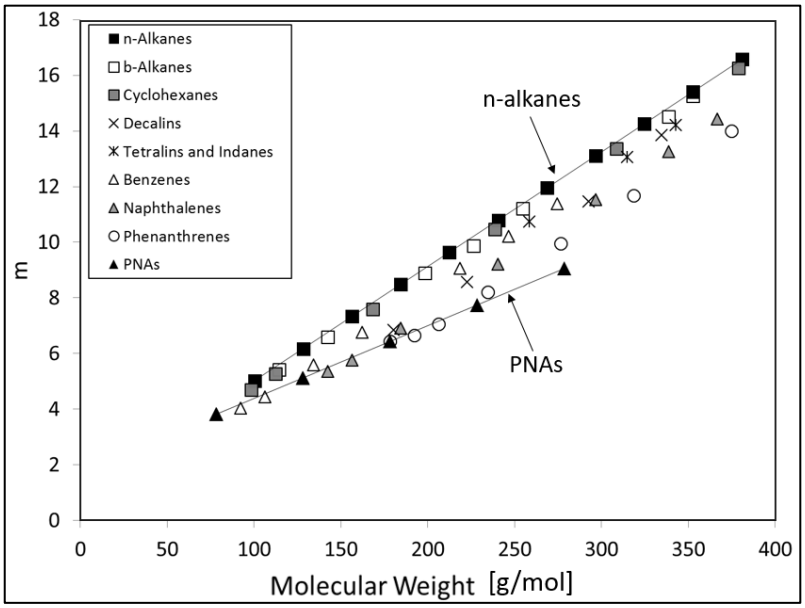

Figure 2.2. PC-SAFT m segment parameter of selected components calculated using GC parameters of Burgess et al. [53].

Figure 2.3 shows the PC-SAFT parameters for the two bounds, n-alkanes and PNAs, as a function of MW. Selected n-alkanes and PNAs are shown to avoid a cluttered graph. Table 2.1 lists correlations for m, $m\sigma$, and ε/k, as a function of MW. The correlations for the PC-SAFT

parameters fit in this study are comparable to those by Burgess et al. [76] but extend the range of MWs to approximately 500 g/mol for n-alkanes and approximately 300 g/mol for PNAs. This higher molecular weight range covers the broad range of compounds typically found in diesel fuels and, therefore, avoids the need for extrapolation.

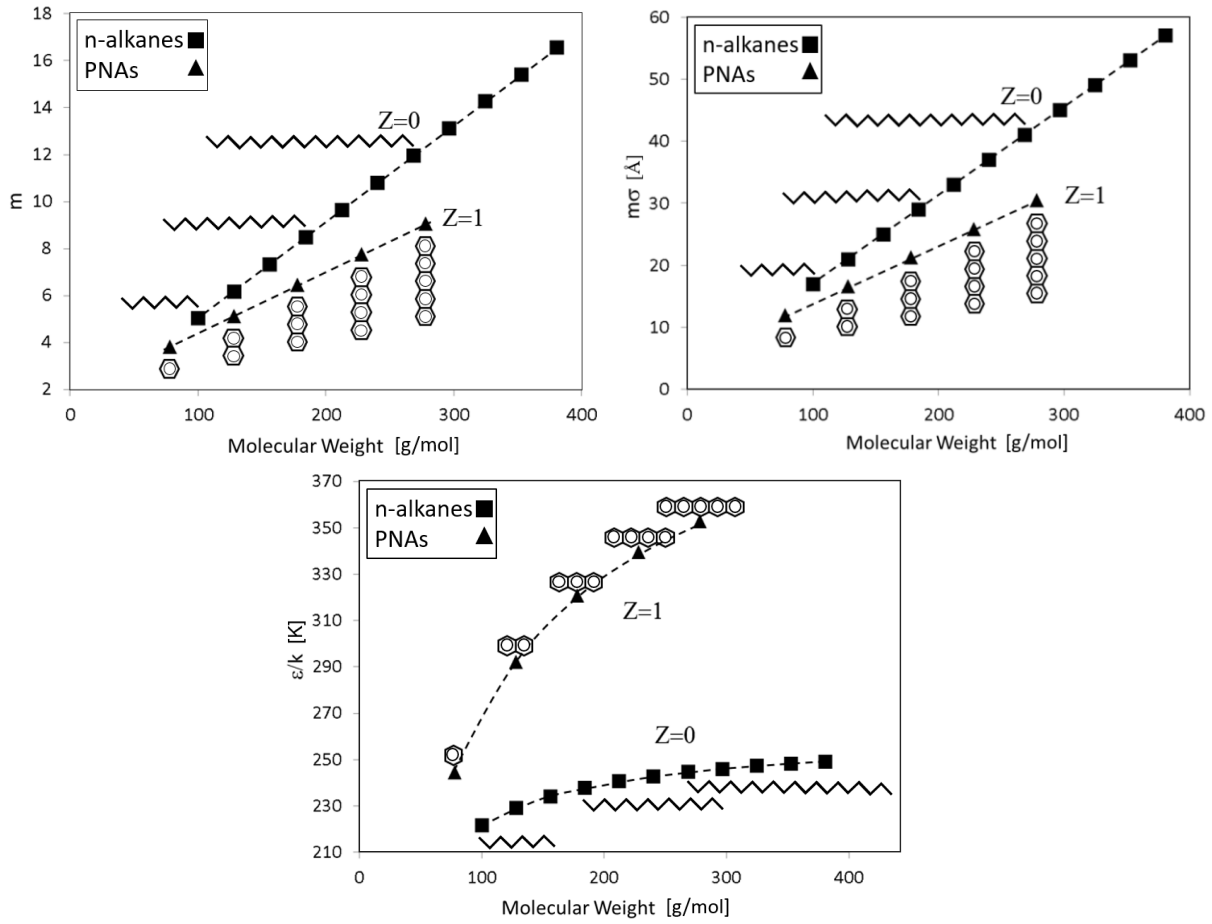

Figure 2.3. PC-SAFT parameters calculated using GC parameters of Burgess et al.[53] as a function of molecular weight for n-alkanes and PNAs. Structures of representative molecules are shown on the graphs. The degree of unsaturation of a mixture is represented through a parameter Z and is described in the text. Z varies from 0 for n-alkanes to 1 for PNAs. Note that the selected n-alkane and PNA compounds with MW up to 400 g/mol are only shown in the figures.

Table 2.1. PC-SAFT parameter correlations as a function of molecular weight (MW (g/mol)) for n-alkanes and PNAs used in this study.

	n-alkanes	PNAs
m	$0.0412\mathrm{MW} + 0.8954$	$0.0262\mathrm{MW} + 1.7750$
$m\sigma\ (\text{Å})$	$0.1430\mathrm{MW} + 2.5847$	$0.0922\mathrm{MW} + 4.7925$
$\varepsilon/_k\ (K)$	$\exp^{(5.5599 - 16.1830/\mathrm{MW})}$	$\exp^{(6.0022 - 39.8810/\mathrm{MW})}$

The pseudo-component PC-SAFT parameters need to account for the MWs and the degree of unsaturation of the compounds in the mixture. The molecular weights of all the compounds in the mixture are averaged to obtain the mixture number averaged MW. Here the degree of unsaturation (DoU) of compounds in a mixture is represented by Z, as calculated in Eq. 2.13. Z varies from 0 for n-alkanes to 1 for PNAs as shown in Figure 2.2. Since the DoU of n-alkanes is zero, Z reduces to the degree of unsaturation of the mixture divided by the degree of unsaturation of a PNA with a MW equal to the mixture number averaged MW. The correlation of $\mathrm{DoU_{PNA}}$ as a function of MW shown in the appendix (Section 2.5) is used to calculate a value for $\mathrm{DoU_{PNA}}$ needed in Eq. 2.12.

$$Z = \frac{\mathrm{DoU_{mixture}} - \mathrm{DoU_{n-alkane}}}{\mathrm{DoU_{PNA}} - \mathrm{DoU_{n-alkane}}} = \frac{\mathrm{DoU_{mixture}}}{\mathrm{DoU_{PNA}}} \qquad 2.12$$

$\mathrm{DoU_{mixture}}$ is calculated by Eq. 2.13 from the average carbon number (CN) and average hydrogen number (HN) of the mixture. The hydrogen to carbon (HN/CN) ratio can either be calculated if all of the mixture components are known or can be obtained from elemental analysis when dealing with a complex fuel mixture.

$$\mathrm{DoU} = \frac{1}{2}(2 \times \mathrm{CN} + 2 - \mathrm{HN}) \quad 2.13$$

Similar to the aromaticity parameter used by Punnapala and Vargas [74], the Z parameter is used to average the contributions of the two bounds (i.e., n-alkanes and PNAs) for each pseudo-component PC-SAFT parameter, Eqs. 2.14-2.16.

$$m_{\mathrm{mixture}} = (1 - Z)m_{\mathrm{n-alkane}} + Zm_{\mathrm{PNA}} \quad 2.14$$

$$(m\sigma)_{\mathrm{mixture}} = (1 - Z)(m\sigma)_{\mathrm{n-alkane}} + Z(m\sigma)_{\mathrm{PNA}} \quad 2.15$$

$$\left(\varepsilon/k\right)_{\mathrm{mixture}} = (1 - Z)\left(\varepsilon/k\right)_{\mathrm{n-alkane}} + Z\left(\varepsilon/k\right)_{\mathrm{PNA}} \quad 2.16$$

The hydrocarbon mixtures and diesel and jet fuels in this study do not contain compounds with DoUs greater than 10 (i.e., phenanthrene). However, DoUs greater than 10 would be calculated for PNAs using the $\mathrm{DoU_{PNA}}$ correlation as a function of MW if the mixture number average MW is greater than that for phenanthrene (i.e. 178 g/mol). Thus, direct application of Eq. 2.12 could underpredict the Z parameter. Instead, an upper bound of 10 is assigned for the DoU of PNAs when the mixture number averaged MW is greater than 178 g/mol, and the Z parameter is redefined as shown in Eq. 2.17.

$$Z = \begin{cases} \dfrac{\mathrm{DoU_{mixture}}}{\mathrm{DoU_{PNA}}}, \mathrm{MW_{mixture}} < 178\ \mathrm{g/mol} \\ \dfrac{\mathrm{DoU_{mixture}}}{10}, \mathrm{MW_{mixture}} \geq 178\ \mathrm{g/mol} \end{cases} \quad 2.17$$

The PC-SAFT parameters of the pseudo-component can be calculated using a combination of either the original expression for the Z parameter (Eq. 2.12) or the alternative expression (Eq. 2.17). Both

approaches are used in the following property predictions for well-characterized hydrocarbon mixtures, four diesel fuels, and two jet fuels. PC-SAFT fluid property calculations are performed using the software VLXE/Blend [131]. For clarity only the isotherms at the lowest and highest temperatures are shown. However, the reported statistical measures include data at all temperatures available from literature. Deviation plots are included in the appendix (Section 2.5). Statistical measures reported, defined by Eqs. 2.18-2.22, include percent deviation, maximum (Max) deviation, standard deviation (SD), MAPD, and bias.

$$\text{Deviation (\%)} = 100 \times \frac{\left(y_{\text{predict}} - y_{\text{exp}}\right)}{y_{\text{exp}}} \tag{2.18}$$

$$\text{Max Deviation (\%)} = \text{Max}\left(100 \times \frac{\left|y_{\text{predict}} - y_{\text{exp}}\right|}{y_{\text{exp}}}\right) \tag{2.19}$$

$$\text{SD (\%)} = \sqrt{\frac{\sum(\text{Deviation} - \text{MAPD})^2}{N-1}} \tag{2.20}$$

$$\text{MAPD (\%)} = \frac{1}{N}\sum 100 \times \frac{\left|y_{\text{predict}} - y_{\text{exp}}\right|}{y_{\text{exp}}} \tag{2.21}$$

$$\text{Bias (\%)} = \frac{1}{N}\sum 100 \times \frac{\left(y_{\text{predict}} - y_{\text{exp}}\right)}{y_{\text{exp}}} \tag{2.22}$$

In Eqs. 2.18-2.22, y_{exp}, y_{predict}, and N denote the experimental data point, the prediction, and number of data points, respectively.

2.3 Results

2.3.1 Well-characterized hydrocarbon mixtures

Table 2.2 lists the composition of the six hydrocarbon mixtures used to evaluate the pseudo-component technique presented here. Baylaucq et al. [132] reported densities for binary mixtures of methyl-cyclohexane (MCH) and n-heptane (nC7) for five different compositions for 3 isotherms at 303, 323, and 343 K and pressures up to 1,000 bar. Ijaz [88] reported densities of a ternary and two quaternary mixtures for 7 isotherms between 298 and 448 K and pressures up to 1,350 bar. Boned et al. [133] measured densities for a ternary and a quinary mixture for 7 isotherms between 293 to 353 K and pressures up to 1,000 bar. Table 2.3 presents the calculated MW, the HN/CN ratio, Z parameter, and the PC-SAFT parameters of the pseudo-components for the six different well-characterized hydrocarbon mixtures using both combinations of approaches to calculate Z.

Table 2.2. Molar composition (mole fraction) of hydrocarbon mixtures studied in this work.

Compounds	M1	M2	M3	M4	M5	M6
n-heptane	0.5 to 1.0	-	-	-	-	-
methyl-cyclohexane	balance	-	-	-	-	-
n-tridecane	-	-	-	-	0.394	0.200
2,2,4,4,6,8,8-hepta-methyl-nonane	-	-	-	-	-	0.162
heptyl-cyclohexane	-	-	-	-	0.348	0.353
heptyl-benzene	-	-	-	-	0.258	0.156
1-methyl-naphthalene	-	-	-	-	-	0.129
n-octane	-	0.460	0.349	0.347	-	-
n-dodecane	-	0.309	0.235	0.235	-	-
n-hexadecane	-	0.232	0.176	0.175	-	-
bi-cyclohexyl	-	-	0.241	-	-	-
di-isopropyl-benzene	-	-	-	0.244	-	-

Table 2.3. Mixture properties and PC-SAFT parameters of the pseudo-components for well-characterized hydrocarbon mixtures predicted in this study. When the number averaged MW of the mixture is less than the MW of phenanthrene, Eq. 2.17 reduces to Eq. 2.12, and the original and alternative Z parameters are the same.

Sample	MW	HN/CN	Z		m	σ (Å)	ε/k (K)
M1 (1.000 mole fraction nC7)	100.2	2.29	Original	0	5.0237	3.3667	221.08
M1 (0.875 mole fraction nC7)	99.9	2.25	Original	0.0236	4.9985	3.3630	222.16
M1 (0.750 mole fraction nC7)	99.7	2.21	Original	0.0472	4.9734	3.3592	223.24
M1 (0.625 mole fraction nC7)	99.4	2.18	Original	0.0711	4.9484	3.3553	224.31
M1 (0.500 mole fraction nC7)	99.2	2.14	Original	0.0950	4.9235	3.3514	225.39
M2	157.6	2.20	Original	0	7.3872	3.4000	234.47
M3	159.7	2.11	Original	0.0439	7.4069	3.3967	238.27
M4	158.7	2..03	Original	0.0971	7.2882	3.3912	242.33
M5	181.6	1.94	Original	0.1363	8.1219	3.3972	249.42
			Alternative	0.1390	8.1169	3.3969	249.65
M6	183.6	1.84	Original	0.2027	8.0768	3.3923	255.49
			Alternative	0.2092	8.0644	3.3917	256.06

Figure 2.4 shows density predictions for the well-characterized hydrocarbon mixtures reported by Baylaucq et al. [132], Ijaz [88], and Boned et al. [133] at the lowest and highest temperatures reported and pressures up to 1,350 bar. For brevity, only the composition containing 0.750 mole fraction n-heptane and 0.250 mole fraction MCH are reported in Figure 2.4. Although relatively higher deviations (i.e., 2.2% MAPD) are achieved for mixture M3, which is likely due to the presence of high concentration of bi-cyclohexyl, the predictions for all six well-characterized hydrocarbon mixtures show quantitative agreement with experiment across all temperatures and

pressures. Only predictions using the original Z equation are shown for mixtures M1-M4, since their number averaged MWs are less than the MW of phenanthrene.

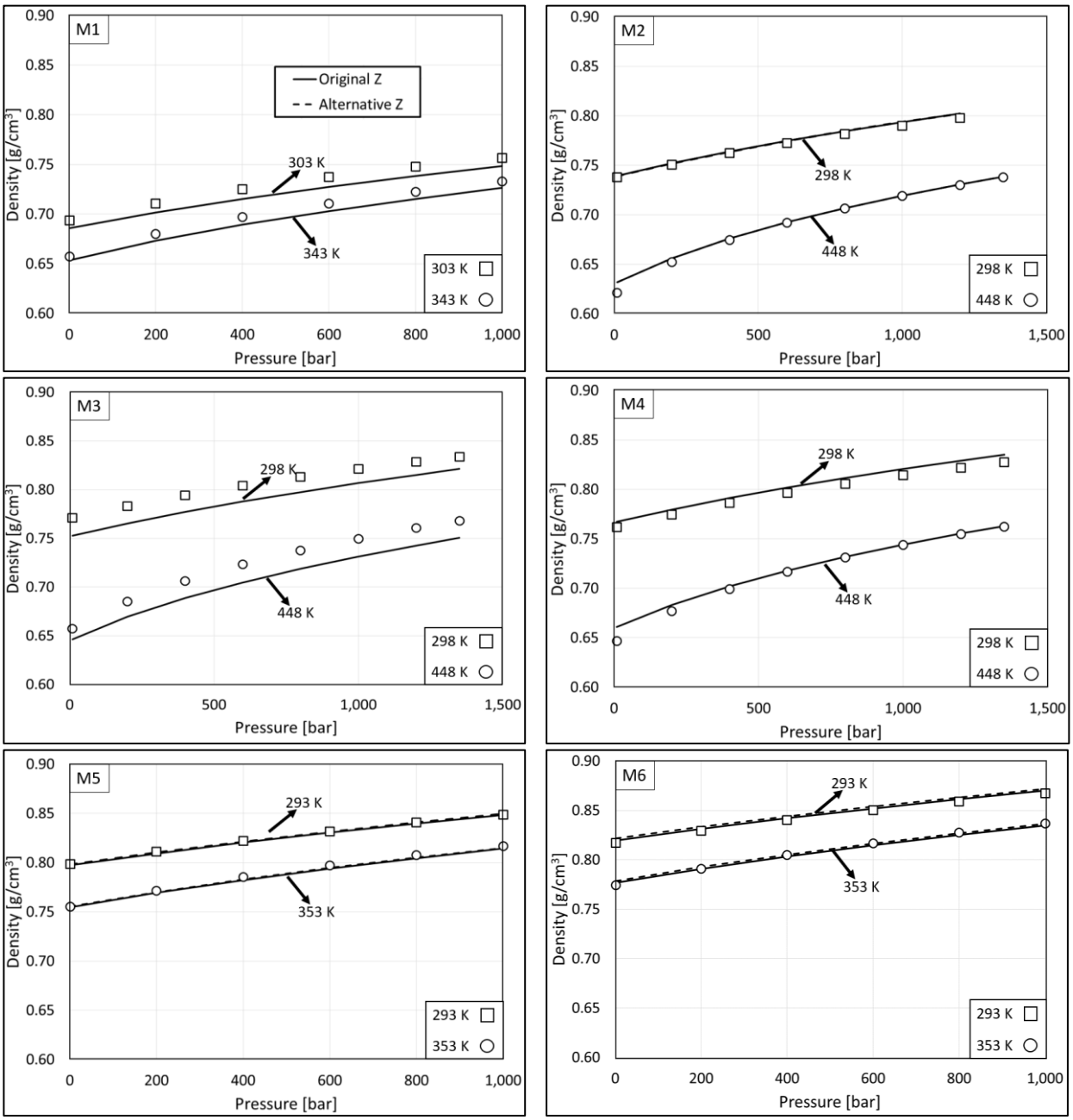

Figure 2.4. Density predictions (lines) compared to experimental data [88, 132, 133] (symbols) for well-characterized hydrocarbon mixtures.

Table 2.4 shows statistical measures for density predictions of the binary mixture (M1) with MAPDs ranging from 0.2 to 2.5%, with an MAPD of 1.2% for all considered mixture compositions. The MAPDs of the density predictions appear to increase monotonically with increasing mole fraction of MCH. This behavior could potentially be due to the relatively low MW of n-heptane and MCH, both of which lie at the extreme lower bound of fitted PC-SAFT correlations. Large concentrations of these compounds are not typically found in diesel and jet fuels.

Table 2.4. The MAPD (%), bias (%), SD (%), and Max Deviation (%) for density predictions of mixture M1 with different compositions of methyl-cyclohexane (MCH) and n-heptane (nC7).

Mole Fraction					
x_{nC7}	x_{MCH}	MAPD	Bias	SD	Max Deviation
1.000	0.000	0.2	0.2	0.2	0.9
0.875	0.125	0.4	-0.4	0.2	0.6
0.750	0.250	1.1	-1.1	0.2	1.3
0.625	0.375	1.8	-1.8	0.2	2.1
0.500	0.500	2.5	-2.5	0.1	2.7
Average		1.2	-1.1	0.9	2.7

Table 2.5 summarizes the density predictions using the original and alternative Z equations for the calculation of the PC-SAFT parameters for the ternary, quaternary, and quinary mixtures studied by Ijaz [88] and Boned et al. [133] (mixtures M2-M6). The density predictions show that the original and alternative equations used to calculate Z provide similarly accurate predictions for these well-defined simple mixtures.

Table 2.5. The MAPD (%), bias (%), SD (%), and Max Deviation (%) for density predictions of mixtures M2-M6. When the number averaged MW of the mixture is less than the MW of phenanthrene, Eq. 2.17 reduces to Eq. 2.12, and the original and alternative Z parameters are the same.

Mixture	Z	MAPD	Bias	SD	Max Deviation
M2	Original	0.3	0.3	0.3	1.8
M3	Original	2.2	-2.2	0.2	2.4
M4	Original	0.6	0.6	0.4	2.4
M5	Original	0.2	-0.2	0.1	0.5
	Alternative	0.1	-0.1	0.1	0.3
M6	Original	0.2	0.0	0.1	1.0
	Alternative	0.3	-0.3	0.2	0.6

Direct experimental measurement of the isothermal compressibility (κ_T) and volumetric thermal expansion coefficient (α_p) is challenging, which is reflected in limited experimental data available in the literature. Therefore, density data are fit to the Tait equation, Eq. 2.23, and the isothermal compressibility (Eq. 2.24) and volumetric thermal expansion coefficient (Eq. 2.25) are calculated from derivatives of the Tait fits to density.

$$\frac{\rho - \rho_0(T)}{\rho} = A \log_{10}\left(\frac{P + B(T)}{P_0 + B(T)}\right) \quad 2.23$$

$$\kappa_T = \frac{1}{\rho}\left(\frac{d\rho}{dP}\right)_T \quad 2.24$$

$$\alpha_p = -\frac{1}{\rho}\left(\frac{d\rho}{dT}\right)_P \quad 2.25$$

In Eq. 2.23, ρ_0 is the density at the reference pressure of 0.1 MPa, B is a temperature dependent parameter, and A is a constant. Values for ρ_0 and B fit to each isotherm were subsequently fit to second order polynomials as a function of temperature, Eqs. 2.26 and 2.27.

$$\rho_0(T) = \sum_{i=0}^{2} e_i T^i \quad 2.26$$

$$B(T) = \sum_{i=0}^{2} b_i T^i \quad 2.27$$

MAPDs less than 0.10%, biases less than -0.02%, SDs less than 0.10%, and Max Deviations less than 0.47% are obtained between data and predictions using the Tait equation for the mixtures considered here. Values for A and the coefficients in Eqs. 2.26 and 2.27 for all of the mixtures are found in the appendix (Section 2.5). For brevity, only the composition containing 0.750 mole fraction n-heptane and 0.250 mole fraction MCH are reported in the following figures. Figure 2.5 presents the predicted mixture κ_T compared to Tait calculations from experimental density data. The effects of temperature and pressure are well predicted quantitatively.

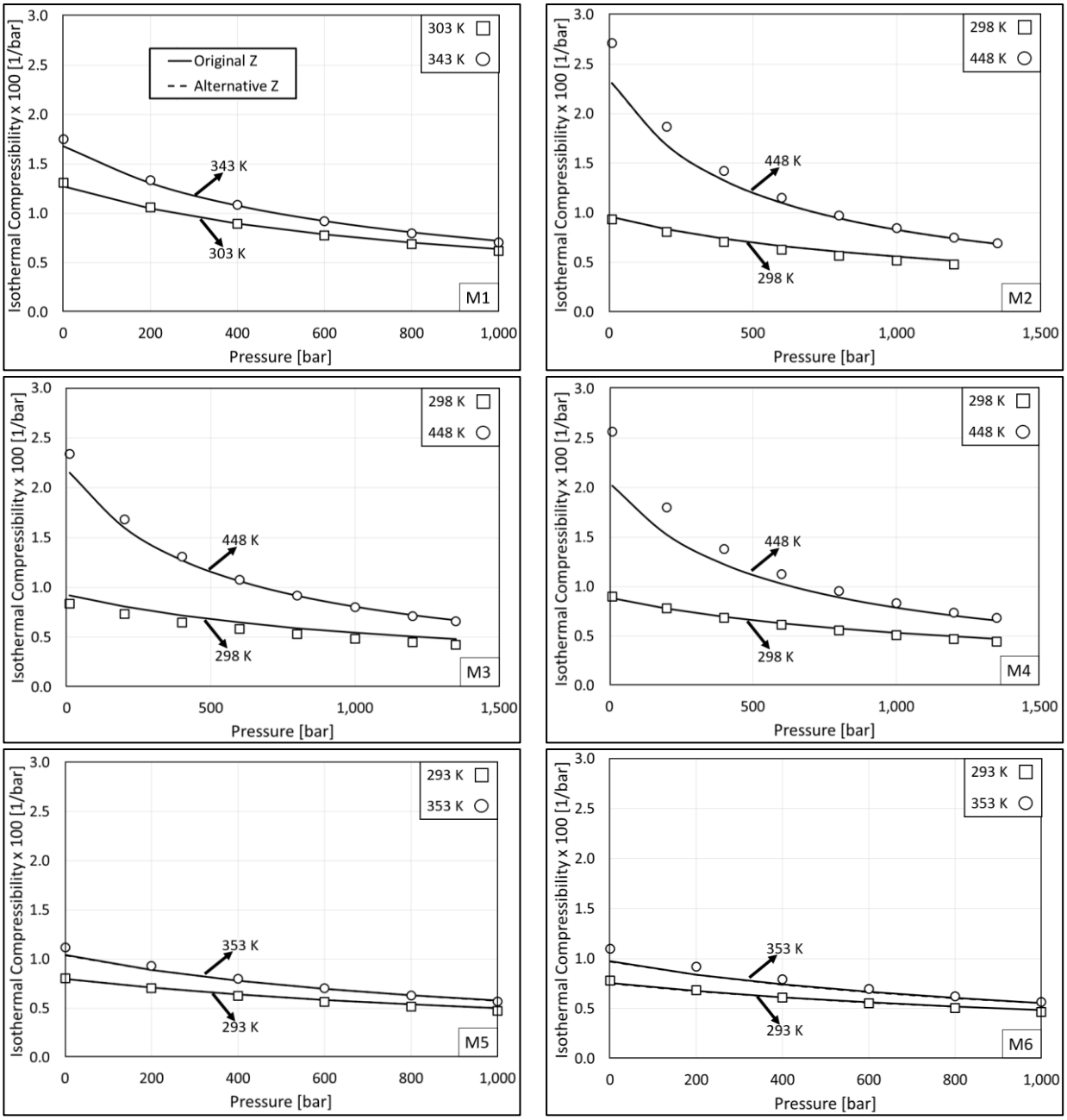

Figure 2.5. Isothermal compressibility predictions (lines) compared to experimental data [88, 132, 133] (symbols) for well-characterized hydrocarbon mixtures.

Figure 2.6 shows predictions for α_p compared to Tait calculations from experimental density data. The predictions capture the qualitative trends with respect to pressure, with the coefficients monotonically decreasing with pressure for all mixtures. The predictions capture the qualitative trends with respect to temperature for mixtures M1-M4. Predictions for mixtures M5 and M6 exhibit an inverse dependence on temperature for all pressures compared to the Tait calculations. A crossover in temperature is observed between 200 and 500 bar for mixtures M1-M4 for predictions and the Tait calculations. A crossover in temperature is observed for the Tait calculations at pressures less than 200 bar and pressures between 200 and 400 bar for mixtures M5 and M6, respectively, but is not observed in the predictions. For pressures below the crossover point, α_p increases with temperature, and for pressures above the crossover point, α_p decreases with temperature. Previous studies observed a crossover in temperature at pressures less than 600 bar for benzene, tetrachloromethane, n-hexane, n-nonane, n-dodecane, n-tridecane, n-pentadecane, mixtures of trialkylimidazolium-based ionic liquids, biodiesel from rapeseed oil, and standard petroleum diesel oil [134-137]. The crossover has been attributed to anharmonicity of intermolecular vibrations [134-136]. Tables 2.6 and 2.7 summarize statistical measures for the κ_T and α_p predictions using the original and alternative Z equations for the calculation of the PC-SAFT parameters for mixtures M1-M6. The alternative equation used to calculate Z does not significantly impact predictions of the derivative properties.

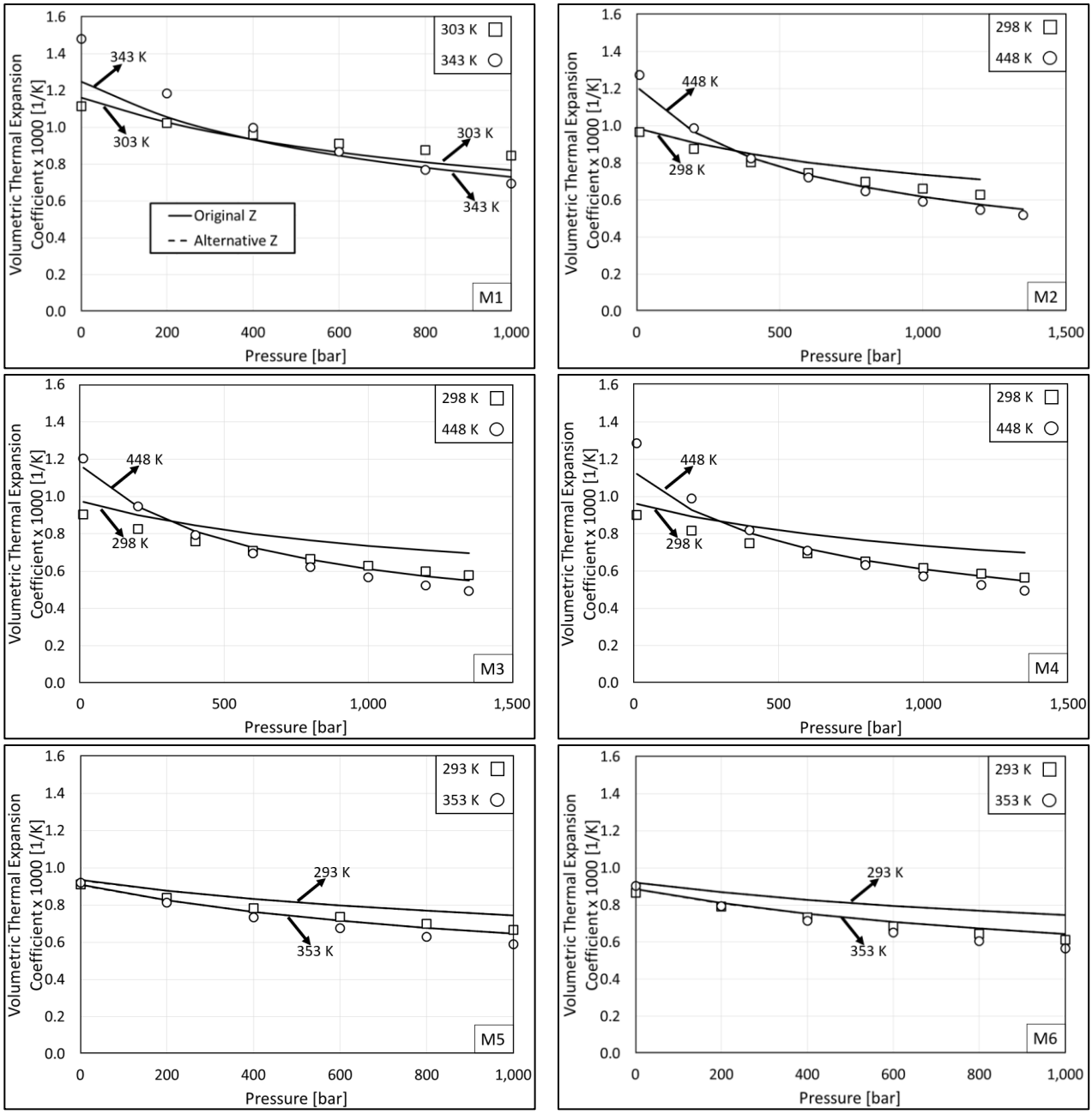

Figure 2.6. Volumetric thermal expansion coefficient predictions (lines) compared to experimental data [88, 132, 133] (symbols) for hydrocarbon mixtures.

Table 2.6. The MAPD (%), bias (%), SD (%), and Max Deviation (%) for isothermal compressibility predictions of well-characterized hydrocarbon mixtures.

Mixture	Z	MAPD	Bias	SD	Max Deviation
M1	Original	1.9	-0.2	1.4	5.6
M2	Original	3.8	-0.7	3.3	14.9
M3	Original	5.6	4.5	3.6	13.2
M4	Original	5.2	-3.5	4.7	20.1
M5	Original	2.5	0.2	1.8	6.7
	Alternative	2.5	0.0	1.8	7.1
M6	Original	3.6	-2.6	2.9	11.5
	Alternative	3.7	-2.7	3.0	12.0

Table 2.7. The MAPD (%), bias (%), SD (%), and Max Deviation (%) for volumetric thermal expansion coefficient predictions of well-characterized hydrocarbon mixtures.

Mixture	Z	MAPD	Bias	SD	Max Deviation
M1	Original	7.2	-5.8	3.7	21.9
M2	Original	4.0	1.3	2.8	13.1
M3	Original	6.3	5.2	4.7	20.5
M4	Original	6.8	3.1	5.5	23.8
M5	Original	5.3	5.1	3.2	11.8
	Alternative	5.3	5.1	3.2	11.8
M6	Original	9.9	9.8	5.7	22.0
	Alternative	9.9	9.8	5.7	22.0

2.3.2 Fuels

Commercially available distillate fuels (e.g., diesel, gasoline, kerosene, jet fuels) are composed of hundreds of hydrocarbons. Composition depends on the source of the crude oil, distillation

conditions, target fuel quality specifications [138, 139], and additional processing and blending with additives. Table 2.8 lists the limited number of experimental studies reporting the density of diesel and jet fuels up to HTHP conditions. Outcalt and colleagues [140, 141] measured the density of jet fuels JP-8 3773 (referred to as JP-8) and Jet A 4658 (referred to as Jet A) at high temperatures between 270 and 470 K and pressures up to 400 bar. Safarov et al. [142] reported density measurements of the Hallen DK B0 diesel fuel from 2015 (referred to as B02015) and 2016 (referred to as B02016) over a wide range of temperatures between 263 and 468 K and pressures up to 2,000 bar. Aquing et al. [25] measured the density of the Middle East SR and Highly Naphthenic diesel fuels at temperatures between 323 and 423 K and pressures up to 3,500 bar.

Table 2.8. Summary of available density data for diesel and jet fuels measured up to high temperatures and pressures.

Author	Year	Fuel	T_{range}/K	P_{max}/bar	Density uncertainty (%)	No. of samples with measured composition
Peters et al. [143]	1990	Diesel	299-450	1,000	-	0
Payri et al. [144]	2011	Diesel	298-343	1,800	0.60	0
Aquing et al. [25]	2012	Diesel	323-423	3,500	0.05	2
Bazile et al. [145]	2012	Diesel	283-423	2,000	0.01	0
Schaschke et al. [26]	2013	Diesel	298-373	5,000	0.20	0
Desantes et al. [146]	2015	Diesel	303-353	2,000	0.01	0
Ivaniš et al. [147]	2016	Diesel	293-413	600	0.01	0
Safarov et al. [142]	2018	Diesel	263-468	2,000	0.04	2 [148]
Outcalt et al. [140]	2009	Jet	278-343	320	0.01	1[a]
Outcalt et al. [141]	2010	Jet	278-343	400	0.01	1[b]
Abdulagatov and Azizov [149]	2010	Jet	301-745	600	0.10	0

[a]Number averaged MW and HN/CN from ref. [150].
[b]Number averaged MW and HN/CN from ref. [151].

Aquing et al. [25] used gas chromatography to characterize the composition of the chemical families in the two diesel fuels shown in Table 2.9. One of the fuels is a conventional diesel fuel distilled from Middle Eastern crude oil (Middle East Straight Run (SR)) and the other is a fuel treated after distillation to hydrogenate aromatic compounds (Highly Naphthenic). Saturated compounds (i.e., normal alkanes, branched alkanes, cyclohexanes, and decalins) comprise 70 mol% of diesel fuel Middle East SR and 65 mol% of diesel fuel Highly Naphthenic. There is a significant difference in concentrations of naphthenes (i.e., cyclohexanes and decalins) and alkanes between the two diesel fuels. Diesel fuel Middle East SR contains 20 mol% naphthenes and about 50 mol% normal and branched alkanes compared to 46 mol% naphthenes and 20 mol% normal and branched alkanes in diesel fuel Highly Naphthenic. Figure 2.7 shows the molecular weight distribution of the 140 different compounds identified in these diesel fuels. The molecular weights of compounds in diesel fuel Middle East SR range from 100 to 370 g/mol with the majority of compounds having molecular weights between 150 to 300 g/mol. The molecular weight distribution of diesel fuel Highly Naphthenic is wider from 100 to 480 g/mol. However, the majority of compounds have lower molecular weights between 100 to 260 g/mol, as compared to diesel fuel Middle East SR. Although not shown here, compositional variability is also observed between the different jet fuels reported in the literature [25, 152, 153]. The composition of the Hallen DK B0 diesel fuel was not reported [142], but the average MW and HN/CN ratio were obtained from private communication [148]. Table 2.10 presents the mixture properties for the four diesel fuels and two jet fuels in this study, the Z parameter, and the PC-SAFT parameters of the pseudo-components for both combinations of approaches.

Table 2.9. Molar composition (%) and carbon number ranges of chemical families found in diesel fuels Middle East SR and Highly Naphthenic obtained from gas chromatography. Data from ref. [25].

	Mole Percent (%)		Carbon Number Range	
Chemical Class	Middle East SR	Highly Naphthenic	Middle East SR	Highly Naphthenic
Normal Alkanes	23	6	7-27	7-29
Branched Alkanes	26	13	7-27	7-29
Cyclohexanes	16	26	8-26	8-28
Decalins	4	20	10-25	10-26
Benzenes	10	10	8-24	8-20
Naphthalenes	7	3	10-21	10-15
Phenanthrenes	3	1	14-20	14-35
Tetralins + Indanes	7	16	9-23	9-22
Other Unsaturates	4	5	12-21	13-35

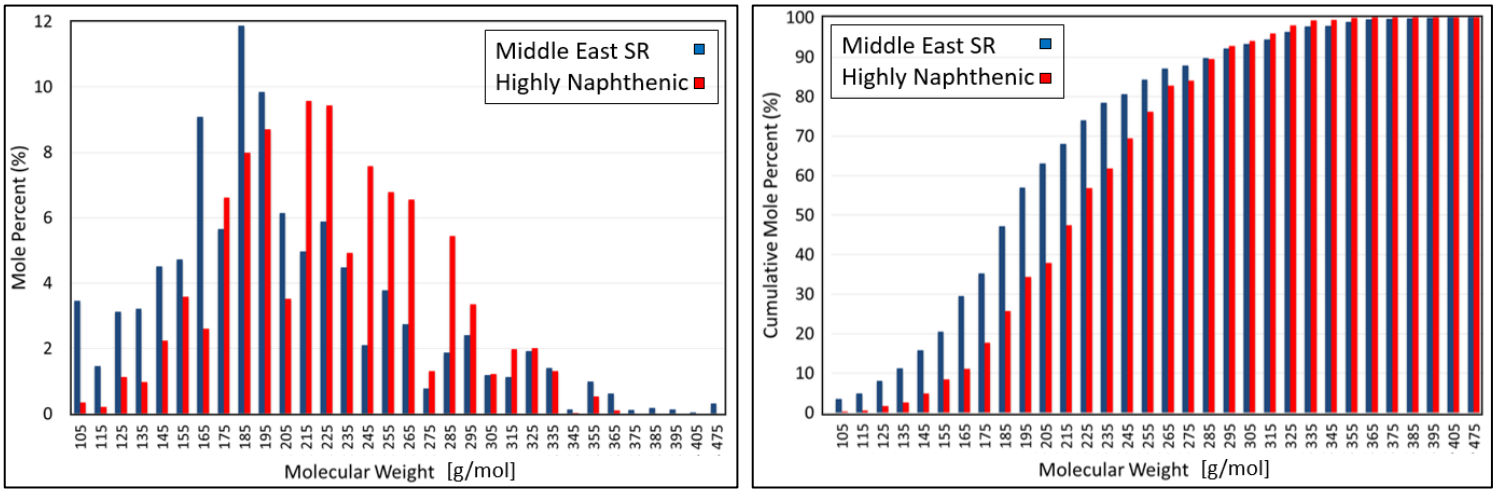

Figure 2.7. Molecular weight distribution (left) and cumulative mole percent (right) of the compounds in diesel fuels Middle East SR and Highly Naphthenic from gas chromatography. Data from ref. [25].

Table 2.10. Mixture properties and PC-SAFT parameters for the pseudo-components of diesel and jet fuels predicted in this study. When the number averaged MW of the mixture is less than the MW of phenanthrene, Eq. 2.17 reduces to Eq. 2.12, and the original and alternative Z parameters are the same.

Sample	MW	HN/CN	Z		m	σ (Å)	ε/k (K)
Middle East SR	225.1[a]	1.85[a]	Original	0.1731	9.7335	3.4085	258.44
			Alternative	0.2217	9.6111	3.4053	263.11
Highly Naphthenic	203.6[a]	1.74[a]	Original	0.2537	8.7269	3.3959	263.24
			Alternative	0.2923	8.6422	3.3928	266.77
B0 2015	215.0	1.92	Original	0.1294	9.4471	3.4087	253.17
			Alternative	0.1579	9.3796	3.4067	255.85
B0 2016	215.0	1.92	Original	0.1294	9.4471	3.4087	253.17
			Alternative	0.1579	9.3796	3.4067	255.85
JP-8 3773	160.0[b]	1.95[b]	Original	0.1444	7.2656	3.3872	246.33
			Alternative	0.1444	7.2656	3.3872	246.33
Jet A4658	157.5[c]	1.96[c]	Original	0.1399	7.1747	3.3864	245.47
			Alternative	0.1399	7.1747	3.3864	245.47

[a]From the gas chromatography results from ref. [25].

[b]From ref. [151].

[c]From ref. [150].

Figure 2.8 shows the predictions and experimental density data for the four diesel fuels and the two jet fuels at the lowest and highest temperatures and a range of pressures. The predictions are in quantitative agreement with experimental data across all temperatures and pressures for all six fuels. Table 2.11 summarizes the statistical measures for the four diesel and two jet fuels, for all temperatures and pressures, using the original and alternative equations for calculating Z needed to calculate the PC-SAFT parameters. The use of the alternative equation for Z improves the accuracy of the density predictions for all of the diesel fuels. However, improvement is not observed

for the jet fuel density predictions since the MW of these fuels is less than the MW of phenanthrene, and the alternative Z equation (Eq. 2.17) reduces to the original equation (Eq. 2.12).

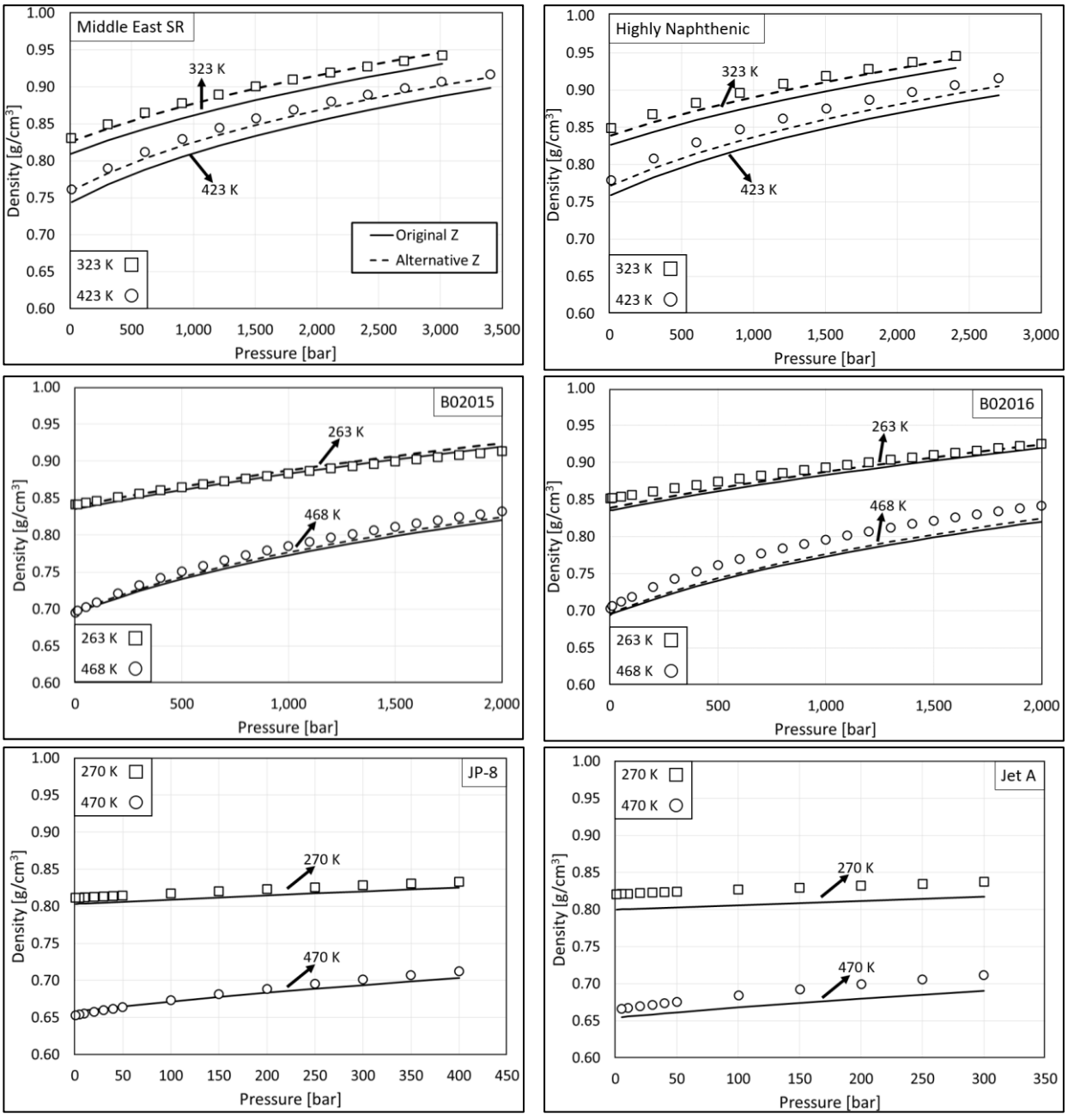

Figure 2.8. Density predictions (lines) compared to experimental data [25, 140-142] (symbols) for diesel and jet fuels.

Table 2.11. The MAPD (%), bias (%), SD (%), and Max Deviation (%) for density predictions of diesel and jet fuels.

Sample	Z	MAPD	Bias	SD	Max Deviation
Middle East SR	Original	2.3	-2.3	0.4	3.0
	Alternative	0.6	-0.6	0.3	1.1
Highly Naphthenic	Original	2.6	-2.6	0.4	3.2
	Alternative	1.2	-1.2	0.4	1.8
B02015	Original	1.0	-1.0	0.4	1.6
	Alternative	0.4	0.0	0.3	1.7
B02016	Original	2.2	-2.2	0.5	2.9
	Alternative	1.2	-1.2	0.5	1.9
JP-8	Original	1.1	-1.1	0.3	1.4
	Alternative	1.1	-1.1	0.3	1.4
Jet A	Original	2.6	-2.6	0.3	3.0
	Alternative	2.6	-2.6	0.3	3.0

The same approach used for the hydrocarbon mixtures is applied to predict the derivative properties of the fuels. The A constant and the coefficients in Eq. 2.26 and 2.27 for the Tait equation fit to diesel and jet fuel density data are included in the appendix (Section 2.5). Figure 2.8 shows the predicted isothermal compressibilities (κ_T) for the fuels compared to Tait calculations from the experimental density data. Predictions are in quantitative agreement with experimental data. However, the model overpredicts at the lowest temperatures and underpredicts at the highest temperatures. Although the predictions in Figure 2.9 for fuels JP-8 and Jet A appear to exhibit a greater deviation compared to predictions for the diesel fuels, note that x-axes are scaled differently in the figures. The MAPDs reported for the κ_T predictions in Table 2.12 show similar values for the diesel and jet fuels. The alternative equation for calculating Z does not significantly improve the κ_T predictions for the fuels studied in this work.

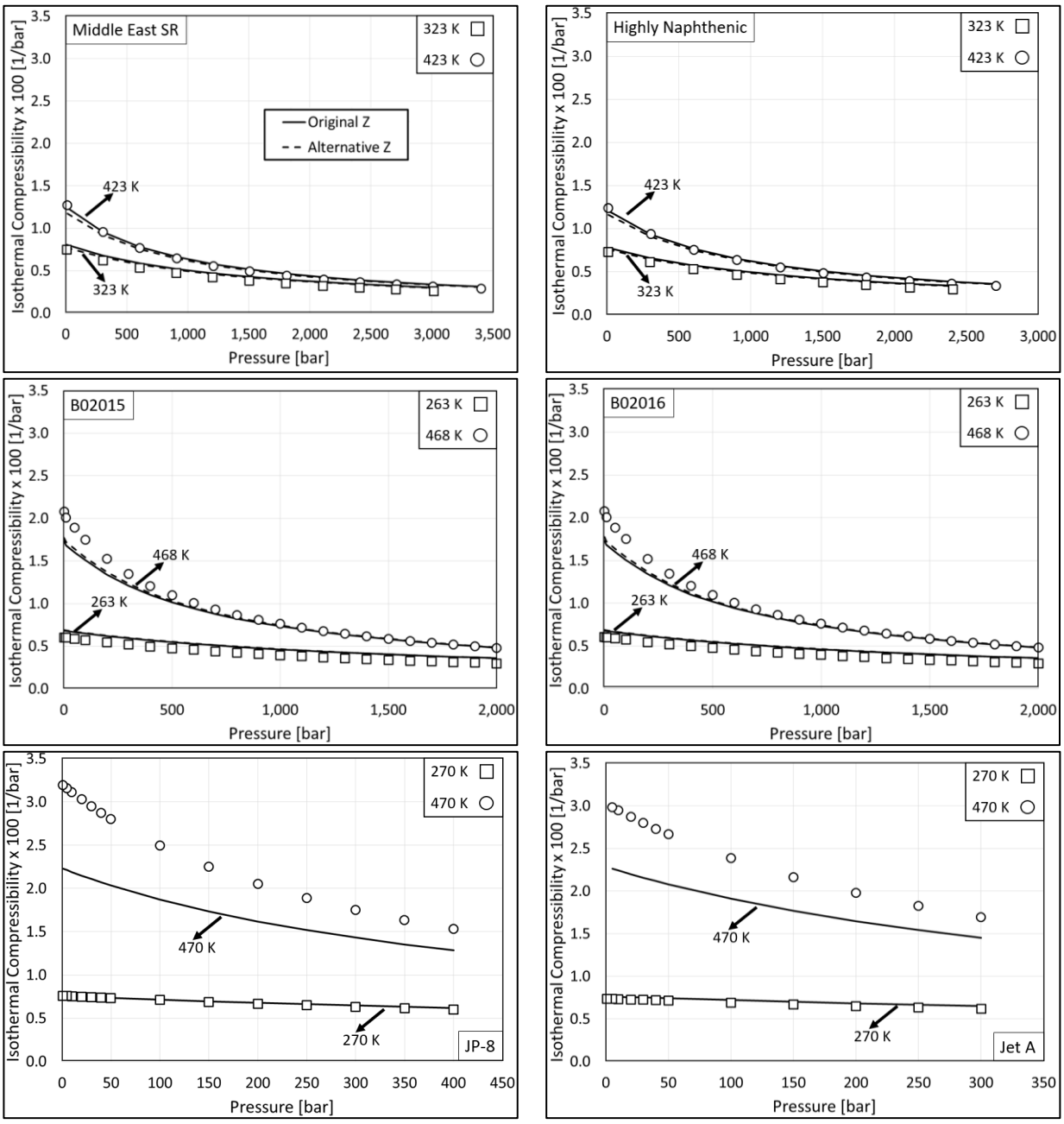

Figure 2.9. Isothermal compressibility predictions (lines) compared to experimental data [25, 140-142] (symbols) for diesel and jet fuels.

Table 2.12. The MAPD (%), bias (%), SD (%), and Max Deviation (%) for isothermal compressibility predictions of diesel and jet fuels.

Sample	Z	MAPD	Bias	SD	Max Deviation
Middle East SR	Original	8.0	7.8	4.3	16.3
	Alternative	6.4	5.3	3.9	14.8
Highly Naphthenic	Original	7.1	6.9	3.8	14.4
	Alternative	5.7	4.8	3.5	13.0
B02015	Original	14.8	14.8	3.8	21.3
	Alternative	13.1	13.1	4.2	20.2
B02016	Original	14.5	14.5	3.9	21.0
	Alternative	12.8	12.8	4.3	20.0
JP-8	Original	13.8	-13.6	8.7	30.3
	Alternative	13.8	-13.6	8.7	30.3
Jet A	Original	11.1	-10.1	7.3	24.2
	Alternative	11.1	-10.1	7.3	24.2

Figure 2.10 shows predicted volumetric thermal expansion coefficients (α_p) compared to Tait calculations from the experimental density data. The predictions for all of the fuels qualitatively capture the observed monotonic decrease in α_p with respect to pressure. All of the predictions for all fuels show better agreement at higher temperatures compared to lower temperatures.

The Tait calculations for the Highly Naphthenic diesel fuel exhibit a temperature crossover between 300 and 600 bar. However, this crossover is not observed with the Middle East SR diesel fuel. In contrast, a predicted temperature crossover is observed for both of these diesel fuels, but at a pressure less than 50 bar. Predicted α_p values exhibit more sensitivity to temperature than experimental values obtained with Tait calculations. Similar trends are observed with predicted α_p values for the B02015 and B02016 diesel fuels, although now the predicted temperature crossover

occurs at pressures less than 10 bar. In contrast the predicted α_p for Jet fuels JP-8 and Jet A show a temperature crossover temperature at approximately 200 bar. However, Tait calculations for α_p, for these four fuels, do not exhibit a temperature crossover.

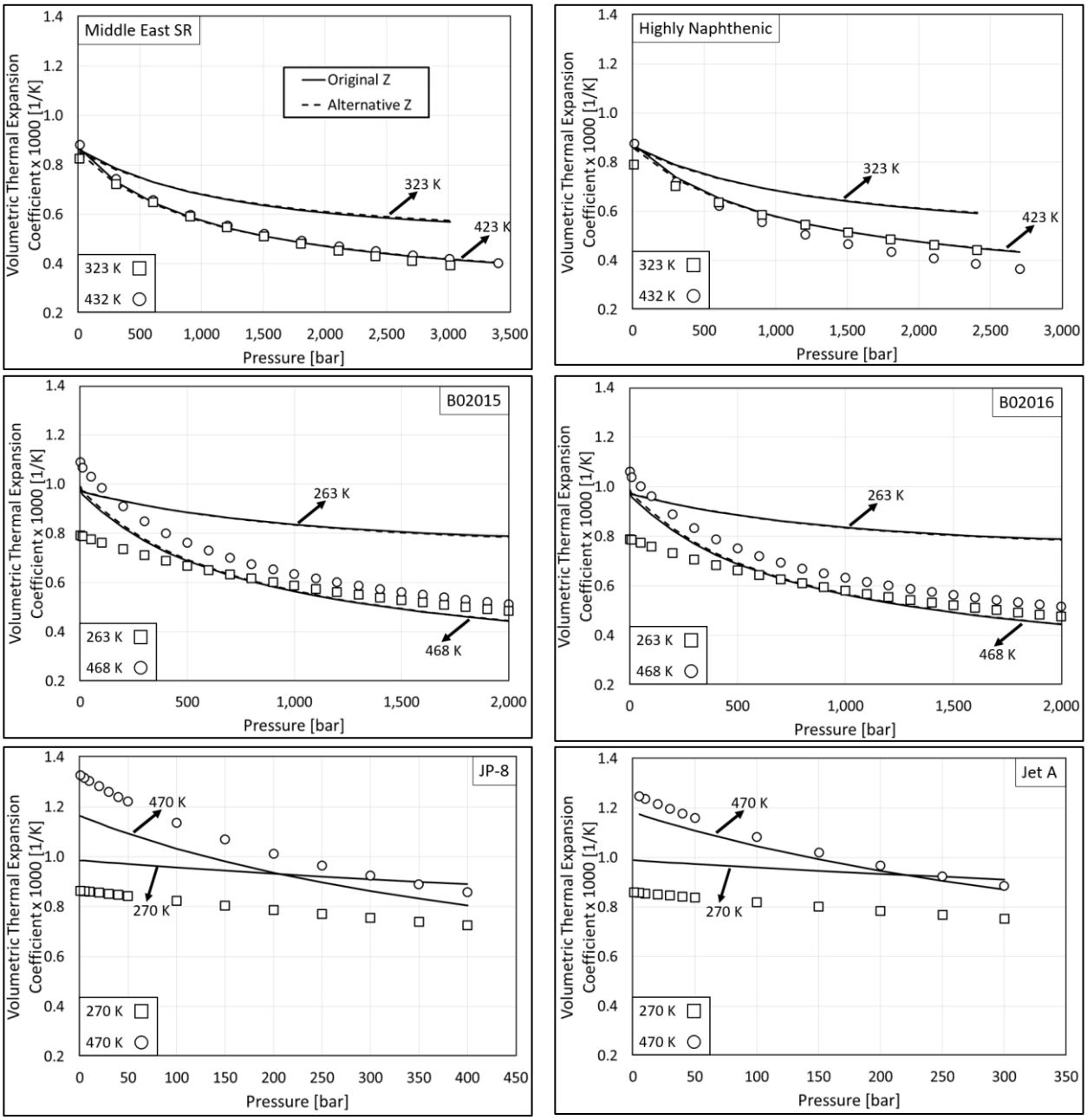

Figure 2.10. Volumetric thermal expansion coefficient predictions (lines) compared to experimental data [25, 140-142] (symbols) for diesel and jet fuels.

Table 2.13 summarizes the statistical measures for predictions of the volumetric thermal expansion coefficient for the four diesel fuels and two jet fuels using the original and alternative approaches for calculating Z for the calculation of the PC-SAFT parameters. For the volumetric thermal expansion coefficient calculations, the alternative approach for calculating Z does not significantly improve the predictions for the fuels studied in this work.

Table 2.13. The MAPD (%), bias (%), SD (%), and Max Deviation (%) for the volumetric thermal expansion coefficient predictions of diesel and jet fuels.

Sample	Z	MAPD	Bias	SD	Max Deviation
Middle East SR	Original	13.3	12.3	13.2	44.9
	Alternative	13.7	12.4	13.6	46.2
Highly Naphthenic	Original	14.6	14.6	8.6	33.8
	Alternative	14.6	14.5	9.0	34.5
B02015	Original	14.2	11.7	15.5	62.6
	Alternative	14.3	11.5	15.7	63.5
B02016	Original	17.4	14.0	14.6	65.5
	Alternative	17.5	13.8	14.7	66.4
JP-8	Original	7.9	-2.3	4.8	22.6
	Alternative	7.9	-2.3	4.8	22.6
Jet A	Original	5.8	0.3	4.6	21.1
	Alternative	5.8	0.3	4.6	21.1

A discussion is found in the appendix (Section 2.5) on the potential sources of error in the derivative property predictions. Lafitte et al. [154] suggest that the inaccuracy in derivative property calculations is a result of the intermolecular potential used in the PC-SAFT EoS. Predictions can be improved if a Mie potential is used instead of the square-well potential used in PC-SAFT. The

Mie potential is used in more recent SAFT variants (i.e., SAFT for variable range interactions with Mie potentials (SAFT-VR Mie [114]) and SAFT-γ-Mie [56]). However, these SAFT variants are not currently as widely used in industry as is PC-SAFT. Predictions could also be improved by simultaneously regressing the PC-SAFT parameters (or the GC parameters) to both density and derivative properties, similar to the approach of de Villiers et al. [46]. Much broader data sets are needed such as saturated liquid density, isochoric heat capacity, vapor pressure, enthalpy of vaporization, and speed of sound as used by de Villiers et al. [46].

2.4 Conclusion

A purely predictive, pseudo-component technique using the Perturbed-Chain Statistical Associating Fluid Theory (PC-SAFT) equation of state was developed to predict the density, isothermal compressibility, and volumetric thermal expansion coefficient of complex hydrocarbon mixtures, such as diesel and jet fuels. This approach negates the need for fitting binary interaction parameters to experimental mixture data. The method in this study is predictive up to high temperatures and pressures, without the need to fit parameters to experimental data. The approach described here only requires the input of two experimentally measured mixture properties: the number averaged molecular weight and the hydrogen to carbon ratio. We speculate that further improvements in the accuracy of this pseudo-component technique, especially for derivative property estimations, can be realized if a different variant of the SAFT equation of state is used instead, such as SAFT-VR Mie [114] or SAFT-γ-Mie [56]. However, these SAFT variants are not as widely applied in industrial practice, and to be used with the pseudo-component technique, it would be necessary to develop a set of correlations specific to these equations of state. The purely predictive, pseudo-component technique described here provides a straightforward, yet powerful,

tool to aid the development of improved fuel injection equipment design and control. This tool will also aid the development and optimization of fuel and fluid formulations for improved performance at extreme operating conditions.

2.5 Appendix for Chapter 2

2.5.1 DoU correlation for PNAs

Figure 2.11 shows the degree of unsaturation (DoU) for poly-nuclear aromatics (PNAs). The DoU of PNAs is correlated to molecular weight (MW) as shown in Eq. 2.28.

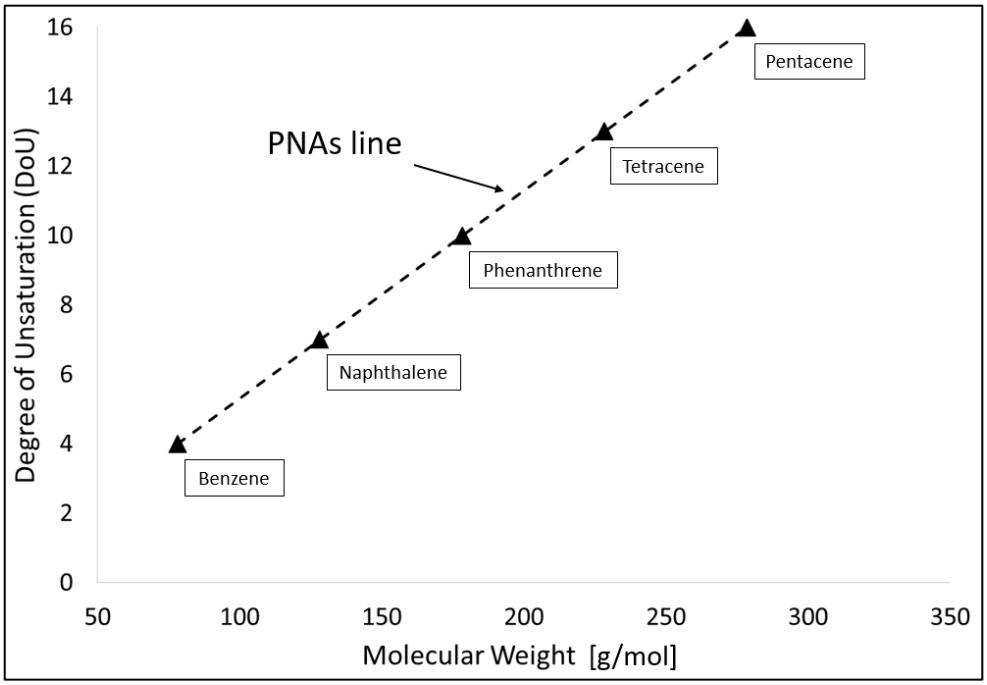

Figure 2.11. The calculated DoU of PNAs. The DoU of tetracene and pentacene are calculated and shown in the figure to provide a more accurate PNAs line, although no tetracene and pentacene are in the diesel and jet fuels.

$$\mathrm{DoU_{PNAs}} = 0.05993 \times \mathrm{MW} - 0.68158 \quad (2.28)$$

2.5.2 Tait coefficients needed for well-characterized hydrocarbon mixtures

Table 2.14. Coefficients for the Tait equation fits to well-characterized hydrocarbon mixture density data [88, 133, 155] .

	M1 (0.750 mole fraction nC7)	M2	M3	M4	M5	M6
A	0.2299	0.2298	0.2301	0.2301	0.2303	0.2301
$10^{-3} \times e_0$ / kg m^{-3}	0.6977	0.9235	0.9495	0.9401	1.034	1.030
$10^{1} \times e_1$ / kg m^{-3} K^{-1}	7.516	-5.283	-4.969	-4.902	-8.797	-7.422
$10^{5} \times e_2$ / kg m^{-3} K^{-2}	-251.700	-31.450	-34.080	-35.860	25.990	5.810
$10^{-2} \times b_0$ / kg m^{-3}	-1.712	3.927	4.168	3.810	3.974	4.454
$10^{0} \times b_1$ / kg m^{-3} K^{-1}	1.963	-1.291	-1.327	-1.188	-1.225	-1.463
$10^{3} \times b_2$ / kg m^{-3} K^{-2}	-3.784	1.104	1.093	0.9429	0.9985	1.3001

Table 2.15. Coefficients for the Tait equation fits to diesel and jet fuel density data [25, 140-142].

	Middle East SR	Highly Naphthenic	B02015	B02016	JP-8	Jet A
A	0.2299	0.2300	0.2300	0.2301	0.2303	0.2300
$10^{-3} \times e_0$ / kg m^{-3}	1.059	1.060	1.002	1.015	0.9701	0.980
$10^{1} \times e_1$ / kg m^{-3} K^{-1}	-7.200	-6.247	-5.494	-5.736	-4.765	-5.261
$10^{5} \times e_2$ / kg m^{-3} K^{-2}	4.811	-7.794	-22.290	-10.870	-41.620	-33.060
$10^{-2} \times b_0$ / kg m^{-3}	5.558	4.667	4.878	4.956	4.347	4.455
$10^{0} \times b_1$ / kg m^{-3} K^{-1}	-1.879	-1.375	-1.590	-1.639	-1.477	-1.514
$10^{3} \times b_2$ / kg m^{-3} K^{-2}	1.766	1.0876	1.389	1.460	1.317	1.353

2.5.3 Pseudo-component parameters and deviation plots for well-characterized hydrocarbon mixtures

Table 2.16. Mixture properties, PC-SAFT parameters for the pseudo-components, and MAPDs (%) for density predictions of well-characterized hydrocarbon mixtures.

Sample	MW	HN/CN	Z		m	σ (Å)	ε/k (K)	MAPD
M1 (1.000 mole fraction nC7)	100.2	2.29	Original	0	5.0237	3.3667	221.08	0.2
M1 (0.875 mole fraction nC7)	99.9	2.25	Original	0.0236	4.9985	3.3630	222.16	0.4
M1 (0.750 mole fraction nC7)	99.7	2.21	Original	0.0472	4.9734	3.3592	223.24	1.1
M1 (0.625 mole fraction nC7)	99.4	2.18	Original	0.0711	4.9484	3.3553	224.31	1.8
M1 (0.500 mole fraction nC7)	99.2	2.14	Original	0.0950	4.9235	3.3514	225.39	2.5
M2	157.6	2.20	Original	0	7.3872	3.4000	234.47	0.3
M3	159.7	2.11	Original	0.0439	7.4069	3.3967	238.27	2.2
M4	158.7	2..03	Original	0.0971	7.2882	3.3912	242.33	0.6
M5	181.6	1.94	Original	0.1363	8.1219	3.3972	249.42	0.2
			Alternative	0.1390	8.1169	3.3969	249.65	0.1
M6	183.6	1.84	Original	0.2027	8.0768	3.3923	255.49	0.2
			Alternative	0.2092	8.0644	3.3917	256.06	0.3

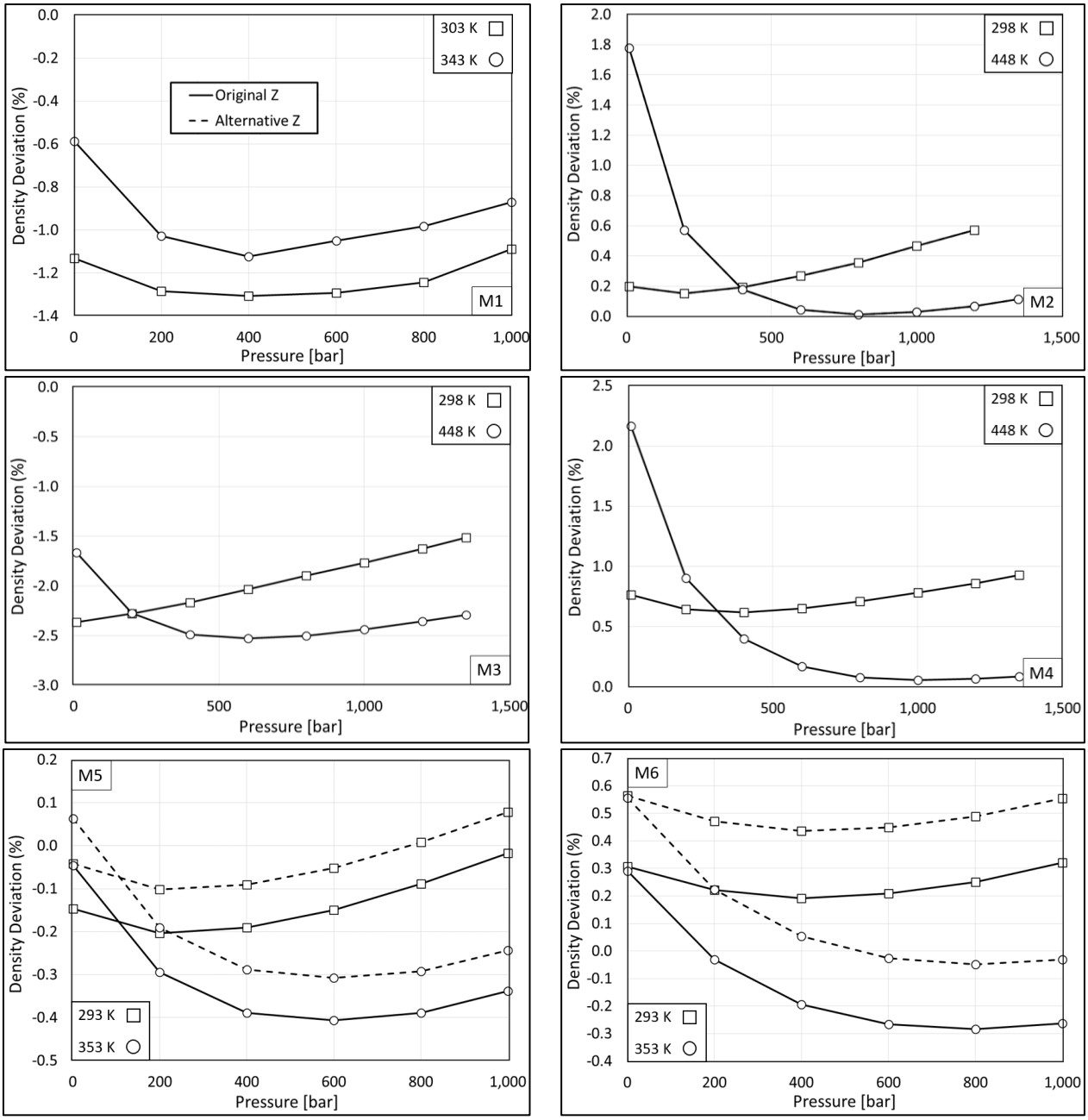

Figure 2.12. Predicted density deviations compared to experimental data [88, 133, 155] for well-characterized hydrocarbon mixtures. Lines are a guide for the eye.

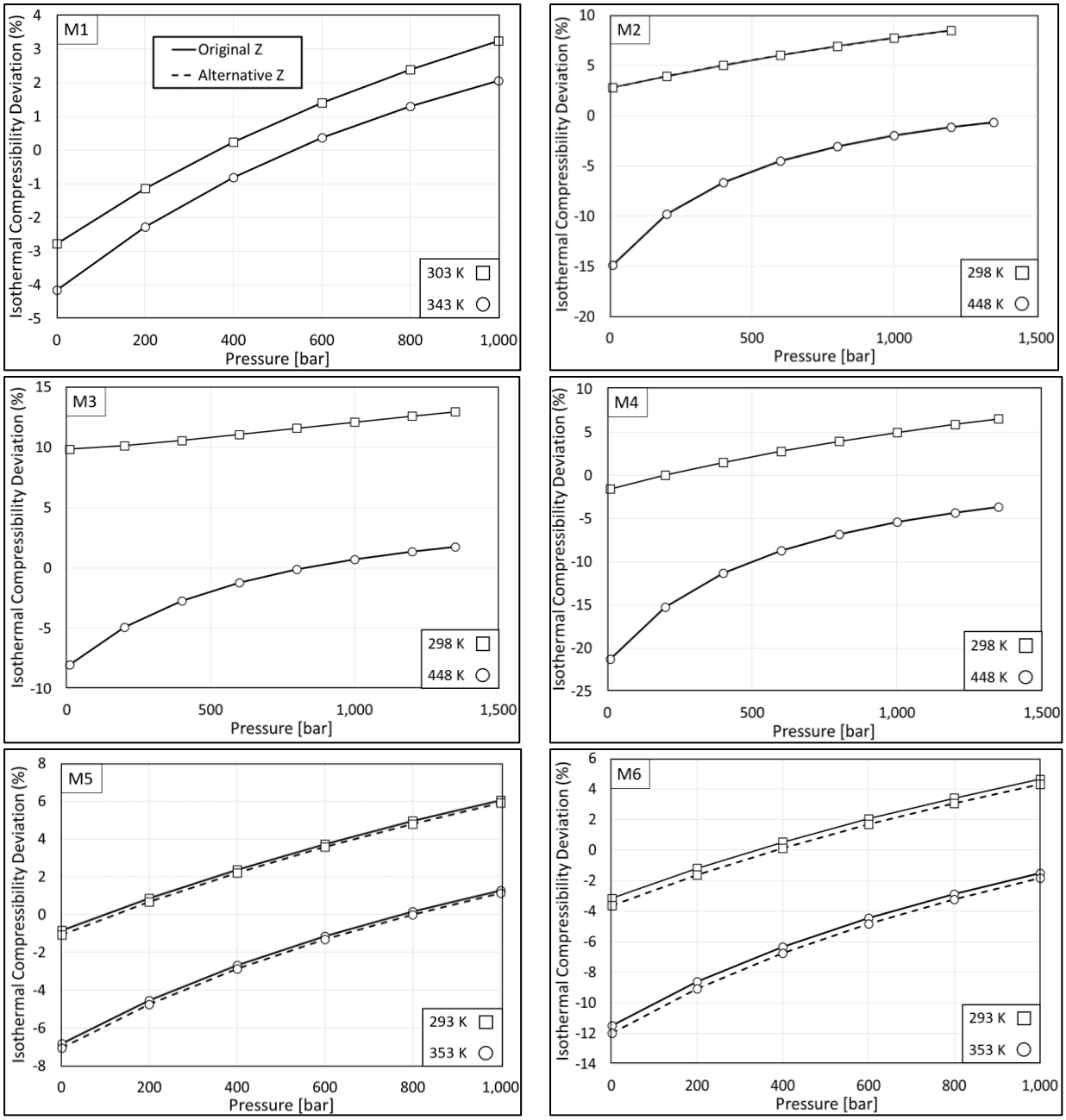

Figure 2.13. Predicted isothermal compressibility deviations compared to experimental data [88, 133, 155] for well-characterized hydrocarbon mixtures. Lines are a guide for the eye.

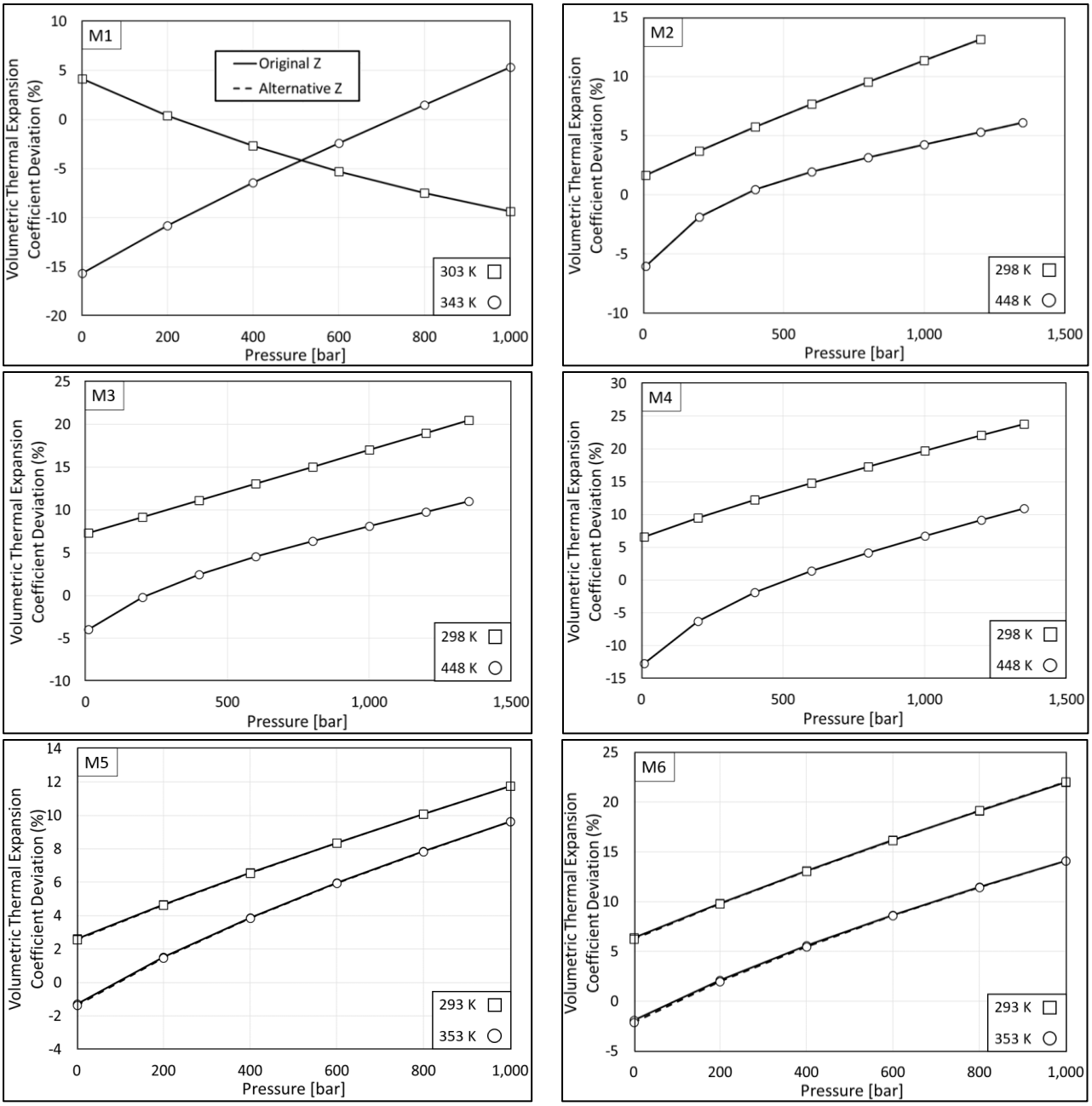

Figure 2.14. Predicted volumetric thermal expansion coefficient deviations compared to experimental data [88, 133, 155] for well-characterized hydrocarbon mixtures. Lines are a guide for the eye.

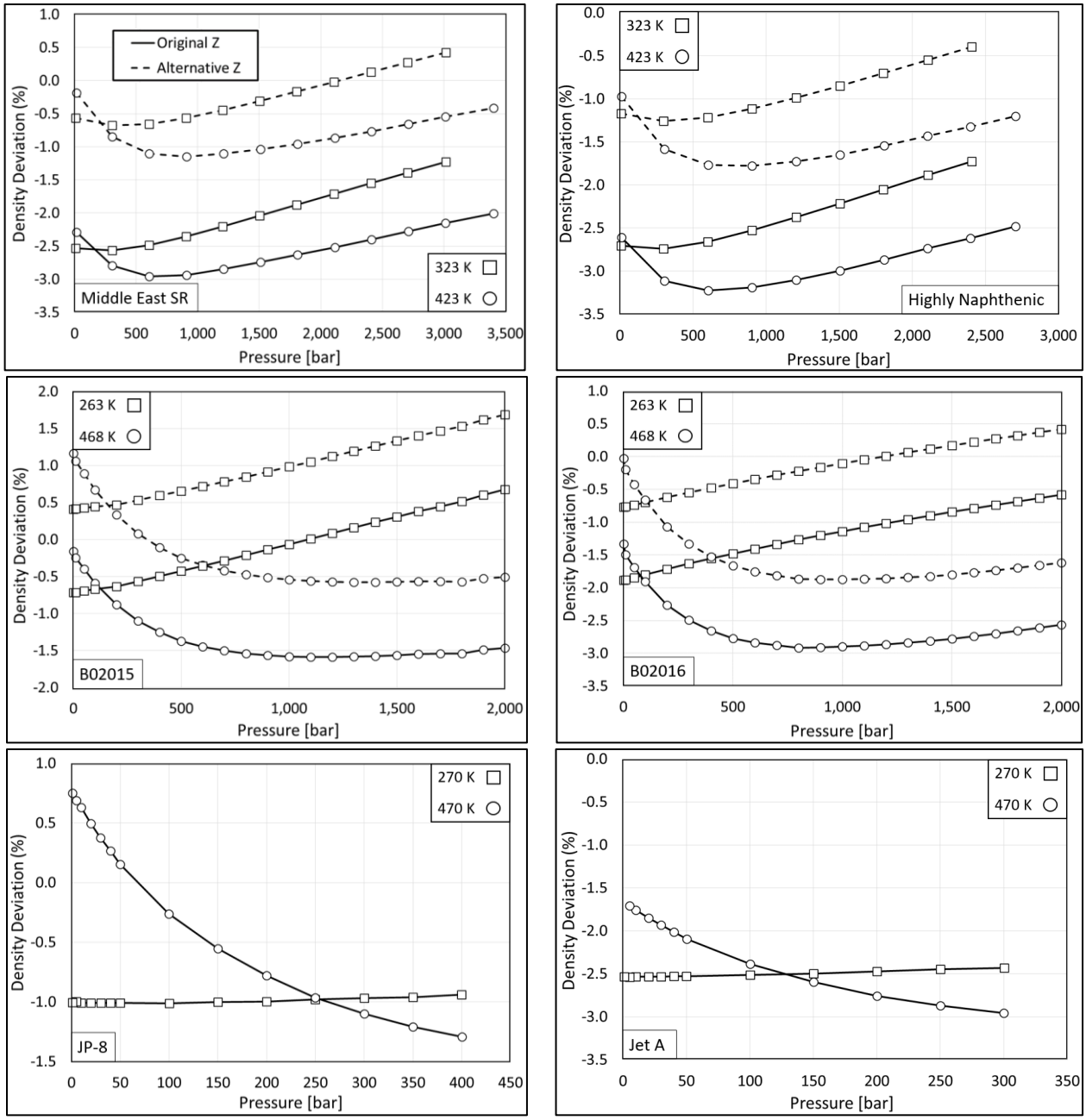

Figure 2.15. Predicted density deviations compared to experimental data [25, 140-142] for diesel and jet fuels. Lines are a guide for the eye.

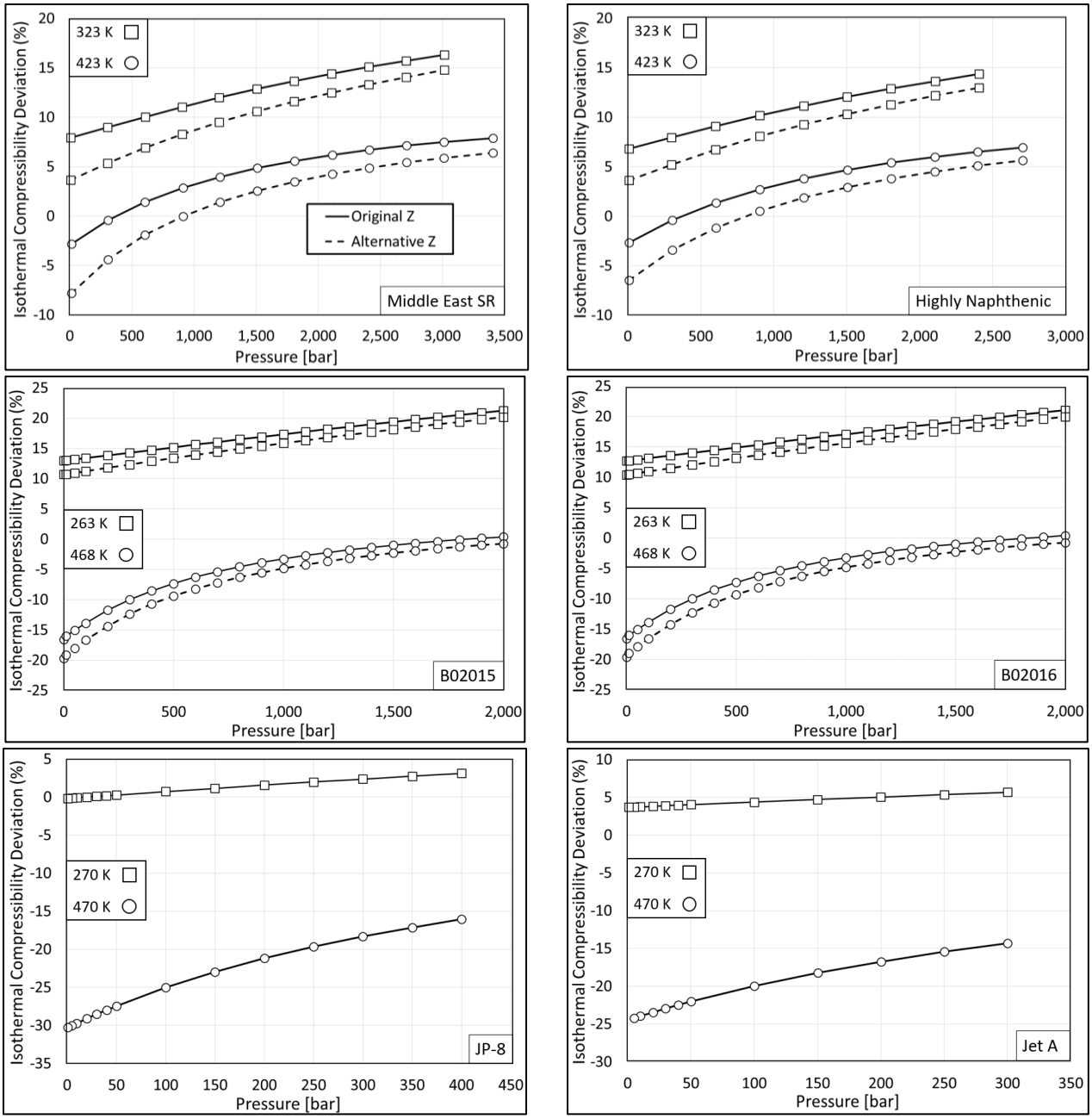

Figure 2.16. Predicted isothermal compressibility deviations compared to experimental data [25, 140-142] for diesel and jet fuels. Lines are a guide for the eye.

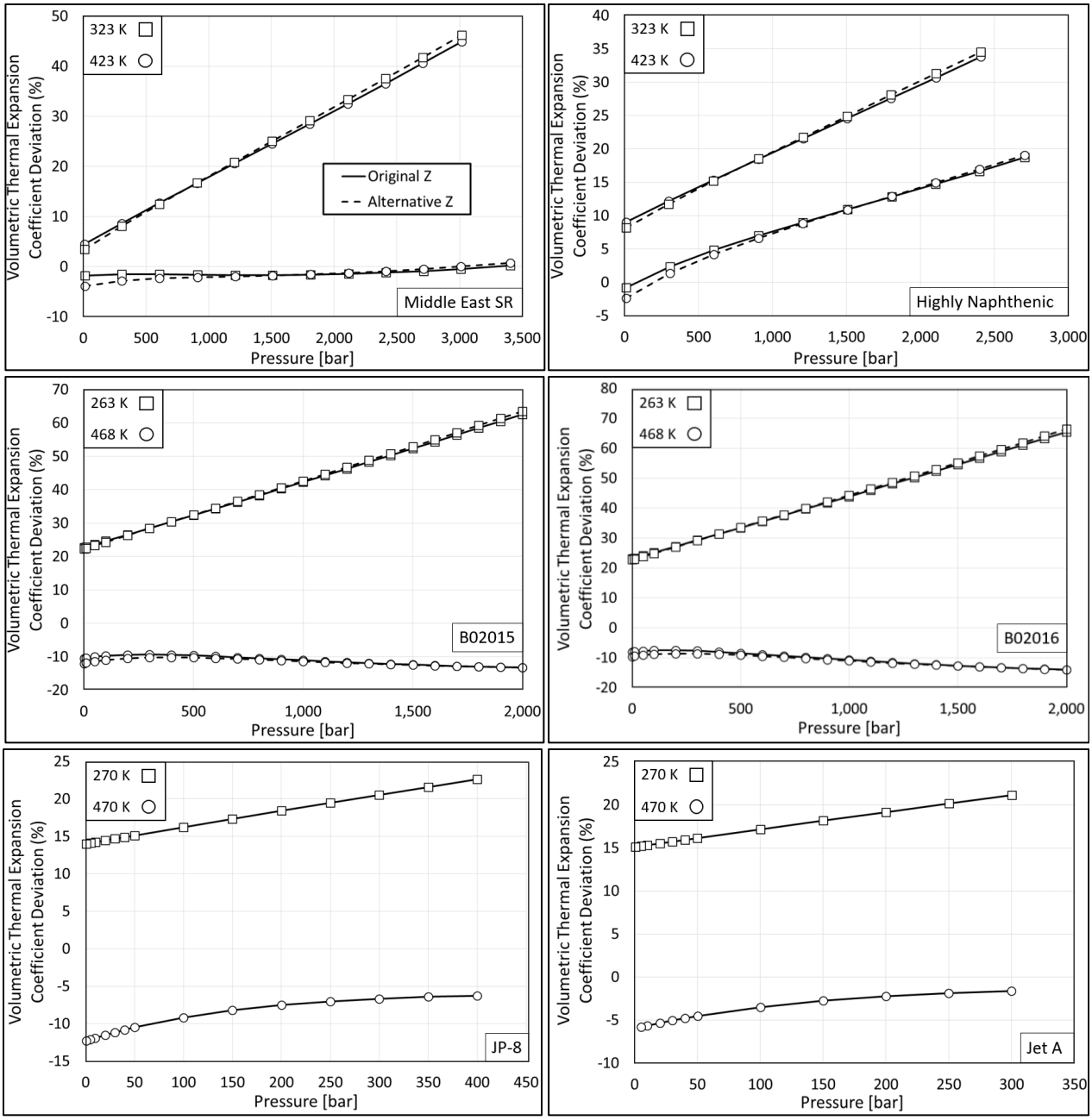

Figure 2.17. Predicted volumetric thermal expansion coefficient deviations compared to experimental data [25, 140-142] for diesel and jet fuels. Lines are a guide for the eye.

2.5.4 Potential source of inaccuracy for the derivative properties

There could be several potential sources of error that contribute to the relatively less accurate α_p predictions compared to the density and κ_T predictions: the pseudo-component

approach, the Tait equation, the PC-SAFT EoS, and limited experimental data for fitting to the Tait equation. It is important to assess and identify the dominant source(s) of error to help recommend improvements for future technique development. A potential source of inaccuracy of κ_T and α_p could be the pseudo-component approach itself. To test this conjecture, α_p was predicted using the pseudo-component parameters using the technique developed in the present study and using the mixing rules for the actual mixture in the PC-SAFT EoS. Figure 2.18 shows the predicted α_p from the PC-SAFT EoS with original mixing rules, from the pseudo-component method using the alternative Z equation, and from Tait calculations from the experimental density data for mixtures M5 and M6. Table 2.17 lists the MAPD, Bias, SD, and Max Deviation of α_p for mixtures M5 and M6 calculated using the pseudo-component and the PC-SAFT EoS with mixing rules. Results for both mixtures M5 and M6 are essentially the same suggesting that the relative inaccuracy of the α_p predictions is not due to the pseudo-component method.

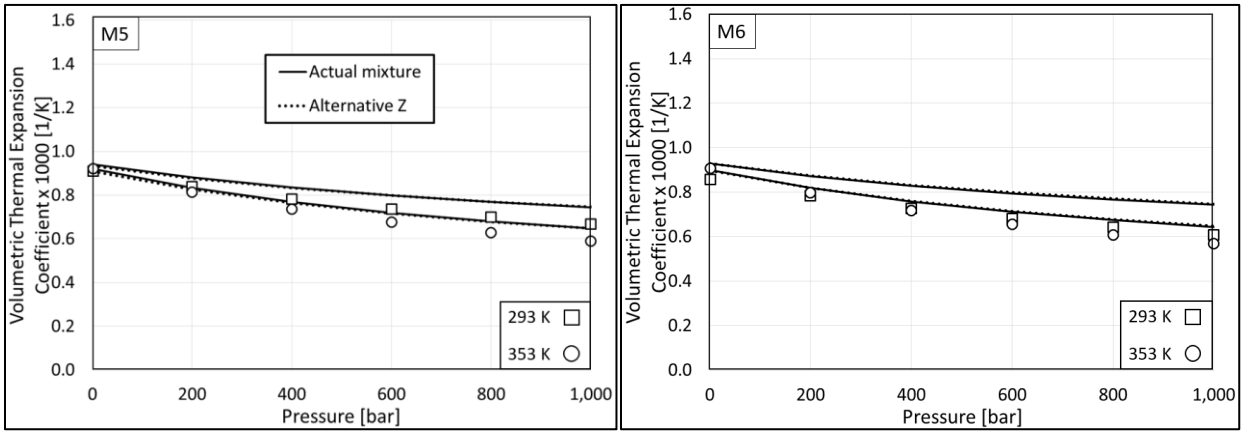

Figure 2.18. Volumetric thermal expansion coefficient predictions compared to experimental data [133] for the M5 and M6 mixtures.

Table 2.17. The MAPD (%), bias (%), SD (%), and Max Deviations (%) for volumetric thermal expansion coefficient predictions of the M5 and M6 mixtures.

Mixture	Predictions using the Pseudo-component				Prediction using the Actual Mixture			
	MAPD	Bias	SD	Max Deviation	MAPD	Bias	SD	Max Deviation
M5	5.3	5.1	3.2	11.8	5.6	5.6	3.2	11.7
M6	9.9	9.7	5.7	22.0	10.0	10.0	5.4	21.4

Another potential source of inaccuracy of α_p could reside in the use of the Tait equation. The experimental derivative properties, including α_p are obtained from the Tait equation fit to experimental density data. Though the Tait equation fit to the experimental density data displayed excellent accuracy for mixtures M5 and M6 with MAPDs of less than 0.06%, biases of smaller than -0.01%, SDs of less than 0.04%, and Max Deviations of less than 0.14%, alternative mathematical and polynomial fitting schemes were evaluated to assess the impact of the Tait equation on accuracy of the derivative properties. None of these alternative schemes significantly improved the accuracy obtained from the Tait equation, and they do not have a noticeable effect on the calculated experimental derivative properties, including α_p. This suggests that the Tait equation is not the dominant contributor to the relative inaccuracy of the α_p predictions.

The next potential source of inaccuracy for α_p could be due to limited experimental data, which affects the quality of the fits to the Tait equation. To assess whether there was insufficient data to ensure a good fit, the Tait equation was fit using a complete dataset and a subset of the complete dataset. The α_p predictions were then compared with predictions using both the pseudo-component technique as well as the PC-SAFT EoS with mixing rules. Boned et al. [133] reported the density data of mixtures M5 and M6 at 293, 303, 313, 323, 333, 343, and 353 K for a range of pressures up to 1,000 bar. In this test, one data set is used that includes the data for all seven

isotherms and a second one is used that includes the data at only 293, 323, and 353 K. The selected sets are fit to the Tait equation with MAPDs of less than 0.03%, biases of smaller than -0.02%, SDs of less than 0.03%, and Max Deviations of less than 0.14%. Table 2.18 summarizes the predictions for α_p using seven and three isotherms in the Tait equation for mixtures M5 and M6. Table 2.18 shows that α_p using the pseudo-component and the actual mixture are comparable. Therefore using limited experimental density data is sufficient for fitting the density of mixtures M5 and M6 and for the Tait calculations of α_p.

Table 2.18. The MAPD (%), bias (%), SD (%), and Max Deviation (%) for volumetric thermal expansion coefficient predictions of mixtures M5 and M6 [133] using 3 and 7 isotherms in the Tait equation.

Mixture		Predictions using the Pseudo-component				Prediction using the Actual Mixture			
		MAPD	Bias	SD	Max Deviation	MAPD	Bias	SD	Max Deviation
M5	3 Isotherms	5.1	4.8	3.2	11.6	5.3	5.3	3.1	11.5
	7 Isotherms	5.3	5.1	3.2	11.8	5.6	5.6	3.2	11.7
M6	3 Isotherms	10.0	9.8	5.8	22.8	10.1	10.1	5.5	22.1
	7 Isotherms	9.9	9.7	5.7	22.0	10.0	10.0	5.4	21.4

The investigations described in the preceding paragraphs suggest that the pseudo-component method, the Tait Equation, and a limited set of experimental data are not the dominant contributors to the relative inaccuracy of α_p predictions. Hence, the relative inaccuracy is likely due to a deficiency of the PC-SAFT approach in predicting derivative properties. The prediction of α_p could potentially be enhanced by improving the intermolecular potential, as suggested by Lafitte et al. [154] The predictions could also be improved by simultaneously regressing the PC-SAFT

parameters, or the GC parameters, to the density and the derivative properties, similar to the approach of de Villiers et al. [46] who fit the PC-SAFT parameters by simultaneously regressing different properties (including saturated liquid density, saturated liquid isochoric heat capacity, vapor pressure, enthalpy of vaporization, and saturated liquid speed of sound) for n-hexane.

3. Chapter 3: Entropy Scaling Based Model for Viscosity[3]

Several correlations and theories have been proposed to model the viscosity of pure components and mixtures as a function of temperature and pressure [157]. These include empirical models and correlations and approaches applied using pseudo-components. Empirical models and correlations [158-165] have been used to predict the viscosity of complex mixtures (e.g., crude oils, bitumens, heavy oils, and diesel and biodiesel fuels) and their blends. Example viscosity mixture models applied using pseudo-components include expanded fluid theory (EFT) [82-85], friction theory (FT) [77-81], free volume theory (FVT) [166, 167], the Dymond-Assael (DA) hard sphere model [86-88], and Eyring's absolute rate theory [168, 169].

Motahhari et al. [83, 84] applied EFT to model the viscosity of several crude oils characterized as mixtures of pseudo-components at temperatures to 473 K and pressures to 552 bar. They fit EFT parameters to atmospheric viscosity data for some crude oils and predicted the parameters for others. Ma et al. [85] used EFT to predict the viscosity of two bitumens characterized with a single pseudo-component at temperatures to 463 K and pressures to 100 bar. Schmidt et al. [80] applied FT to model the viscosity of a North Sea crude oil represented as a mixture of pseudo-components to temperatures of 375 K and pressures to approximately 500 bar. They obtained the values for the FT parameters by fitting individual isotherms for pressures to approximately 350 bar. In a different study, Quiñones-Cisneros et al. [78, 79] applied FT to model the viscosity of crude oils represented as mixtures of pseudo-components to pressures up to 400 bar. These authors fit FT parameters to viscosity data above the saturation pressure and made predictions below the

[3]Adapted from Ref. [156] Rokni HB, Moore JD, Gupta A, M^{c}Hugh MA, Gavaises M. Entropy scaling based viscosity predictions for hydrocarbon mixtures and diesel fuels up to extreme conditions. Fuel **2019**;241:1203-13. doi.org/10.1016/j.fuel.2018.12.043

saturation pressure. Abutaqiya et al. [81] applied FT to model the viscosity of ten Middle Eastern crude oils represented as mixtures of pseudo-components. These authors proposed a new fitting approach for FT and reduced the required number of input parameters for each pseudo-component from two to one. The parameter was fit to a single data point at saturation, and viscosities were predicted for temperatures to 400 K and pressures to 600 bar.

Using FVT, Khoshnamvand and Assareh [166] modeled the viscosity of live oils. Their model defined mixtures containing multiple components including a pseudo-component representing C7+ (i.e., compounds with carbon numbers (CNs) greater than 6). They fit FVT parameters to experimental data for 22 live oils as a training set, and they predicted viscosity of six other oils. Ijaz [88] predicted the viscosity of crude oils through single pseudo-components using the DA hard sphere model [86, 87], fitting four parameters in the model to experimental data and predicted the viscosity of crude oils up to 448 K and 1,400 bar. In a different approach, Macias-Salinas et al. [168] represented several crude oils through mixtures of pseudo-components and modeled the mixture viscosity using Eyring's absolute rate theory [169]. They used a tuning factor to scale density and viscosity predictions, which required fitting the model to experimental data.

Entropy scaling is another approach reported for modeling viscosity. First proposed by Rosenfeld [170], entropy scaling effectively reduces the temperature and pressure dependence of viscosity to a mono-variable dependence on residual entropy. Recently, Lötgering-Lin and Gross utilized Rosenfeld's entropy scaling approach to develop a group contribution (GC) method using PC-SAFT to predict the viscosity of pure components [171] and mixtures [172]. Fouad and Vega [173, 174] also used entropy scaling to model the viscosity of hydroflurocarbon and hydrofluroolefin refrigerants, fitting parameters to experimental saturated viscosity data.

This chapter describes an entropy scaling based, pseudo-component technique using the PC-SAFT EoS [171] to predict the viscosity of hydrocarbon mixtures and diesel fuels. The pseudo-component technique [36] is applied to correlate reduced viscosity to residual entropy through a third order polynomial using the GC method of Lötgering-Lin and Gross [171]. The model is not fit to viscosity data but is predictive up to HTHP conditions using two calculated or measured mixture properties: the number averaged MW and HN/CN ratio. Deviations in predictions are found when the mixture contains large concentrations of iso-alkanes and cyclohexanes. However, this deviation is reduced when a third mixture property, viscosity at a chosen reference state, is used to fix the value of one of the model parameters. Pseudo-component viscosity predictions are compared to experimental data for 54 different hydrocarbon mixture compositions and two diesel fuels over a wide range of temperatures and pressures.

3.1 Entropy scaling approach and pseudo-component technique development

Rosenfeld [170, 175] showed a mono-variable relationship existed between reduced viscosity (i.e., $\eta^* = \eta/\eta_{\text{reference}}$) and residual entropy (i.e., $\tilde{s}^{\text{res}}$, the difference between absolute entropy and its ideal gas at the same conditions) for spherical monoatomic systems. Chopra et al. [176] used entropy scaling to describe the reduced transport properties of water, using molecular dynamics to calculate the transport properties. Goel et al. [177] applied entropy scaling to Lennard-Jones chains and showed that the entropy scaling parameters were dependent on chain length. Galliero et al. [178] extended the work of Goel et al. [177] and applied entropy scaling to model viscosity of normal alkanes. Novak [179-182] showed that η^*scales nearly linearly with $\tilde{s}^{\text{res}}$, when the Chapman-Enskog viscosity is used as the reference viscosity, and proposed [180] a

PC-SAFT parameter-based residual entropy correlation to predict viscosity for normal alkanes to temperatures of 650 K and pressures up to 5,000 bar with an MAPD of 7 %.

Similar to the approach taken by Novak [180], Lötgering-Lin and Gross [171] used perturbed-chain polar SAFT (PCP-SAFT), with the Chapman-Enskog reference viscosity, and correlated η^* to $\tilde{s}^{\mathrm{res}}$ using a third order polynomial, developing a GC entropy scaling method to predict viscosity of 110 pure compounds, from 12 different chemical families, with a 5 % MAPD. The GC entropy scaling method overcomes the limitation of requiring multiple fitted viscosity model parameters needed in other approaches (e.g., FVT – see section 3.4.3 for a comparison between FVT and entropy scaling). This approach is extended in this section and applied to develop a pseudo-component technique to predict viscosity of hydrocarbon mixtures and fuels.

For self-consistency within the GC entropy scaling method, GC PC-SAFT parameters of Sauer et al. [58] were used to develop different PC-SAFT parameter correlations for pure-component n-alkanes and PNAs than are used for predicting density in Chapter 2, and these correlations are listed in Table 3.1. Knowing the pseudo-component PC-SAFT parameters, calculated using the approach described in Chapter 2, Eq. 3.1 can now be used with the PC-SAFT EoS to calculate reduced residual entropy, $\tilde{s}^{\mathrm{res}}$ (i.e., the molar residual entropy, $\bar{s}^{\mathrm{res}}$, divided by the gas constant, *R*), using commercial software (VLXE/Blend [131]). The next section describes the steps needed for the calculation of the viscosity, knowing $\tilde{s}^{\mathrm{res}}$.

$$\tilde{s}^{\mathrm{res}}(V,T) = -\left(\frac{\partial \tilde{a}^{\mathrm{res}}}{\partial T}\right)_V \qquad 3.1$$

Table 3.1. PC-SAFT parameter correlations as a function of MW (g/mol) for n-alkanes and PNAs using the GC parameters of Sauer et al. [58].

	n-alkane	PNA
m	$0.0325\text{MW} + 0.2463$	$0.0231\text{MW} + 0.7392$
$m\sigma$ (Å)	$0.1265\text{MW} + 0.7564$	$0.0874\text{MW} + 2.6366$
$\varepsilon/_k$ (K)	$\exp(5.4762 - 1.3302/\text{MW})$	$\exp(5.8137 - 15.5549/\text{MW})$

Rosenfeld [170] showed that reduced viscosity, $\eta^* = \eta/\eta_{\text{reference}}$, scales with $\tilde{s}^{\text{res}}$. Here $\eta_{\text{reference}}$ is set equal to the Chapman-Enskog viscosity (Eq. 3.2), as recommended by Novak [179, 180] who showed that a straightforward scaling of $\tilde{s}^{\text{res}}$ can be obtained over the entire fluid phase space.

$$\eta_{\text{reference}} = \frac{5}{16}\frac{\sqrt{\text{MW}kT/\left(mN_{\text{A}}\pi\right)}}{\sigma^2\Omega^{(2,2)*}} \qquad 3.2$$

where m and σ are the PC-SAFT parameters for a pure compound when calculating viscosity for a pure compound or are those of a pseudo-component when calculating viscosity of a pseudo-component. In Eq. 3.2, T, k, N_{A}, and $\Omega^{(2,2)*}$ are temperature, Boltzmann's constant, Avogadro's number, and the reduced collision integral, respectively. The correlation of Neufeld et al. [183] is used to calculate $\Omega^{(2,2)*}$. Lötgering-Lin and Gross [171] modified Novak's approach to calculate η^* using a third-order polynomial (Eq. 3.3) in reduced dimensionless residual entropy, s^* (Eq. 3.4).

$$ln(\eta^*) = A + Bs^* + C{s^*}^2 + D{s^*}^3 \qquad 3.3$$

$$s^* = \left(\frac{\tilde{s}^{\text{res}}(V,T)}{m}\right) \qquad 3.4$$

In Eq. 3.3, A, B, C, and D are the viscosity coefficients of either a pure compound or pseudo-component needed to calculate the viscosity. For a pure compound, these viscosity coefficients are found to best correlate to MW when each coefficient is multiplied by m^2. As a typical result, Figure 3.1 shows the variation of Am^2 with MW for selected compounds found in diesel fuels, where A is calculated using the GC method of Lötgering-Lin and Gross [171] and $m = m_{\text{pure compound}}$. The Am^2 values that fall outside the alkane and PNA curves are ignored since these compounds have MWs less than those of the diesels considered in this study [36]. Figure 3.2 shows the variation of Am^2, Bm^2, Cm^2, and Dm^2 with MW for n-alkanes and PNAs and Table 3.2 lists the coefficients for the polynomial fits needed to calculate each viscosity coefficient. The Z parameter, which is calculated using Eq. 2.17 in Chapter 2, is now used in Eqs. 3.5-3.8 to calculate the pseudo-component viscosity coefficients needed in Eq. 3.3.

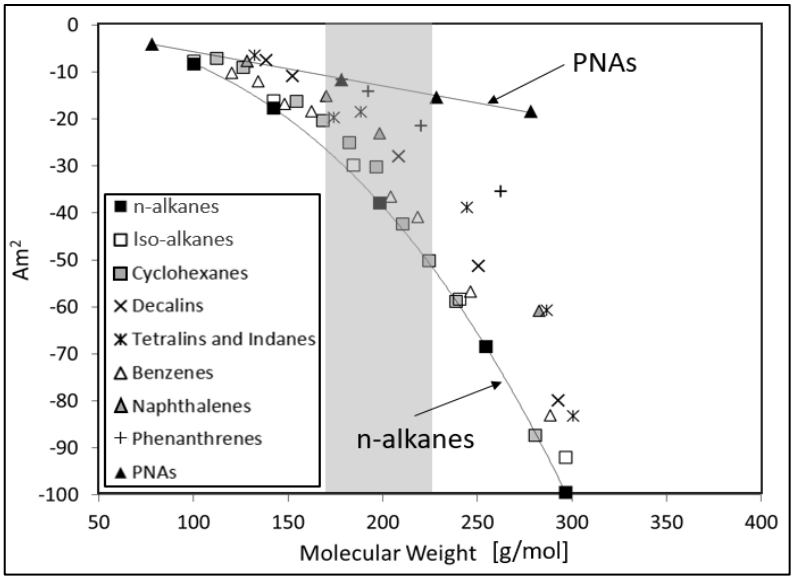

Figure 3.1. Effect of molecular weight on Am^2 for selected compounds with A calculated using the GC method of Lötgering-Lin and Gross [171] and with $m = m_{\text{pure compound}}$. The shaded region shows the number averaged MW range (i.e., 172 to 228 g/mol) for the diesel fuels studied by Aquing et al. [25].

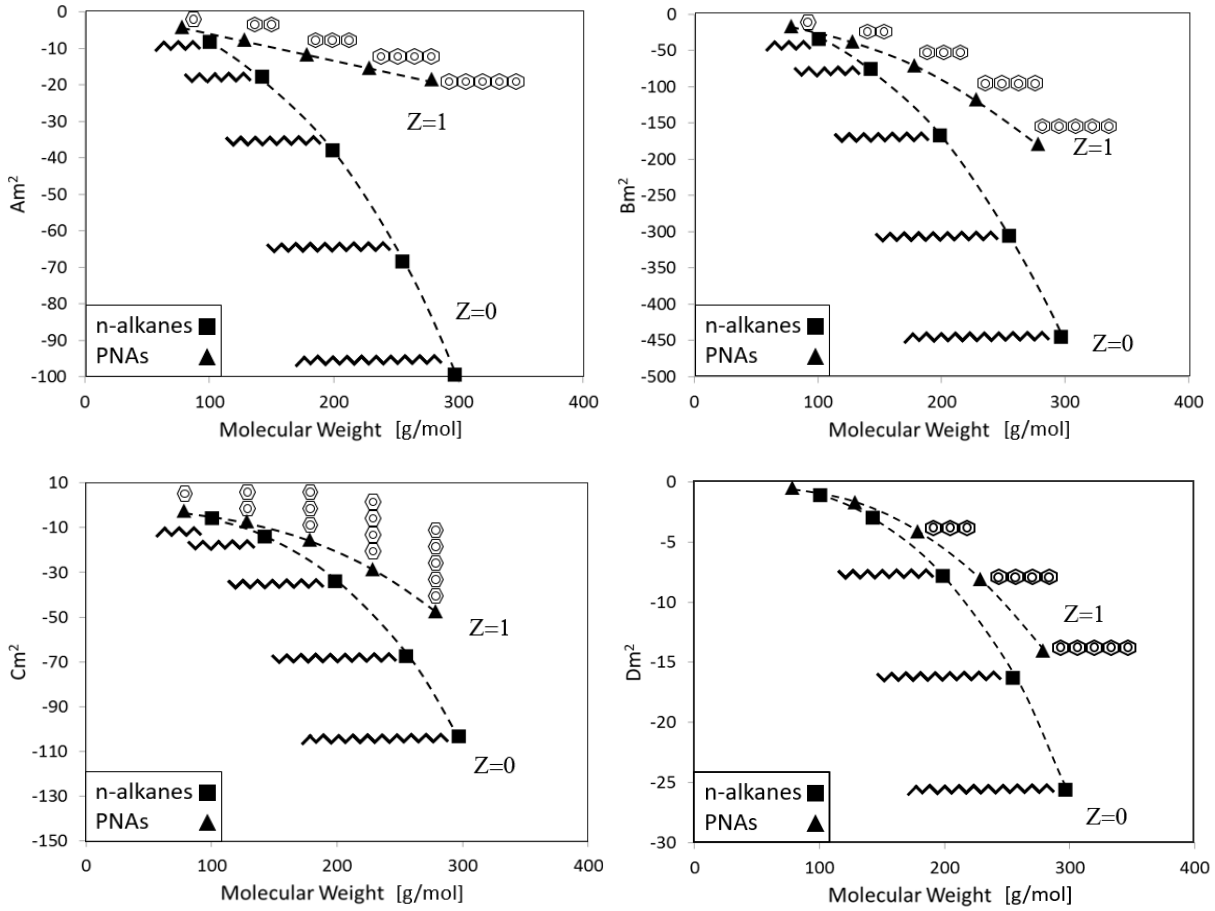

Figure 3.2. Effect of molecular weight on the viscosity coefficients for n-alkanes and PNAs calculated using the GC method of Lötgering-Lin and Gross [171] and with $m = m_{\text{pure compound}}$. Structures of representative compounds are shown in the figures.

Table 3.2. Parameters for the 3rd order polynomial correlation as a function of MW (g/mol) for the viscosity coefficients of n-alkanes and PNAs: $Ym^2 = \sum_{i=0}^{3}\left(e_i MW^i\right)$. Y is a viscosity coefficient (A, B, C or D) and e is the coefficient in the polynomial equation for n-alkanes and PNAs.

	n-alkane				PNA			
	e_0	e_1	e_2	e_3	e_0	e_1	e_2	e_3
Am^2	-3.000×10^{-2}	-8.028×10^{-3}	-5.510×10^{-4}	-1.860×10^{-6}	-3.996×10^{-1}	-2.420×10^{-2}	-3.431×10^{-4}	7.111×10^{-7}
Bm^2	-1.602×10^{1}	3.079×10^{-1}	-4.279×10^{-3}	-5.524×10^{-6}	-2.194×10^{0}	-4.339×10^{-2}	-1.522×10^{-3}	-2.172×10^{-6}
Cm^2	-9.298×10^{-3}	-2.639×10^{-3}	-2.107×10^{-4}	-3.215×10^{-6}	-1.020×10^{-1}	-7.812×10^{-3}	-1.895×10^{-4}	-1.408×10^{-6}
Dm^2	1.085×10^{-4}	-2.519×10^{-5}	-1.232×10^{-5}	-9.383×10^{-7}	1.644×10^{-3}	-4.411×10^{-4}	-3.231×10^{-5}	-5.288×10^{-7}

$$\left(Am^2\right)_{\text{pseudo}-\text{component}} = (1-Z)\left(Am^2\right)_{\text{n}-\text{alkane}} + Z\left(Am^2\right)_{\text{PNA}} \quad 3.5$$

$$\left(Bm^2\right)_{\text{pseudo}-\text{component}} = (1-Z)\left(Bm^2\right)_{\text{n}-\text{alkane}} + Z\left(Bm^2\right)_{\text{PNA}} \quad 3.6$$

$$\left(Cm^2\right)_{\text{pseudo}-\text{component}} = (1-Z)\left(Cm^2\right)_{\text{n}-\text{alkane}} + Z\left(Cm^2\right)_{\text{PNA}} \quad 3.7$$

$$\left(Dm^2\right)_{\text{pseudo}-\text{component}} = (1-Z)\left(Dm^2\right)_{\text{n}-\text{alkane}} + Z\left(Dm^2\right)_{\text{PNA}} \quad 3.8$$

It should be noted that improved predictions can be obtained in some cases if *D* is fit to a single viscosity data point rather than calculating *D* with Eq. 3.8. Both approaches shown in the following section require information on the mixture number averaged MW and HN/CN ratio. For convenience, *D* is fit to a viscosity experimental data point at the lowest reported temperature and pressure (e.g., 323 K and ~10 bar for the two diesel fuels in this study). An equally appropriate

approach is to fit *D* to the kinematic viscosity at 40 °C (KV40 [184]) or to the viscosity at atmospheric pressure and room temperature since both types of data are commonly measured in industry.

Viscosity predictions are compared with 1822 literature data points for the hydrocarbon mixtures and diesel fuels. For mixtures where experimental data for more than three isotherms are available, only the lowest, a central, and the highest temperature isotherms are shown for clarity. However, all predictions for available experimental data are included in the calculation of percent deviation, Max deviation, SD, MAPD, and bias (Eqs. 2.19-2.23).

3.2 Results

3.2.1 Well-characterized hydrocarbon mixtures

Table 3.3 lists the molar compositions of hydrocarbon mixtures used to evaluate the viscosity pseudo-component technique. Zeberg-Mikkelsen et al. [185] measured the viscosity of ternary mixtures (referred to as M1) containing methyl-cyclohexane (MCH), decalin, and 2,2,4,4,6,8,8-heptamethyl-nonane (i.e., iso-cetane) for three different compositions at seven temperatures (293, 303, 313, 323, 343, and 353 K) and pressures up to 1,000 bar. Baylaucq et al. [186] reported the viscosity for ternary mixtures (referred to as M2) containing n-heptane (nC7), MCH, and methyl-naphthalene for twenty-one compositions at three temperatures (303, 323, and 343 K) and pressures up to 1,000 bar. Boned et al. [133] reported viscosity measurements for a ternary (referred to as M3) and a quinary (referred to as M4) mixture at seven temperatures (293, 303, 313, 323, 333, 343, and 353 K) and pressures up to 1,000 bar. Dauge et al. [187] measured the viscosity of binary mixtures (referred to as M5) containing iso-cetane and n-tridecane (nC13) for seven compositions at seven temperatures (293, 303, 313, 323, 333, 343, and 353 K) and pressures

up to 1,000 bar. Zeberg-Mikkelsen et al. [188] reported the viscosity for ternary mixtures (referred to as M6) containing iso-cetane, nC13, and methyl-naphthalene for twenty-one compositions at seven temperatures (293, 303, 313, 323, 333, 343, and 353 K) and pressures up to 1,000 bar.

Table 3.3. Molar composition of the mixtures studied in this work [133, 185-188] and viscosity of compounds present in these mixtures at 298 K and 1 atmosphere [189-197].

Compound	Chemical Family	Viscosity (cP)	M1	M2	M3	M4	M5	M6
n-heptane	n-alkanes	0.388	-	0.125-0.750	-	-	-	-
n-tridecane	n-alkanes	2.130	-	-	0.394	0.200	0.125-0.875	0.125-0.750
2,2,4,4,6,8,8-heptamethyl-nonane	Iso-alkanes	3.354	balance	-	-	0.162	balance	0.125-0.750
methyl-cyclohexane	Cyclohexanes	0.681	0.125-0.333	0.125-0.750	-	-	-	-
heptyl-cyclohexane	Cyclohexanes	2.473	-	-	0.348	0.353	-	-
decalin	Decalins	2.469	0.125-0.333	-	-	-	-	-
heptyl-benzene	Benzenes	2.100	-	-	0.258	0.156	-	-
methyl-naphthalene	Naphthalenes	2.913	-	balance	-	0.129	-	balance

Figures 3.3 and 3.4 show the viscosity predictions and deviations from experiment, respectively, for the hydrocarbon mixtures reported by Zeberg-Mikkelsen et al. [185], Baylaucq et al. [186], Boned et al. [133], Dauge et al. [187], and Zeberg-Mikkelsen et al. [188]. For brevity, only central compositions are included in the figures. For mixture viscosities measured by Zeberg-Mikkelsen et al. [185], only the data for mixture composition containing 0.250 mole fraction MCH, 0.250 mole fraction decalin, and 0.500 mole fraction iso-octane (referred to as M1-2) are shown in

the figures. For mixture viscosities measured by Baylaucq et al. [186], only the data for mixture composition containing 0.250 mole fraction nC7, 0.625 mole fraction MCH, and 0.125 mole fraction of methyl-naphthalene (referred to as M2-11) are shown in the figures. For mixture viscosities measured by Dauge et al. [187], only the data for mixture composition containing 0.500 mole fraction nC13 and 0.500 mole fraction of iso-cetane (referred to as M5-4) are shown in the figures. For mixture viscosities measured by Zeberg-Mikkelsen et al. [188], only the data for mixture composition containing 0.125 mole fraction iso-cetane, 0.625 mole fraction nC13, and 0.250 mole fraction of methyl-naphthalene (referred to as M6-11) are shown in the figures. Table 3.4 lists the calculated MW, HN/CN ratio, Z parameter, viscosity experimental data point (η_o) at the lowest reported temperature and pressure used to fit D in the three-parameter model, the PC-SAFT parameters, and the viscosity coefficients for the pseudo-components for the hydrocarbon mixtures shown in the figures. Table 3.5 summarizes viscosity predictions of the hydrocarbon mixtures. Parameters and MAPDs are reported in the appendix (Section 3.4) for all hydrocarbon mixture compositions in this study.

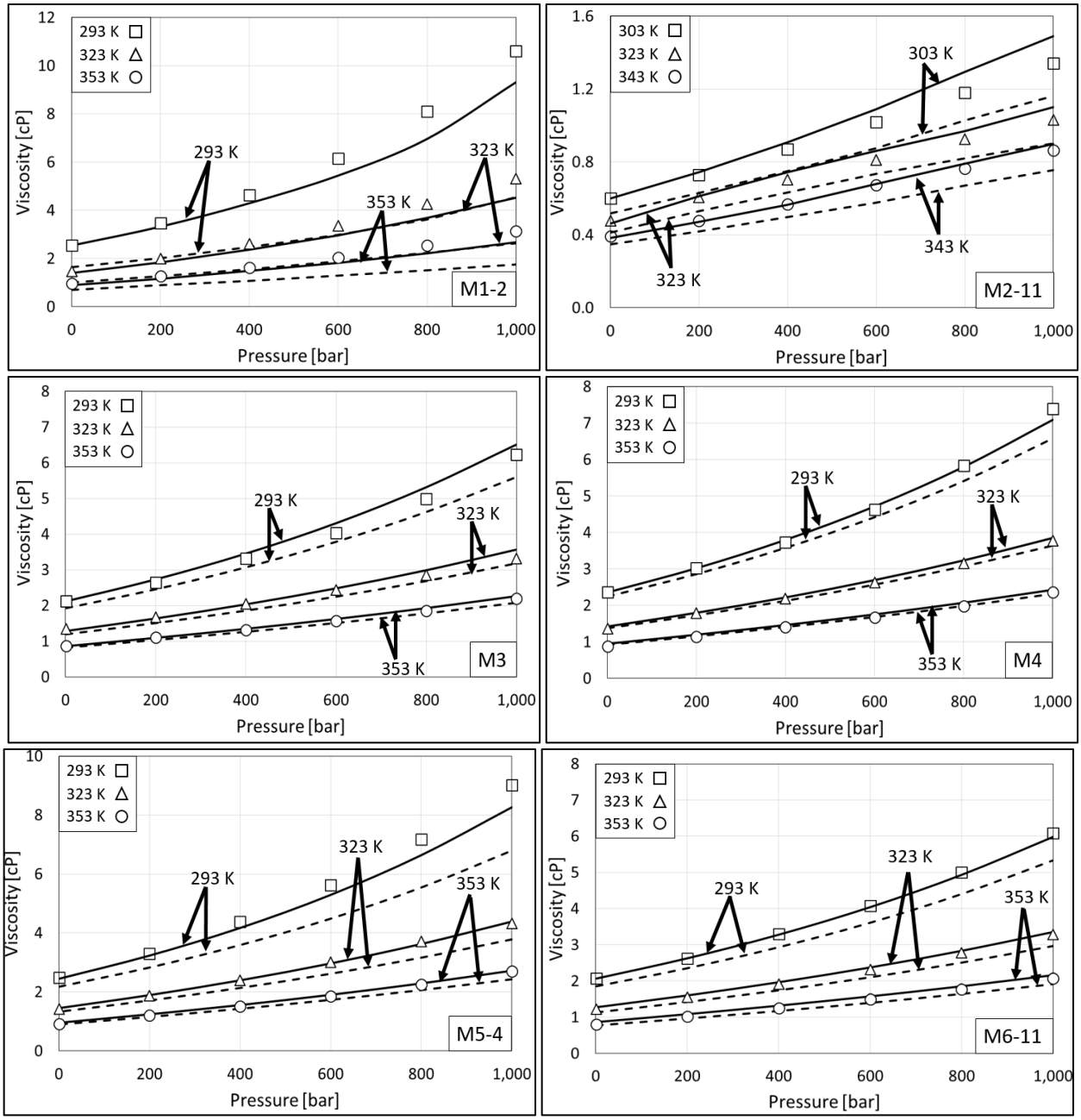

Figure 3.3. Pseudo-component viscosity predictions compared to experimental data [133, 185-188] (symbols) for hydrocarbon mixtures listed in Table 3: two-parameter (dashed lines) and three-parameter (solid lines) models. Note that the y-axis scale is different in each figure.

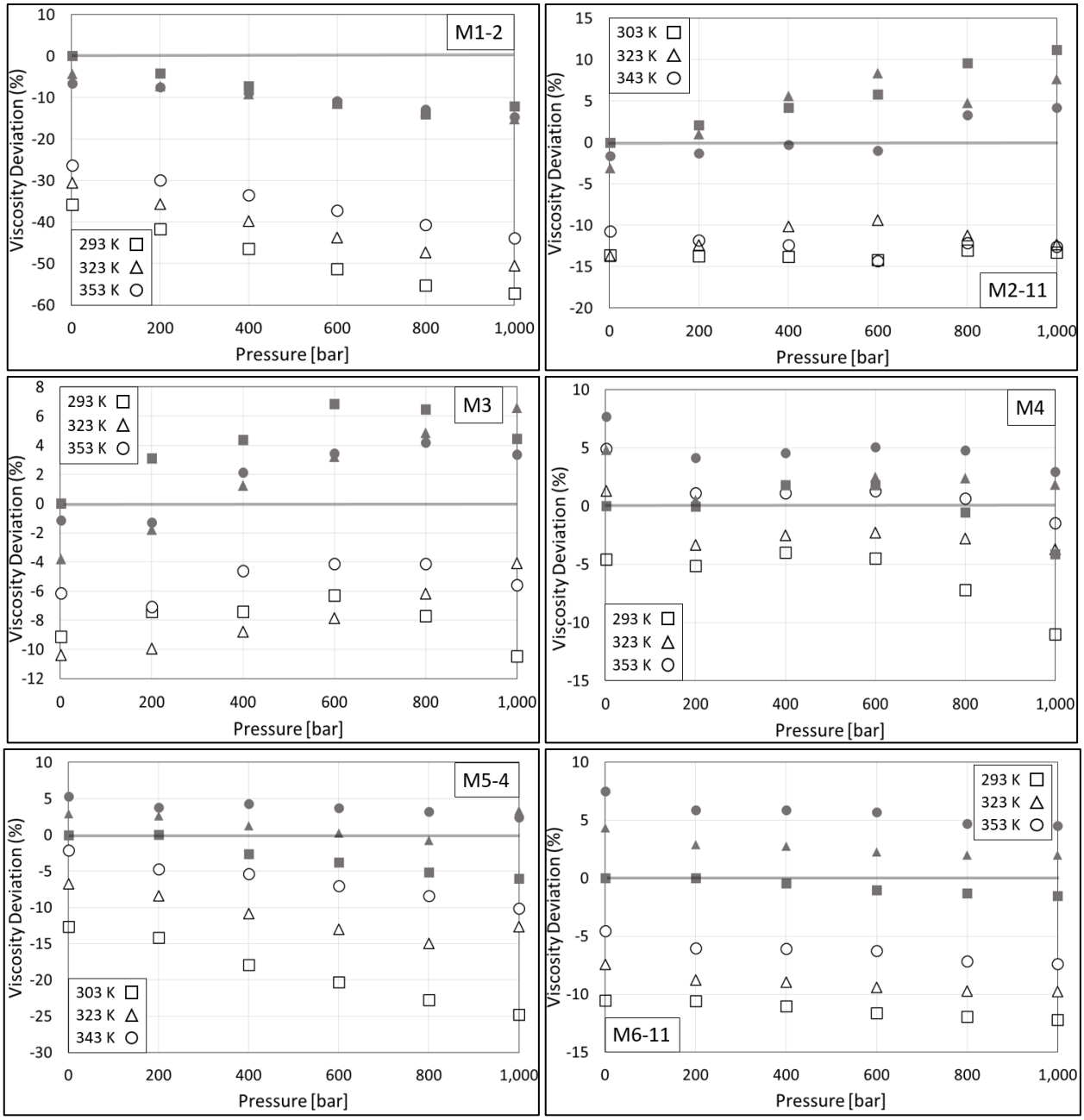

Figure 3.4. Pseudo-component viscosity deviations compared to experimental data [133, 185-188] for hydrocarbon mixtures listed in Table 3: two-parameter (open symbols) and three-parameter (filled symbols) models. Note that the y-axis scale is different in each figure.

Table 3.4. Pseudo-component properties and parameters for mixtures shown in Figure 3. η_o is the viscosity data point at the lowest reported temperature and pressure (1 bar) used to fit D, now termed D^{fit}, in the three-parameter model.

Mixture	MW	HN/CN	Z	η_o / cP	m	σ (Å)	ε/k (K)	A	B	C	D	D^{fit}
M1-2	172.3	2.01	0.097	2.54 at 293 K	5.736	3.849	244.5	-0.781	-3.439	-0.678	-0.153	-0.199
M2-11	104.2	1.94	0.220	0.60 at 303 K	3.526	3.816	248.0	-0.665	-2.754	-0.470	-0.093	-0.111
M3	181.6	1.94	0.139	2.12 at 293 K	5.980	3.847	247.6	-0.788	-3.519	-0.706	-0.162	-0.172
M4	183.8	1.84	0.206	2.36 at 293 K	5.965	3.841	252.2	-0.776	-3.520	-0.712	-0.165	-0.169
M5-4	205.4	2.14	0	2.49 at 293 K	6.922	3.863	237.4	-0.857	-3.511	-0.779	-0.181	-0.196
M6-11	179.1	1.84	0.204	2.07 at 293 K	5.824	3.840	251.4	-0.770	-3.476	-0.698	-0.161	-0.158

Table 3.5. The MAPD (%), bias (%), SD (%), and Max Deviation (%) for pseudo-component viscosity predictions of hydrocarbon mixtures compared to the literature data [133, 185-188].

	Two-parameter						Three-parameter					
	M1	M2	M3	M4	M5	M6	M1	M2	M3	M4	M5	M6
MAPD	35.0	8.0	7.2	3.1	14.0	10.2	11.0	4.8	3.4	2.8	4.6	5.2
Bias	-35.0	-4.8	-7.2	-2.1	-14.0	-7.9	-10.9	3.5	2.1	2.5	-0.3	-2.2
SD	10.1	5.1	2.1	2.1	8.8	7.5	7.3	4.2	2.1	1.9	4.2	4.7
Max Deviation	56.7	24.4	11.6	11.0	49.0	38.7	26.7	24.6	7.8	7.7	22.9	25.5

Viscosities are predicted for mixtures M1 and M2 with MAPDs of 35 and 8%, respectively when using the two-parameter model. Although the MAPD for viscosity predictions for compositions of mixture M2 is less than for compositions of mixture M1, the MAPDs for both mixtures are shown in the appendix (refer to section 3.4.1) to increase with MCH concentration. When using the two-parameter model, viscosities are predicted for mixture M1-3 (33.3 mol%

MCH) and mixture M2-6 (75.0 mol% MCH) with 45 and 20% MAPDs, respectively. More accurate viscosities are predicted using the two-parameter model for mixtures M3 and M4 (7.2 and 3.1% MAPD, respectively), which do not contain MCH. Viscosities of mixtures M5 and M6, which contain large concentrations of iso-cetane, are predicted with MAPDs of 14 and 10%, respectively using the two-parameter model. Due to the definition of DoU (Eq. 2.13), the pseudo-component technique does not distinguish normal and iso-alkanes, which could be a reason for viscosity prediction deviations, when significant concentrations of iso-alkanes are present in the mixtures. Predictions for all hydrocarbon mixtures in this study are improved by fitting the *D* coefficient (three-parameter model).

It should be noted that MCH (MW = 98.18 g/mol) lies at the extreme lower bounds of the fitted PC-SAFT and viscosity coefficient correlations, where the n-alkane and PNA correlations converge to the approximately the same value. Thus, the two-parameter pseudo-component model does not adequately distinguish low MW cycloalkanes from low MW n-alkanes or PNAs. Decalin concentration may also play a role in higher deviations for viscosity predictions using the two-parameter model. However, decalin's effect is unclear as it was present in compositions of only mixture M1.

Another reason for deficiencies in the model could be due to the constant value of the *D* coefficient for every functional group in Lötgering-Lin and Gross [171]'s GC viscosity model. Extending their model to fit functional group dependent *D* coefficients could possibly lead to more accurate viscosity predictions without fitting *D* in the three-parameter model. It is also noted that in the work of Lötgering-Lin and Gross, the pure component GC viscosity coefficients were fit using the homosegmented GC parameters of Sauer et al. [58], where iso and normal alkane functional groups were not differentiated when fitting parameters.

Nevertheless, the two-parameter model and the Z parameter from Eq. 2.17 do not appear to accurately represent mixtures containing significant concentrations of MCH and iso-alkanes. Inclusion of a single viscosity data point at a chosen reference state to fit the *D* coefficient offers the potential for improved viscosity predictions in the three-parameter model. Viscosity is predicted for hydrocarbon mixtures using the three-parameter model with an MAPD of 7.3% for all compositions of all mixtures in this study. This result is comparable to the viscosity predictions of Gross and co-workers [172] (i.e., 6.2% MAPD) for non-polar binary mixtures.

3.2.2 Fuels

Table 3.6 lists the limited number of experimental studies reporting the viscosity of diesel fuels up to HTHP conditions. Detailed composition of diesel fuels, required for our analysis, was found only in Aquing et al. [25]. Although, Politte [198] provides limited fuel compositional information, their reported average CN and average MW were not found to be self-consistent. Therefore, the diesel fuel investigated by Politte [198] is not considered in this study. Further explanation for its exclusion is included in the SI. Aquing et al. [25] reported gas chromatography results of two diesel fuels (referred to in this study as Middle East SR and Highly Naphthenic) and measured the viscosity of these diesel fuels from 323 to 423 K and up to 3,500 bar. Table 3.7 lists the molar composition and CN range for different classes of compounds in the diesel fuels. Table 8 lists the number averaged MW, the HN/CN ratio, viscosity experimental data point (η_O) at the lowest reported temperature and pressure (i.e., 323 K and ~10 bar) used to fit D in the three-parameter model, PC-SAFT parameters (Eqs. 2.15-2.17), and viscosity coefficients (Eqs. 3.5-3.8) of the pseudo-components for the two diesel fuels.

Table 3.6. Summary of viscosity data for diesel fuels measured up to high temperatures and pressures.

Author	Year	T_{range}/K	P_{max}/bar	Uncertainty (%)	No. of Samples with Composition
Schaschke et al. [26]	2013	298-373	5,000	2	0
Aquing et al. [25]	2012	323-423	3,500	2	2
Duncan et al. [199]	2012	283-373	1,311	-	0
Bazile et al. [145]	2012	293-353	2,000	1	0
Duncan et al. [200]	2010	283-373	1,311	-	0
Robertson and Schaschkle [201]	2009	273-294	1,600	-	0
Politte [198]	1985	298-422	1,000	-	1[a]

[a]Sample is not considered in this study. Explanation is provided in the appendix (Section 3.4).

Table 3.7. Molar composition (%) and carbon number ranges of chemical classes in diesel fuels measured by gas chromatography. Data from ref. [25].

	Mole Percent (%)		Carbon Number Range	
Chemical Class	Middle East SR	Highly Naphthenic	Middle East SR	Highly Naphthenic
n-alkanes	23	6	7-27	7-29
iso-alkanes	26	13	7-27	7-29
cyclohexanes	16	26	8-26	8-28
decalins	4	20	10-25	10-26
benzenes	10	10	8-24	8-20
naphthalenes	7	3	10-21	10-15
phenanthrenes	3	1	14-20	14-35
tetralins and Indanes	7	16	9-23	9-22
other unsaturates	4	5	12-21	13-35

Table 3.8. Pseudo-component properties and parameters for diesel fuels. η_O is the viscosity data point at the lowest reported temperature and pressure (i.e., 323 K and ~10 bar) used to fit D, now termed D^{fit}, in the three-parameter model.

Diesel	MW	HN/CN	Z	η_O / cP	m	σ (Å)	ε/k (K)	A	B	C	D	D^{fit}
Middle East SR	225.1	1.85	0.222	2.97	7.202	3.846	254.6	-0.829	-3.885	-0.837	-0.203	-0.226
Highly Naphthenic	203.6	1.74	0.292	2.57	6.448	3.836	259.0	-0.780	-3.668	-0.771	-0.185	-0.211

Figures 3.5 and 3.6 show viscosity predictions and deviations from experiment, respectively, for diesel fuels Middle East SR and Highly Naphthenic for three isotherms (323 K, 373 K, and 423 K) and pressures up to 3,500 bar. Viscosity is predicted across all conditions for both diesel fuels with an MAPD of 22.0% using the two-parameter model and 9.3% using the three-parameter model. Table 3.9 presents the statistics for viscosity predictions of the diesel fuels. The composition of the diesel fuels in this study contain significant concentrations of iso-alkanes (i.e., 26 mol% for diesel fuel Middle East SR and 13 mol% for diesel fuel Highly Naphthenic) and cyclohexanes (16 mol% and 26 mol% for diesel fuels Middle East SR and Highly Naphthenic, respectively). Large concentrations of iso-alkanes and cyclohexanes in the diesel fuels are possibly the cause of less accurate predictions using the two-parameter model, similar to the compositions of mixtures M1 and M2. The Highly Naphthenic diesel fuel also contains 20 mol% decalins, which possibly is another cause of viscosity prediction deviations based on our observations for compositions of mixture M1. Inclusion of a single viscosity data point as a third parameter to fit a model parameter improves viscosity predictions for the diesel fuels in this study.

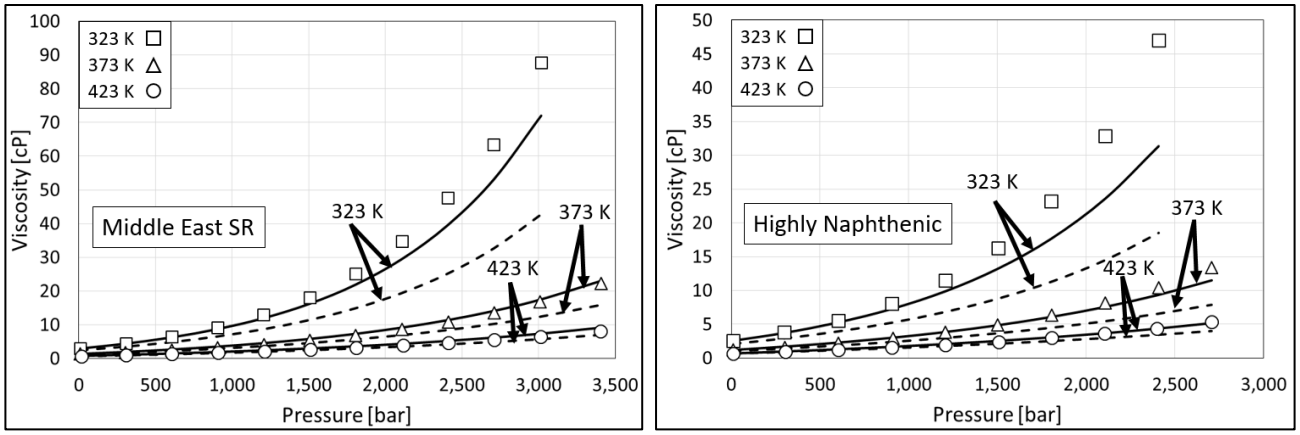

Figure 3.5. Pseudo-component viscosity predictions compared to experimental data [25] (symbols) for diesel fuels: two-parameter (dashed lines) and three-parameter (solid lines). Note that the y-axis scale is different in each figure.

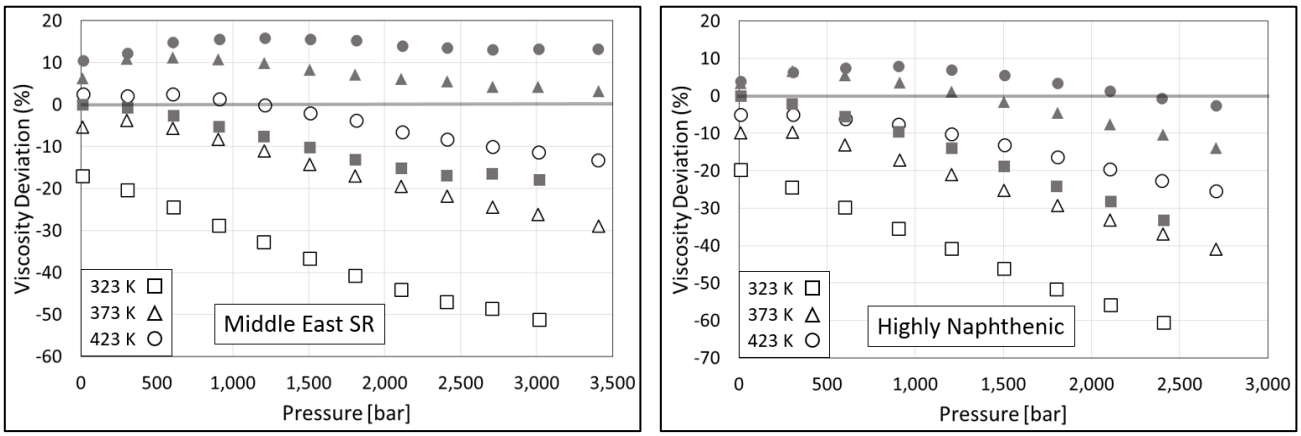

Figure 3.6. Pseudo-component viscosity deviations compared to experimental data [25] for diesel fuels: two-parameter (open symbols) and three-parameter (filled symbols) models. Note that the y-axis scale is different in each figure.

Table 3.9. The MAPD (%), bias (%), SD (%), and Max Deviation (%) for pseudo-component viscosity predictions of diesel fuels compared to experimental data [25].

	Two-parameter		Three-parameter	
	Middle East SR	Highly Naphthenic	Middle East SR	Highly Naphthenic
MAPD	18.3	25.2	10.3	8.3
Bias	-17.8	-25.2	4.3	-3.9
SD	15.2	15.7	5.0	8.3
Max Deviation	51.3	60.6	17.9	33.2

3.3 Conclusion

A pseudo-component technique based upon residual entropy scaling using the Perturbed-Chain Statistical Associating Fluid Theory was developed to predict the viscosity of hydrocarbon mixtures and diesel fuels. The model predicts viscosity without fitting to high temperature and pressure experimental data and requires input of only two calculated or experimentally measured mixture properties: the number averaged molecular weight and the hydrogen-to-carbon ratio. Inclusion of a third parameter, the viscosity data point at a chosen reference state, to fit a model parameter was shown to improve predictions for mixtures that contained significant concentrations of iso-alkanes and cyclohexanes. The ability to predict accurate viscosities for complex hydrocarbon mixtures such as diesel fuel up to extreme conditions, using relatively simple inputs will aid the future development of fuel injection equipment design and support the development and optimization of fuel and fluid formulations for improved performance at extreme conditions.

3.4 Appendix for Chapter 3

3.4.1 The pseudo-component properties for hydrocarbon mixtures

Tables 3.10-3.14 list the pseudo-component properties, the reference viscosity, the PC-SAFT parameters, the viscosity coefficients, and MAPDs for viscosity predictions of hydrocarbon mixtures [133, 185-188] listed in Table 3.3.

Table 3.10. Mixture properties, data point (η_O) at the lowest reported temperature and pressure (1 bar), the PC-SAFT parameters, the viscosity coefficients, and MAPDs (%) of pseudo-component viscosity predictions for mixtures M1-2 (with 0.250 mole fraction MCH and 0.250 mole fraction decalin) [185], M2-11 (with 0.250 mole fraction nC7 and 0.625 mole fraction MCH) [186], M3 [133], M4 [133], M5-4 (with 0.500 mole fraction nC13 and 0.500 mole fraction iso-cetane) [187], and M6-11 (with 0.250 mole fraction MNP, 0.625 mole fraction nC13, and 0.125 mole fraction iso-cetane) [188]. η_O is used to fit D, now termed D^{fit}, in the three-parameter model.

Mixture	MW	HN/CN	Z	η_o (cP)	m	σ (Å)	ε/k (K)	A	B	C	D	MAPD	D^{fit}	MAPD
M1-2	172.3	2.01	0.0973	2.54 at 293 K	5.736	3.849	244.5	-0.781	-3.439	-0.678	-0.153	41.1	-0.199	9.3
M2-11	104.2	1.94	0.2200	0.60 at 303 K	3.526	3.814	248.0	-0.665	-2.754	-0.470	-0.093	12.6	-0.111	4.2
M3	181.6	1.94	0.1390	2.12 at 293 K	5.980	3.847	247.6	-0.788	-3.519	-0.706	-0.162	7.2	-0.172	3.4
M4	183.8	1.84	0.2092	2.36 at 293 K	5.961	3.841	252.5	-0.776	-3.519	-0.712	-0.165	3.1	-0.169	2.8
M5-4	205.4	2.14	0	2.49 at 293 K	6.922	3.863	237.4	-0.857	-3.511	-0.779	-0.181	12.4	-0.196	2.3
M6-11	179.1	1.84	0.204	2.07 at 293 K	5.824	3.840	251.4	-0.770	-3.476	-0.698	-0.161	8.5	-0.158	3.0

Table 3.11. Pseudo-component properties, viscosity experimental data point (η_O) at atmospheric pressure and 293 K, the PC-SAFT parameters, the viscosity coefficients, and MAPDs (%) of pseudo-component viscosity predictions for mixtures M1 [185] with varying composition of methyl-cyclohexane (MCH), decalin, and iso-cetane. x is mole fraction. η_O is used to fit D, now termed D^{fit}, in the three-parameter model.

Mixture	X_{MCH}	$X_{decalin}$	$X_{iso\text{-}cetane}$	MW	HN/CN	Z	η_o (cP)	m	σ (Å)	ε/k (K)	A	B	C	D	MAPD	D^{fit}	MAPD
M1-1	0.125	0.125	0.750	199.4	2.07	0.0505	3.12	6.657	3.858	241.8	-0.835	-3.712	-0.760	-0.176	35.2	-0.210	11.0
M1-2	0.250	0.250	0.500	172.3	2.01	0.0973	2.54	5.736	3.849	244.5	-0.781	-3.439	-0.678	-0.153	41.1	-0.199	9.3
M1-3	0.333	0.333	0.334	154.3	1.98	0.1296	2.18	5.137	3.842	246.1	-0.748	-3.252	-0.623	-0.137	45.3	-0.197	4.8

Table 3.12. Pseudo-component properties, viscosity experimental data point (η_O) at atmospheric pressure and 303 K, the PC-SAFT parameters, the viscosity coefficients, and MAPDs (%) of pseudo-component viscosity predictions for mixtures M2 [186] with varying composition of n-heptane (nC7), methyl-cyclohexane (MCH), and methyl-naphthalene (MNP). x is mole fraction. η_O is used to fit D, now termed D^{fit}, in the three-parameter model.

Mixture	X_{nC7}	X_{MCH}	X_{MNP}	MW	HN/CN	Z	η_o (cP)	m	σ (Å)	ε/k (K)	A	B	C	D	MAPD	D^{fit}	MAPD
M2-1	0.125	0.125	0.750	131.4	1.22	0.6771	1.50	4.014	3.780	277.4	-0.628	-2.885	-0.545	-0.123	10.2	-0.137	8.7

M2-2	0.125	0.250	0.625	125.9	1.35	0.5915	1.22	3.930	3.787	271.4	-0.643	-2.868	-0.531	-0.117	9.2	-0.130	6.7
M2-3	0.125	0.375	0.500	120.4	1.49	0.5008	0.99	3.839	3.795	265.3	-0.654	-2.845	-0.517	-0.111	9.6	-0.125	7.1
M2-4	0.125	0.500	0.375	114.9	1.63	0.4121	0.87	3.739	3.802	259.5	-0.660	-2.815	-0.502	-0.104	14.9	-0.122	6.0
M2-5	0.125	0.625	0.250	109.4	1.76	0.3323	0.75	3.624	3.808	254.4	-0.663	-2.782	-0.486	-0.099	14.8	-0.116	4.6
M2-6	0.125	0.750	0.125	103.9	1.90	0.2476	0.68	3.503	3.813	249.3	-0.663	-2.748	-0.469	-0.093	19.8	-0.124	10.4
M2-7	0.250	0.125	0.625	126.2	1.39	0.5624	1.12	3.958	3.791	269.8	-0.648	-2.878	-0.533	-0.117	3.5	-0.123	5.2
M2-8	0.250	0.250	0.500	120.7	1.53	0.4720	0.93	3.866	3.798	263.7	-0.658	-2.854	-0.518	-0.111	6.6	-0.122	6.0
M2-9	0.250	0.375	0.375	115.2	1.66	0.3907	0.80	3.760	3.804	258.4	-0.663	-2.822	-0.503	-0.105	7.0	-0.115	5.0
M2-10	0.250	0.500	0.250	109.7	1.80	0.3044	0.68	3.648	3.811	253.0	-0.666	-2.788	-0.487	-0.099	8.4	-0.108	3.6
M2-11	0.250	0.625	0.125	104.2	1.94	0.2200	0.60	3.526	3.816	248.0	-0.665	-2.754	-0.470	-0.093	12.5	-0.111	4.2
M2-12	0.375	0.125	0.500	120.9	1.56	0.4507	0.68	3.886	3.801	262.6	-0.661	-2.860	-0.519	-0.111	2.9	-0.112	3.3
M2-13	0.375	0.250	0.375	115.4	1.70	0.3627	0.74	3.782	3.807	256.9	-0.666	-2.829	-0.503	-0.104	2.7	-0.108	2.7
M2-14	0.375	0.375	0.250	109.9	1.83	0.2835	0.65	3.665	3.813	251.9	-0.668	-2.793	-0.487	-0.099	4.7	-0.105	4.4
M2-15	0.375	0.500	0.125	104.4	1.97	0.1994	0.56	3.542	3.818	246.9	-0.667	-2.758	-0.471	-0.093	6.8	-0.103	3.1
M2-16	0.500	0.125	0.375	115.7	1.73	0.3416	0.69	3.803	3.810	255.8	-0.668	-2.835	-0.505	-0.104	3.6	-0.103	2.5
M2-17	0.500	0.250	0.250	110.2	1.87	0.2559	0.59	3.689	3.816	250.5	-0.670	-2.800	-0.488	-0.099	3.5	-0.102	4.7
M2-18	0.500	0.375	0.125	104.7	2.01	0.1721	0.52	3.564	3.821	245.6	-0.669	-2.764	-0.472	-0.093	9.0	-0.088	3.4
M2-19	0.625	0.125	0.250	110.5	1.91	0.2284	0.56	3.713	3.818	249.1	-0.673	-2.806	-0.489	-0.099	6.7	-0.097	4.2
M2-20	0.625	0.250	0.125	104.9	2.04	0.1518	0.49	3.581	3.823	244.6	-0.671	-2.767	-0.473	-0.093	4.1	-0.090	1.7
M2-21	0.750	0.125	0.125	105.2	2.08	0.1248	0.46	3.603	3.826	243.2	-0.673	-2.773	-0.474	-0.093	5.7	-0.084	3.6

Table 3.13. Pseudo-component properties, viscosity experimental data point (η_O) at atmospheric pressure and 293 K, the PC-SAFT parameters, the viscosity coefficients, and MAPDs (%) of pseudo-component viscosity predictions for mixtures M5 [187] with varying composition of n-tridecane (nC13) and heptamethyl-nonane (iso-cetane). x is mole fraction. η_O is used to fit D, now termed D^{fit}, in the three-parameter model.

Mixture	X_{nC13}	$X_{\text{iso-cetane}}$	MW	HN/CN	Z	η_o (cP)	m	σ (Å)	ε/k (K)	A	B	C	D	MAPD	D^{fit}	MAPD
M5-1	0.125	0.875	221.2	2.13	0	3.28	7.435	3.865	237.5	-0.884	-3.674	-0827	-0.195	24.8	-0.218	8.6
M5-2	0.250	0.750	215.9	2.13	0	2.98	7.264	3.864	237.5	-0.875	-3.621	-0.811	-0.190	19.4	-0.210	5.7
M5-3	0.375	0.625	210.7	2.14	0	2.69	7.093	3.864	237.4	-0.866	-3.567	-0.795	-0.185	15.3	-0.201	4.2
M5-4	0.500	0.500	205.4	2.14	0	2.49	6.922	3.863	237.4	-0.857	-3.511	-0.779	-0.181	12.4	-0.196	2.3
M5-5	0.625	0.375	200.1	2.14	0	2.29	6.751	3.862	237.4	-0.857	-3.511	-0.779	-0.176	10.4	-0.190	1.8
M5-6	0.750	0.250	194.9	2.15	0	2.14	6.580	3.682	237.3	-0.838	-3.398	-0.747	-0.171	8.1	-0.186	4.6
M5-7	0.875	0.125	189.6	2.15	0	1.98	6.409	3.861	237.3	-0.829	-3.340	-0.731	-0.167	7.6	-0.181	4.9

Table 3.14. Pseudo-component properties, viscosity experimental data point (η_O) at atmospheric pressure and 303 K, the PC-SAFT parameters, the viscosity coefficients, and MAPDs (%) of pseudo-component viscosity predictions for mixtures M6 [188] with varying composition of methyl-naphthalene (MNP), n-tridecane (nC13), and heptamethyl-nonane (iso-cetane). x is mole fraction. η_O is used to fit D, now termed D^{fit}, in the three-parameter model.

Mixture	X_{MNP}	X_{nC13}	$X_{\text{iso-cetane}}$	MW	HN/CN	Z	η_o (cP)	m	σ (Å)	ε/k (K)	A	B	C	D	MAPD	D^{fit}	MAPD
M6-1	0.125	0.125	0.750	210.7	1.98	0.1176	3.1	6.918	3.853	246.1	-0.838	-3.797	-0.794	-0.188	15.1	-0.196	9.6
M6-2	0.125	0.250	0.625	205.4	1.98	0.1145	3.2	6.757	3.853	245.8	-0.830	-3.750	-0.778	-0.183	15.2	-0.187	8.5
M6-3	0.125	0.375	0.500	200.1	1.98	0.1116	2.5	6.596	3.852	245.4	-0.823	-3.702	-0.762	-0.178	11.4	-0.181	5.8
M6-4	0.125	0.500	0.375	194.9	1.99	0.1087	2.5	6.434	3.852	245.1	-0.815	-3.654	-0.746	-0.173	9.6	-0.176	3.8
M6-5	0.125	0.625	0.250	189.6	1.99	0.1061	2.1	6.272	3.851	244.8	-0.807	-3.605	-0.730	-0.169	16.5	-0.189	1.1
M6-6	0.125	0.750	0.125	184.4	1.99	0.1035	2.1	6.109	3.851	244.5	-0.799	-3.555	-0.714	-0.164	20.7	-0.122	8.0
M6-7	0.250	0.125	0.625	200.1	1.82	0.2267	2.9	6.436	3.842	253.8	-0.794	-3.663	-0.761	-0.180	19.0	-0.194	9.1
M6-8	0.250	0.250	0.500	194.9	1.83	0.2208	2.9	6.284	3.842	253.2	-0.788	-3.618	-0.745	-0.176	16.2	-0.188	6.5
M6-9	0.250	0.375	0.375	189.6	1.83	0.2150	2.4	6.131	3.841	252.6	-0.782	-3.571	-0.729	-0.171	7.4	-0.167	5.5
M6-10	0.250	0.500	0.250	184.3	1.84	0.2094	2.3	5.978	3.841	252.0	-0.776	-3.524	-0.713	-0.166	5.9	-0.163	3.2
M6-11	0.250	0.625	0.125	179.1	1.84	0.2039	2.1	5.824	3.840	251.4	-0.770	-3.476	-0.698	-0.161	8.5	-0.158	3.0
M6-12	0.375	0.125	0.500	189.6	1.67	0.3266	3.0	5.987	3.830	260.5	-0.753	-3.529	-0.727	-0.173	8.8	-0.167	8.5
M6-13	0.375	0.250	0.375	184.3	1.68	0.3178	2.5	5.843	3.830	259.6	-0.749	-3.485	-0.712	-0.168	6.9	-0.162	6.1

M6-14	0.375	0.375	0.250	179.1	1.68	0.3092	2.3	5.698	3.830	258.8	-0.745	-3.441	-0.696	-0.163	6.4	-0.159	3.9
M6-15	0.375	0.500	0.125	173.8	1.68	0.3090	2.1	5.543	3.829	258.5	-0.739	-3.392	-0.680	-0.158	5.9	-0.155	2.8
M6-16	0.500	0.125	0.375	179.1	1.52	0.4169	2.7	5.570	3.819	266.3	-0.717	-3.397	-0.693	-0.165	7.8	-0.161	6.3
M6-17	0.500	0.250	0.250	173.8	1.52	0.4165	2.4	5.420	3.818	265.9	-0.712	-3.351	-0.678	-0.160	6.4	-0.156	4.4
M6-18	0.500	0.375	0.125	168.5	1.53	0.4181	2.1	5.268	3.817	265.6	-0.707	-3.303	-0.662	-0.155	6.0	-0.151	2.9
M6-19	0.625	0.125	0.250	168.5	1.37	0.5283	2.6	5.147	3.806	273.1	-0.678	-3.255	-0.659	-0.157	7.1	-0.155	4.3
M6-20	0.625	0.250	0.125	163.3	1.37	0.5304	2.2	5.000	3.804	272.8	-0.674	-3.209	-0.643	-0.152	6.5	-0.150	3.2
M6-21	0.750	0.125	0.125	158.0	1.22	0.6461	2.6	4.740	3.790	279.9	-0.640	-3.111	-0.623	-0.148	7.8	-0.152	2.9

3.4.2 Exclusion of diesel viscosity data

Politte [198] did not report detailed composition of the diesel fuel but did report the carbon number distribution and the average molecular weight (MW). Typically, this information should be sufficient to calculate the degree of unsaturation (DoU). For the diesel sample reported by Politte [198], Eq. 3.9 is used to calculate the hydrogen number (HN) of the diesel fuel from the reported average MW and the calculated average CN from gas chromatography. Eq. 3.10 shows that the calculated degree of unsaturation for the sample is negative, which is unrealistic. This indicates that the reported average MW is not consistent with the carbon number distribution. Therefore, the degree of unsaturation of the sample cannot be ascertained with confidence. Since this information is needed to calculate the PC-SAFT parameters for the pseudo-component, this sample is excluded from the present study.

$$\mathrm{HN_{diesel}} = \frac{\mathrm{MW_{diesel}} - 12.01\mathrm{CN_{diesel}}}{1.01} = \frac{212.0 - 12.01 \times 14.7}{1.01} = 35.2 \tag{3.9}$$

$$\mathrm{DoU_{diesel}} = \frac{1}{2}(2 \times \mathrm{CN_{diesel}} + 2 - \mathrm{HN_{diesel}}) = \frac{1}{2}(2 \times 14.7 + 2 - 35.2) = -1.89 \tag{3.10}$$

3.4.3 Performance of entropy scaling compared to free volume theory (FVT)

Free volume theory (FVT) [202] is compared with the entropy scaling approach for pure compounds from different chemical families and diesel fuels. The densities required in the FVT model are calculated using the PC-SAFT EoS of Gross and Sadowski [38]. For entropy scaling, the GC parameters of Sauer et al. [58] are used to calculate the PC-SAFT parameters for pure compounds, and the correlations developed in Chapter 2 using the parameters listed in Table 3.1 are used to calculate the PC-SAFT parameters for the diesel fuels. The FVT model parameters (i.e., α, l, and B_i) are fit to viscosity data at one isotherm, and the fitted parameters are used to predict viscosity for other isotherms. It is possible to fit temperature dependent FVT parameters to data at multiple isotherms, which would result in more accurate FVT predictions. However, here, we consider only a FVT predictive technique with minimal inputs by fitting temperature independent parameters to a single isotherm.

Table 3.15 lists the pure compounds (i.e., n-octane (nC8), n-dodecane (nC12), and n-octadecane (nC16)), branched alkanes (i.e., isooctane (iC8), iso-cetane (iC16)), and aromatics (i.e., m-xylene and toluene)) and diesel fuels for which viscosity is predicted up to high temperatures and pressures using either FVT or the GC entropy scaling method. Baled et al. [203] measured the viscosity of nC8 and iC8 at temperatures from 304 to 523 K and pressures up to 2,400 bar. Caudwell et al. [204] reported the viscosity for nC12 at

temperatures from 298 to 473 K and pressures up to 1,900 bar. Baled et al. [205] reported viscosity measurements for nC18 up to 534 K and 2,430 bar. Zeberg-Mikkelsen et al. [188] measured iC16 at temperatures from 293 to 3535 K and pressures up to 1,000 bar. Caudwell et al. [206] reported viscosity for m-xylene up to 473 K and 1,970 bar. Rowane et al. [207] measured the viscosity of toluene up to 531 K and 2,200 bar. Aquing et al. [25] measured the viscosity of two diesel fuels up to 423 K and 3,500 bar.

Unlike the GC entropy scaling method developed by Lötgering-Lin and Gross [171], no study has reported group contribution FVT parameters. Therefore, viscosity data are required to fit the three FVT parameters. The lowest reported isotherm is used to fit the FVT parameters for the pure compounds and diesel fuels. Table 3.15 lists the fitted FVT and entropy scaling parameters required to predict viscosity. The GC entropy scaling method developed by Lötgering-Lin and Gross [171] is used for pure compounds, and the three-parameter pseudo-component technique described in Chapter 3 is used for diesel fuels. Predictions are summarized in Table 3.16 and show that entropy scaling yields more accurate viscosity predictions compared to FVT, when minimal inputs are used by fitting FVT parameters to a single isotherm.

Table 3.15. Model parameters for selected compounds and diesel fuels. Data from [25, 188, 203-207].

		PC-SAFT				FVT		Viscosity Entropy Scaling			
Fluid	MW	m	σ (Å)	ε/k (K)	l (Å)	α ($m^5mol^{-1}s^{-2}$)	$B_i \times 10^3$	A	B	C	D
nC8	114.2	3.960	3.839	236.2	1.184	118.8	4.851	-0.696	-2.869	-0.501	-0.100
nC12	170.3	5.785	3.855	237.1	2.017	146.8	4.639	-0.794	-3.455	-0.671	-0.149
nC18	254.5	8.521	3.867	237.7	2.517	216.6	3.309	-0.942	-4.209	-0.927	-0.224
iC8	114.2	2.989	4.091	264.3	0.958	94.4	7.192	-0.599	-2.524	-0.460	-0.100
iC16	226.4	5.009	4.277	284.8	1.209	133.1	8.885	-0.575	-3.264	-0.758	-0.199
m-xylene	106.2	3.225	3.748	281.6	0.953	88.2	6.080	-0.689	-2.566	-0.509	-0.100
toluene	92.1	2.882	3.739	278.4	0.885	82.8	7.457	-0.658	-2.513	-0.451	-0.087
Middle East	225.1	7.202	3.841	254.6	1.403	188.2	5.481	-0.829	-3.885	-0.837	-0.226
Highly Naphthenic	203.6	6.448	3.831	259.0	0.954	171.5	6.785	-0.780	-3.668	-0.771	-0.210

Table 3.16. The MAPD (%), bias (%), SD (%), and Max Deviation (%) for FVT and entropy scaling viscosity predictions of selected compounds and diesel fuels compared to literature data [25, 188, 203-207]. Table 3.16 also lists the MAPD, bias, SD, and Max Deviation achieved for only the single isotherm used to fit the FVT parameters for each fluid.

Fluid	FVT prediction for all data points				FVT prediction for fitted single isotherm				Entropy scaling prediction for all data points			
	MAPD	Bias	SD	Max Deviation	MAPD	Bias	SD	Max Deviation	MAPD	Bias	SD	Max Deviation
nC8	8.1	7.9	6.6	22.0	0.5	-0.3	0.6	1.8	2.8	2.0	1.9	7.4
nC12	27.6	27.6	16.6	55.5	2.4	-0.1	0.3	0.9	3.3	0.4	1.9	7.5
nC18	59.0	58.9	35.6	112.7	0.4	-0.2	0.4	1.4	10.9	10.1	9.2	27.8
iC8	2.1	-1.2	2.1	7.7	0.7	0.0	0.5	1.5	5.5	0.0	2.8	12.9
iC16	12.7	12.4	8.3	30.9	1.5	-0.3	1.2	2.8	4.1	-3.1	3.0	12.3
m-xylene	5.8	5.7	3.5	11.3	0.4	0.0	0.3	0.8	3.2	-3.1	1.9	8.2
toluene	5.3	1.6	3.9	13.9	0.9	-0.2	0.9	3.8	3.6	2.4	1.8	8.3
Middle East	39.6	7.5	34.9	120.3	1.1	-0.5	1.2	4.2	10.3	4.3	5.0	17.9
Highly Naphthenic	22.8	3.8	21.6	70.2	2.4	-0.9	2.2	7.0	8.3	-3.9	8.3	33.4

4. Chapter 4: Entropy Scaling Based Model for Thermal Conductivity[4]

Limited experimental thermal conductivity data are available for pure compounds and well-characterized hydrocarbon mixtures up to extreme conditions, and there is a greater lack of thermal conductivity data available for complex mixtures, such as rocket propellant (RP), jet, and diesel fuels. Various correlations and theories have been developed for the prediction of thermal conductivity for pure hydrocarbons [209-233] and their mixtures [214, 222-224, 231, 234-238] including structure-based, group contribution methods [239-245].

A few pseudo-component based methodologies have been developed to model the thermal conductivity of complex mixtures, such as crude oil and its fractions. These methodologies include an expanded fluid-based (EFB) model [238, 246] and a corresponding-states approach defined by an effective carbon number (ECN) [222]. Yarranton and co-workers [238] used EFB to model the thermal conductivity of several crude oils up to 100 bar and 398 K. They fit four EFB pseudo-component parameters for the crude oils to available experimental data and predicted the thermal conductivity within 1% MAPD compared to experimental data [238]. They extended this work by developing structure independent correlations to calculate the EFB parameters and obtained predictions within 3% MAPD [246]. Teja and Tarlneu [222] used the ECN-based approach to predict the thermal conductivity of different cuts of three crude oils at temperatures from 308 to 528 K and atmospheric pressure within 7% MAPD. Their ECN-based model required as inputs the average molecular weight (MW) and critical properties of the pseudo-components, which were

[4]Adapted from Ref. [208] Rokni HB, Moore JD, Gupta A, M^{c}Hugh MA, Mallepally RR, Gavaises M. General method for prediction of thermal conductivity for well-characterized hydrocarbon mixtures and fuels up to extreme conditions using entropy scaling. Fuel **2019**;245:594-604. doi.org/10.1016/j.fuel.2019.02.044

calculated using the reported boiling temperature and specific gravity of the pseudo-components [247] through the correlations developed by Kesler and Lee [248].

The two-abovementioned pseudo-component based techniques capture the effect of composition only through the mixture average MW and are limited in predictive capability by the need for multiple pseudo-components or for fitting to experimental data. Hence, a technique is needed that considers the effects of both the molecular structure and MW of compounds present in mixtures while only requiring a minimum number of parameters fit to experimental data.

In this chapter, a pseudo-component technique is developed using the residual entropy scaling based thermal conductivity correlation of Hopp and Gross [227] and the PC-SAFT [38] EoS. Thermal conductivities of well-characterized hydrocarbon mixtures and fuels are predicted up to high temperature and high pressure (HTHP) conditions using two mixture properties: the number averaged MW and the HN/CN ratio. Less accurate predictions are obtained using the two-parameter model for the mixtures containing high amounts of iso-alkanes, but the predictions are improved when a single thermal conductivity data point at a reference condition is used to fix the value of one model parameter. The technique described here accurately predicts thermal conductivity up to HTHP conditions for fourteen well-characterized hydrocarbon mixtures and six fuels.

4.1 Pseudo-component Entropy scaling technique

Pure compound PC-SAFT parameters are determined by directly fitting to properties (e.g., saturated liquid density and vapor pressure data) or using group contribution (GC) methods [58-60]. In this chapter, the PC-SAFT parameters are determined using the GC parameters of Sauer et al. [58] to be consistent with the technique to predict viscosity in Chapter 3. However, in general, other PC-SAFT GC parameters could be used, such as those reported by Tihic et al. [61] or Burgess

et al. [53]. PC-SAFT parameters are fit as a function of molecular weight (MW) for a given chemical family. The correlations reported in Table 3.1 for m, $m\sigma$, and ε/k for n-alkanes and poly-nuclear aromatics (PNAs) are used here to be consistent with the viscosity pseudo-component technique.

Similar to reduced viscosity, as observed by Rosenfeld [170], reduced thermal conductivity, λ^*, (Eq. 4.1) of a pure compound scales with the residual entropy. Hopp and Gross [227] investigated several choices of a reference thermal conductivity including Chapman Enskog (CE), CE with Eucken correction, and the reference proposed by Liang and Tsai [249] based on the work of Stiel and Thodos [250]. None of these references was completely successful in describing the nonlinear entropy scaling behavior for the complete fluid space from low-density gas to dense liquid. Hopp and Gross [227] proposed a new, empirically-based reference that did correlate the complete fluid space and allowed for a mono-variable dependence of λ^* with reduced residual entropy. Hopp and Gross [227] showed that the CE reference thermal conductivity (Eq. 4.2) can adequately reproduce λ^* in the dense fluid region, which is the region of interest in the present study. Hence, the CE reference term is used as the reference thermal conductivity in the present study.

$$\lambda^* = \frac{\lambda}{\lambda_{\text{reference}}} \tag{4.1}$$

$$\lambda_{\text{reference}} = \lambda_{\text{CE}} = \frac{5}{16}\frac{\sqrt{\text{MW}kT/\left(mN_{\text{A}}\pi\right)}}{\sigma^2\Omega(2,2)*} \tag{4.2}$$

where, k, T, N_A, and $\Omega^{(2,2)*}$ are Boltzmann's constant, temperature, Avogadro's number, and the reduced collision integral, respectively. In Eq. 4.2, m and σ are the PC-SAFT parameters of a pure compound when calculating thermal conductivity for a pure compound or are those of a pseudo-

component when calculating thermal conductivity of a pseudo-component. Hopp and Gross [227] modified the third-order polynomial reported by Lötgering-Lin and Gross [171] for viscosity and proposed Eq. 4.3 to correlate λ^* to the reduced, dimensionless residual, entropy, s^* (Eq. 4.4).

$$ln(\lambda^*) = A + Bs^* + C(1.0 - \exp(s^*)) + Ds^{*2} \quad 4.3$$

$$s^* = \left(\frac{\tilde{s}^{res}(V,T)}{m}\right) \quad 4.4$$

where A, B, C, and D are the thermal conductivity coefficients. In the present study, instead of using Eq. 4.3 to calculate λ^*, the simpler expression in Eq. 4.5 is used since it adequately describes liquid-phase thermal conductivities.

$$ln(\lambda^*) = A + Bs^* + Cs^{*2} + Ds^{*3} \quad 4.5$$

where the thermal conductivity coefficients of a pure compound are used when calculating thermal conductivity of a pure compound or those of a pseudo-component are used when calculating the thermal conductivity of a pseudo-component.

Hopp and Gross [227] used Eq. 4.3 to fit thermal conductivity coefficients for 148 pure compounds that included normal and iso-alkanes, alkenes, aldehydes, ethers, esters, ketones, alcohols, acids, and benzenes. However, they did not report parameters for some compounds from chemical classes present in petroleum fuels including cyclohexanes, decalins, tetralins, indanes, naphthalenes, and phenanthrenes due to the limited amount of thermal conductivity data available in the literature. In the pseudo-component approach, n-alkanes and PNAs are the two bounds for values of the thermal conductivity coefficients. Since Hopp and Gross [227] did not report

coefficients for n-alkanes and PNAs using only the CE reference term, new pure compound liquid phase thermal conductivity coefficients (i.e., *A,B,C,* and *D*) are fit in the present study.

For many n-alkanes and PNAs, experimental thermal conductivity data at HTHP conditions are not reported in the literature. Thus, experimental thermal conductivities at atmospheric pressure are utilized here to fit the n-alkane parameters. Experimental data is lacking for PNAs even at atmospheric pressure, with the exception of benzene. Briggs [251] reported a thermal conductivity correlation as a function of temperature at atmospheric pressure for some PNAs (i.e., benzene, naphthalene, and phenanthrene). However, thermal conductivities of benzene using the Briggs correlation deviate by up to 8% compared to data reported in the Dortmund Data Bank (DDB) [252] containing data of Rastorguev and Pugach [253]. Here we use the model of Gharagheizi et al. [239] for benzene at atmospheric pressure to predict thermal conductivity within 4% of the DDB. Furthermore, since no other experimental data for heavier PNAs are available to assess the accuracy of the Briggs correlation [251], the model of Gharagheizi et al. [239] is also used to calculate the thermal conductivities of naphthalene and phenanthrene (PNAs) at atmospheric pressure. More information on the differences between the thermal conductivities of benzene, naphthalene, and phenanthrene using these two approaches is reported in the appendix (Section 4.4). Table 4.1 lists coefficients A, B, C, and D fit to Eq. 4.5 for selected n-alkanes and PNAs. For n-alkanes, A does not vary monotonically with MW. B decreases with MW, whereas C and D appear constant for n-alkanes. For PNAs, A, B, and C monotonically increase with MW, whereas D is a constant. Figure 4.1 shows these coefficients plotted versus MW for n-alkanes and PNAs, and the correlations are listed in Table 4.2.

Table 4.1. Thermal conductivity coefficients fit to atmospheric pressure data using Eq. 4.5 for selected n-alkanes and PNAs.

Compounds	A	B	C	D	T_{range} / K	λ_{range} / $Wm^{-1}K^{-1}$	Reference
n-octane	0.482	-0.972	-0.001	0.013	298-348	0.127-0.112	Kashiwagi et al. [254]
n-decane	0.482	-0.990	-0.001	0.013	303-373	0.130-0.110	Kashiwagi et al. [254]
n-undecane	0.482	-1.002	-0.001	0.013	292-364	0.135-0.120	Wada et al. [255]
n-dodecane	0.482	-1.008	-0.001	0.013	298-373	0.136-0.119	Kashiwagi et al. [254]
n-tetradecane	0.506	-1.009	-0.001	0.013	284-363	0.143-0.126	Wada et al. [255]
n-hexadecane	0.506	-1.024	-0.001	0.013	296-362	0.144-0.132	Wada et al. [255]
benzene	0.303	-1.362	-0.217	-0.013	279-413	0.145-0.118	Gharagheizi et al. [239]
naphthalene	0.367	-1.307	-0.195	-0.013	354-545	0.126-0.088	Gharagheizi et al. [239]
phenanthrene	0.415	-1.293	-0.183	-0.013	375-483	0.129-0.107	Gharagheizi et al. [239]

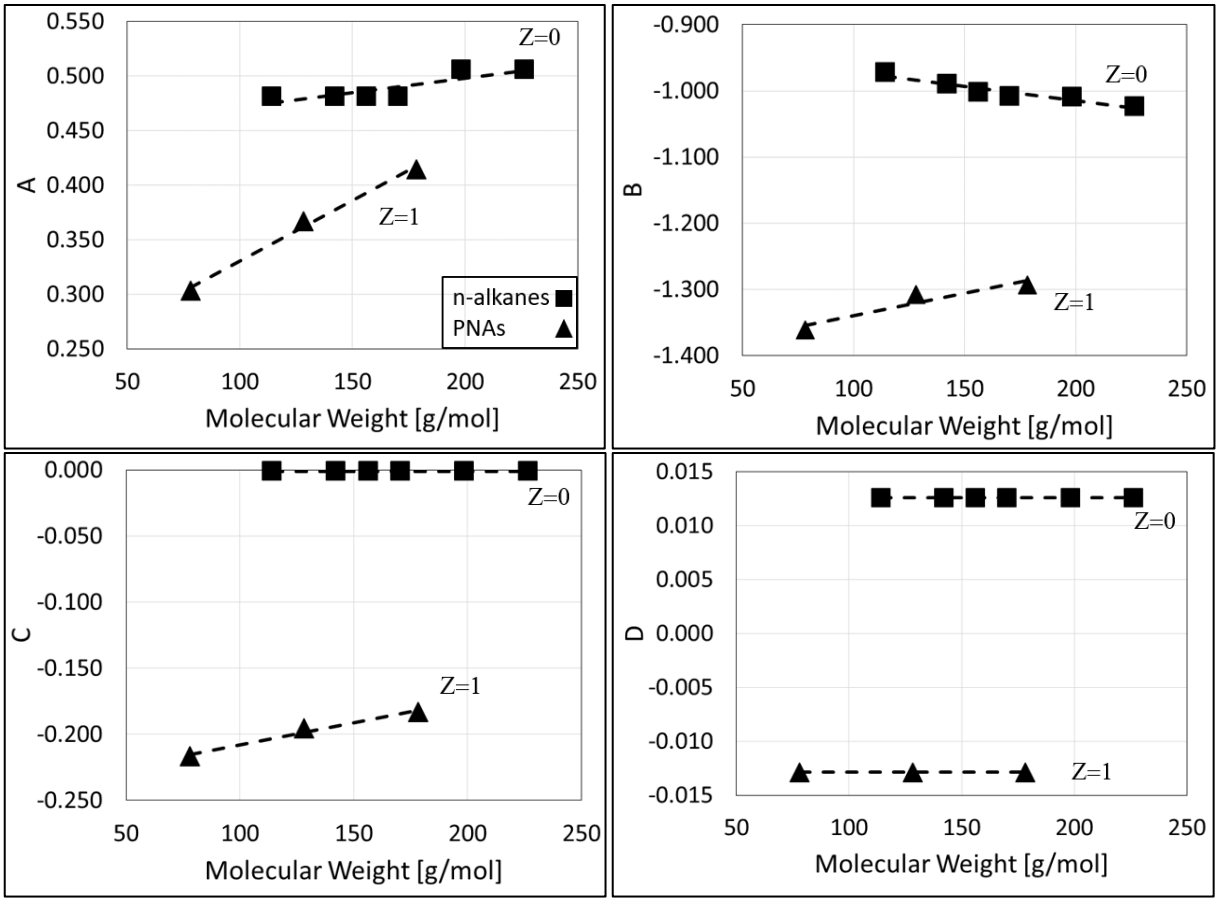

Figure 4.1. Effect of molecular weight (g/mol) on thermal conductivity coefficients for selected compounds from n-alkanes and PNAs. Note that the y-axis scale is different in each figure.

Table 4.2. Thermal conductivity coefficient correlations as a function of MW (g/mol) fit to selected compounds from n-alkanes and PNAs.

Coefficient	n-alkanes	PNAs
A	$2.6702 \times 10^{-4}\mathrm{MW} + 4.4472 \times 10^{-1}$	$1.1140 \times 10^{-3}\mathrm{MW} + 2.1893 \times 10^{-1}$
B	$-4.2810 \times 10^{-4}\mathrm{MW} - 9.2891 \times 10^{-1}$	$6.8258 \times 10^{-4}\mathrm{MW} - 1.4083 \times 10^{0}$
C	-1.0012×10^{-3}	$3.3215 \times 10^{-4}\mathrm{MW} - 2.4099 \times 10^{-1}$
D	1.2568×10^{-2}	-1.2867×10^{-2}

In the viscosity pseudo-component technique [156], the viscosity coefficients for chemical classes present in fuel were scaled with the PC-SAFT parameter *m*, so that parameter values for n-alkanes and PNAs bounded parameter values for all other chemical families. Due to the lack of thermal conductivity data available in the literature for the pure compounds from different chemical classes found in fuels, only the thermal conductivity coefficients for n-alkanes and PNAs are considered here and the coefficients for the two chemical groups are assumed to be the two bounds for the pseudo-component thermal conductivity coefficients in Eq. 4.5. The Z value, calculated using Eq. 2.17, is used in Eqs. 4.6-4.9 to calculate the pseudo-component thermal conductivity coefficients needed for the calculation of the reduced thermal conductivity using Eq. 4.5.

$$A_{\text{pseudo}-\text{component}} = (1-Z)A_{\text{n}-\text{alkane}} + ZA_{\text{PNA}} \quad 4.6$$

$$B_{\text{pseudo}-\text{component}} = (1-Z)B_{\text{n}-\text{alkane}} + ZB_{\text{PNA}} \quad 4.7$$

$$C_{\text{pseudo}-\text{component}} = (1-Z)C_{\text{n}-\text{alkane}} + ZC_{\text{PNA}} \quad 4.8$$

$$D_{\text{pseudo}-\text{component}} = (1-Z)D_{\text{n}-\text{alkane}} + ZD_{\text{PNA}} \quad 4.9$$

When applying this approach to well-characterized hydrocarbon mixtures and fuels, thermal conductivity predictions improve by fitting B to a single reference state data point. In this study, the reference state is chosen as the experimental data point at the lowest reported temperature and pressure for the mixtures of interest. Coefficient B is fit to reproduce the thermal conductivity at the reference state, while A, C, and D are determined from Eqs. 4.6, 4.8, and 4.9, respectively. The results for the two-parameter and three-parameter models are described in the following sections for well-characterized hydrocarbon mixtures and fuels.

The thermal conductivity predictions are compared with 655 data points for well-characterized hydrocarbon mixtures, rocket propellant fuels, and jet fuels. The performance of the approach is characterized by the percent deviation, Max deviation, SD, MAPD, and bias (Eqs. 2.18-2.22).

4.2 Results

4.2.1 Well-characterized hydrocarbon mixtures

The pseudo-component technique is applied to several binary and ternary hydrocarbon mixtures [255-257]. Wakeham et al. [256] measured the thermal conductivity for binary mixtures containing benzene and 2,2,4-trimethylpentane (i.e., iso-octane) (TMP) (referred to as M1) for two different compositions at temperatures from 313 to 345 K and pressures up to 3,500 bar. Fareleira et al. [257] and Wakeham et al. [256] reported thermal conductivity data for binary mixtures containing n-heptane (nC7) and TMP (referred to as M2) for three different compositions at temperatures from 308 to 360 K and pressures up to 4,500 bar. Wada et al. [255] reported the thermal conductivity data for binary mixtures containing nC7 and n-undecane (nC11), nC7 and n-hexadecane (nC16), and nC11 and nC16 (referred to as M3, M4, and M5, respectively) for three different compositions for each mixture at atmospheric pressure and a range of temperatures from 295 to 345 K. Wada et al. [255] also reported the thermal conductivity for ternary mixtures (referred to as M6) including nC7, nC11, and nC16 for three compositions at temperatures from 295 to 345 K and 1 bar. Table 4.3 lists the molar composition of these mixtures. For brevity, only central compositions of mixtures M3-M6 (referred to as M3-2, M4-2, M5-2, and M6-2, respectively) are shown in the figures. However, all mixture compositions of mixtures M3-M6 are included in the reported statistical metrics.

Table 4.3. Molar composition (mol%) of the well-characterized hydrocarbon mixtures studied in this work. Data from ref. [255-257]

Compound	Chemical Family	M1	M2[a]	M3	M4	M5	M6
n-heptane	n-alkanes	-	48.9 74.4 75.1	25.0 50.0 75.0	-	25.0 50.0 75.0	10.0 33.4 59.9
n-undecane	n-alkanes	-	-	balance	25.0 50.0 75.0	- -	29.9 33.3 30.0
n-hexadecane	n-alkanes	-	-	-	balance	balance	balance
2,2,4-trimethylpentane (TMP)	iso-alkanes	25.0 75.0	balance	-	-	-	-
benzene	benzenes	balance	-	-	-	-	-

[a] The composition of mixture M2 containing 74.4 mol% nC7 and 25.6 mol% TMP measured by Fareleira et al. [257] is close to that of the mixture containing 75.1 mol% nC7 and 24.9 mol% TMP measured by Wakeham et al. [256], and the two data sets agree within 0.05%. Both sets of data are included in the reported statistics in Table 4.4, but only the data reported by Wakeham et al. [256], which have a greater temperature range, are shown in Figures 4.2 and 4.4.

Figures 4.2 and 4.3 present the thermal conductivity predictions for the investigated hydrocarbon mixtures at different temperatures and pressures. Figures 4.4 and 4.5 show the thermal conductivity prediction deviations for these mixtures. The appendix (Section 4.4) provides information on the calculated MW, the HN/CN ratio, Z parameter, thermal conductivity experimental data point (λ_o) at the lowest reported temperature and pressure used to fit B in the three-parameter model, the PC-SAFT parameters, and the thermal conductivity coefficients for the pseudo-components for all of the well-characterized hydrocarbon mixtures considered in this study. Table 4.4 summarizes the statistical metrics of the thermal conductivity predictions for these mixtures.

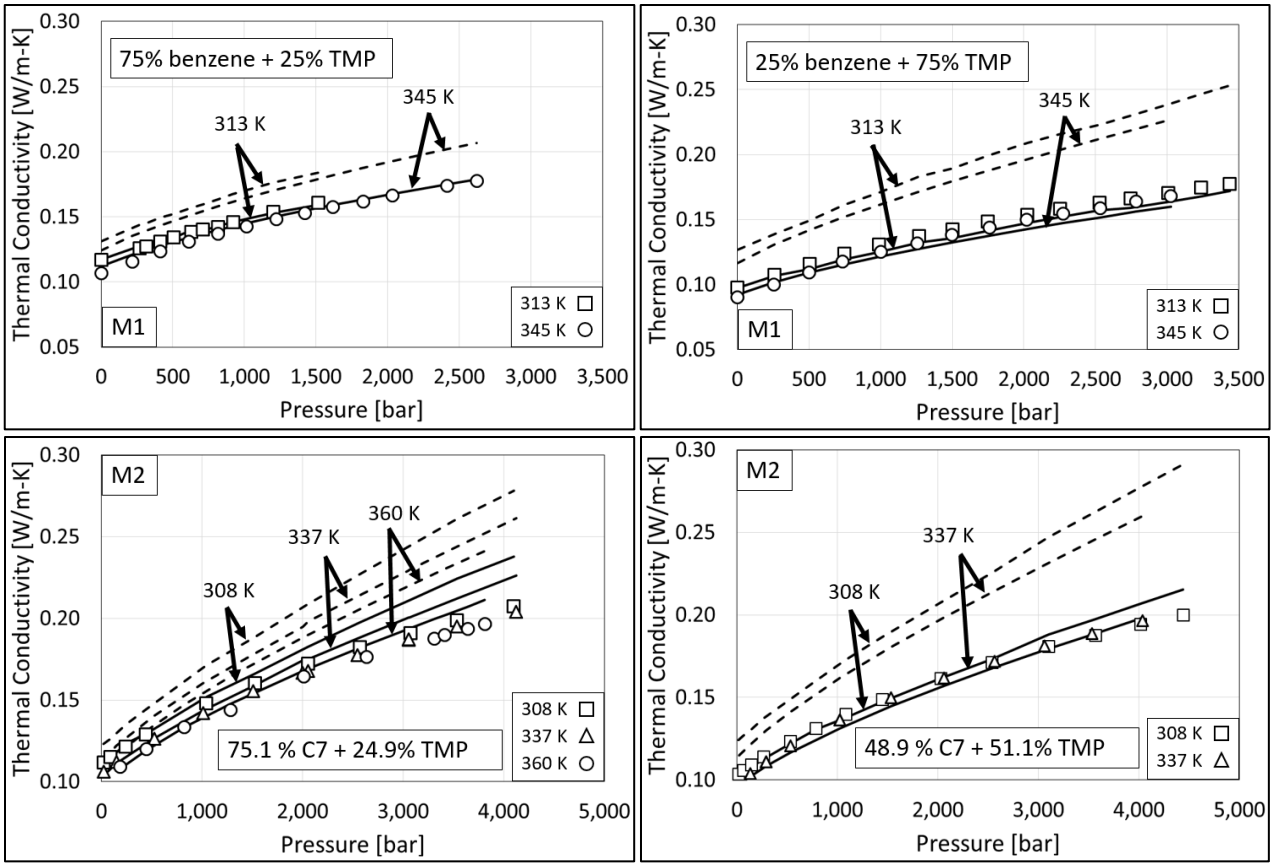

Figure 4.2. Pseudo-component thermal conductivity predictions compared to experimental data [256, 257] (symbols) for mixtures M1 and M2. Dashed lines show the two-parameter predictions and solid lines show the three-parameter predictions.

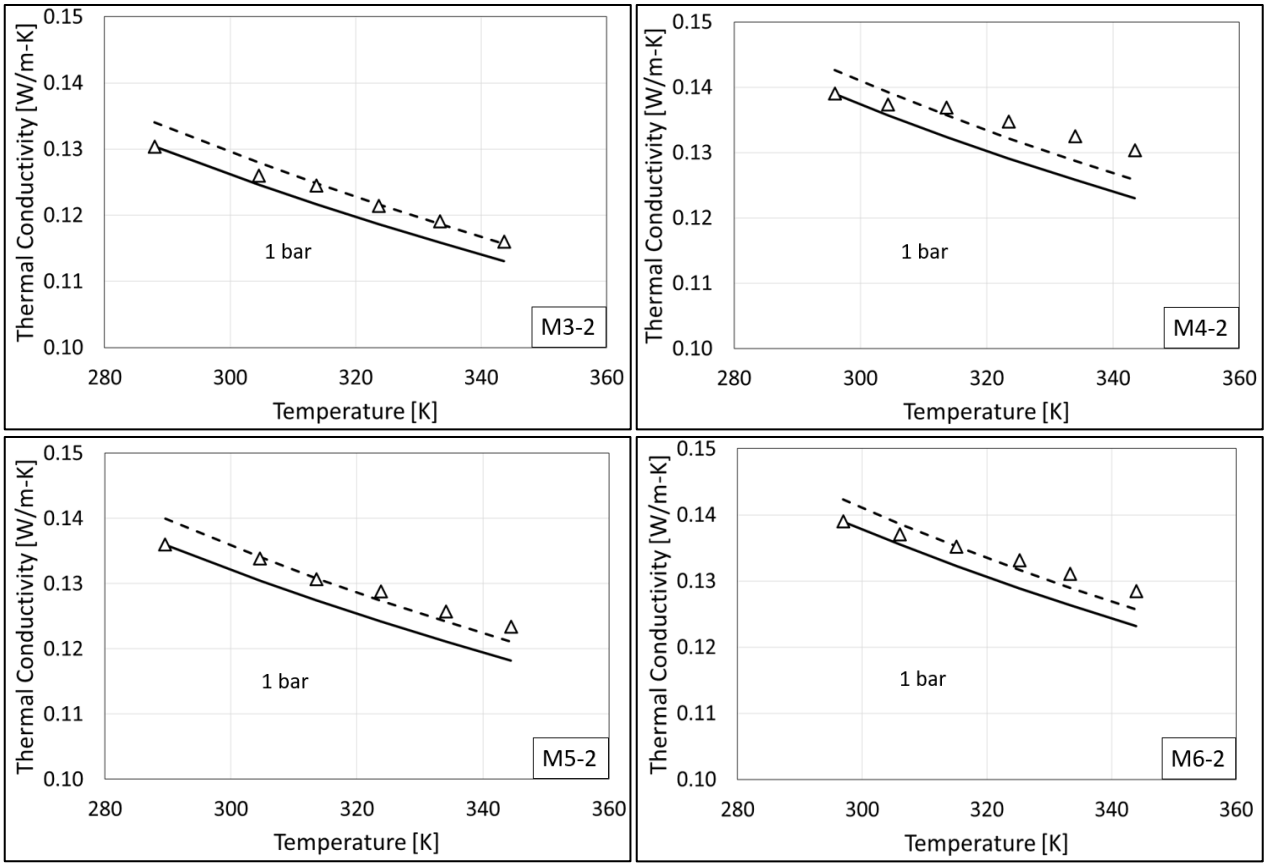

Figure 4.3. Pseudo-component thermal conductivity predictions compared to experimental data [255] (symbols) for mixtures M3-2 to M6-2. Dashed lines show the two-parameter predictions and solid lines show the three-parameter predictions.

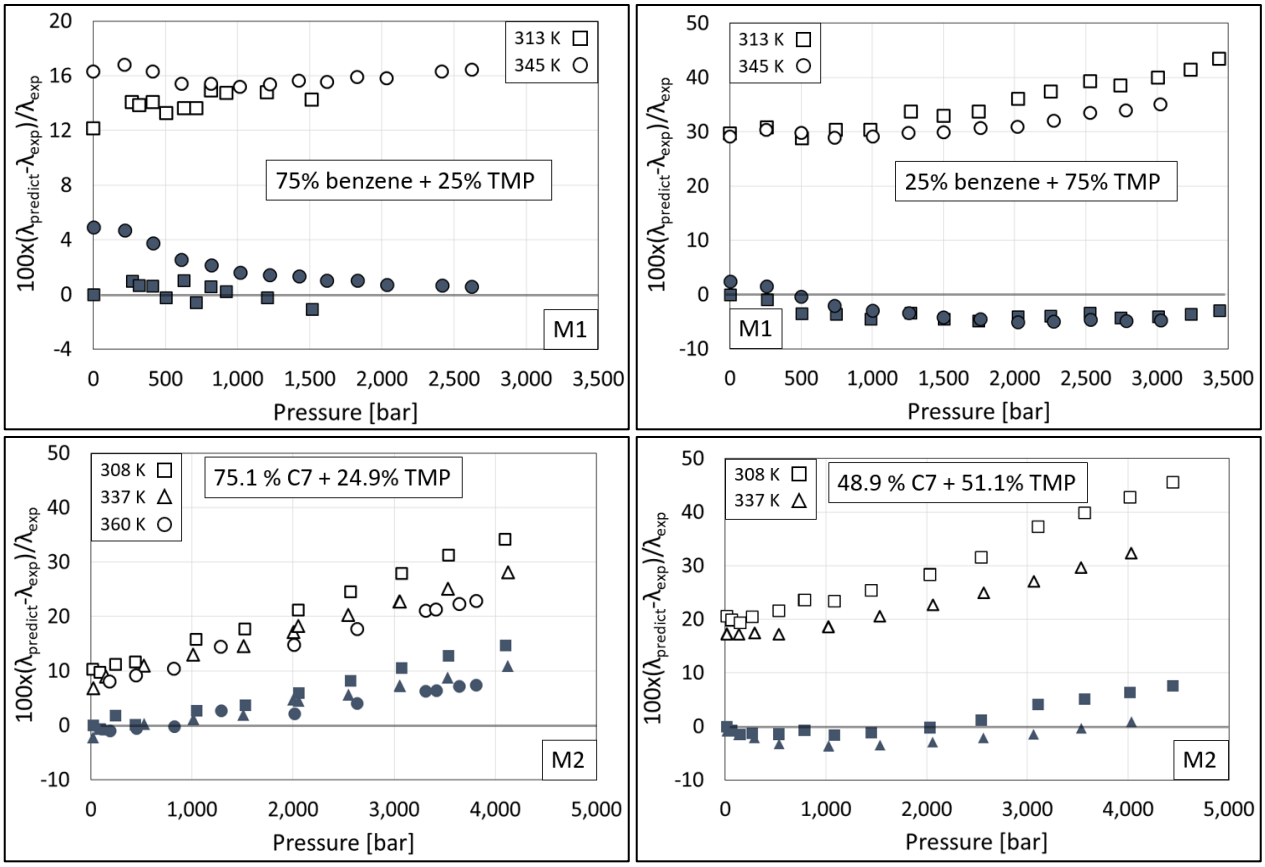

Figure 4.4. Pseudo-component thermal conductivity prediction deviations compared to experimental data [256, 257] for mixtures M1 and M2: two-parameter (open symbols) and three-parameter (filled symbols) models.

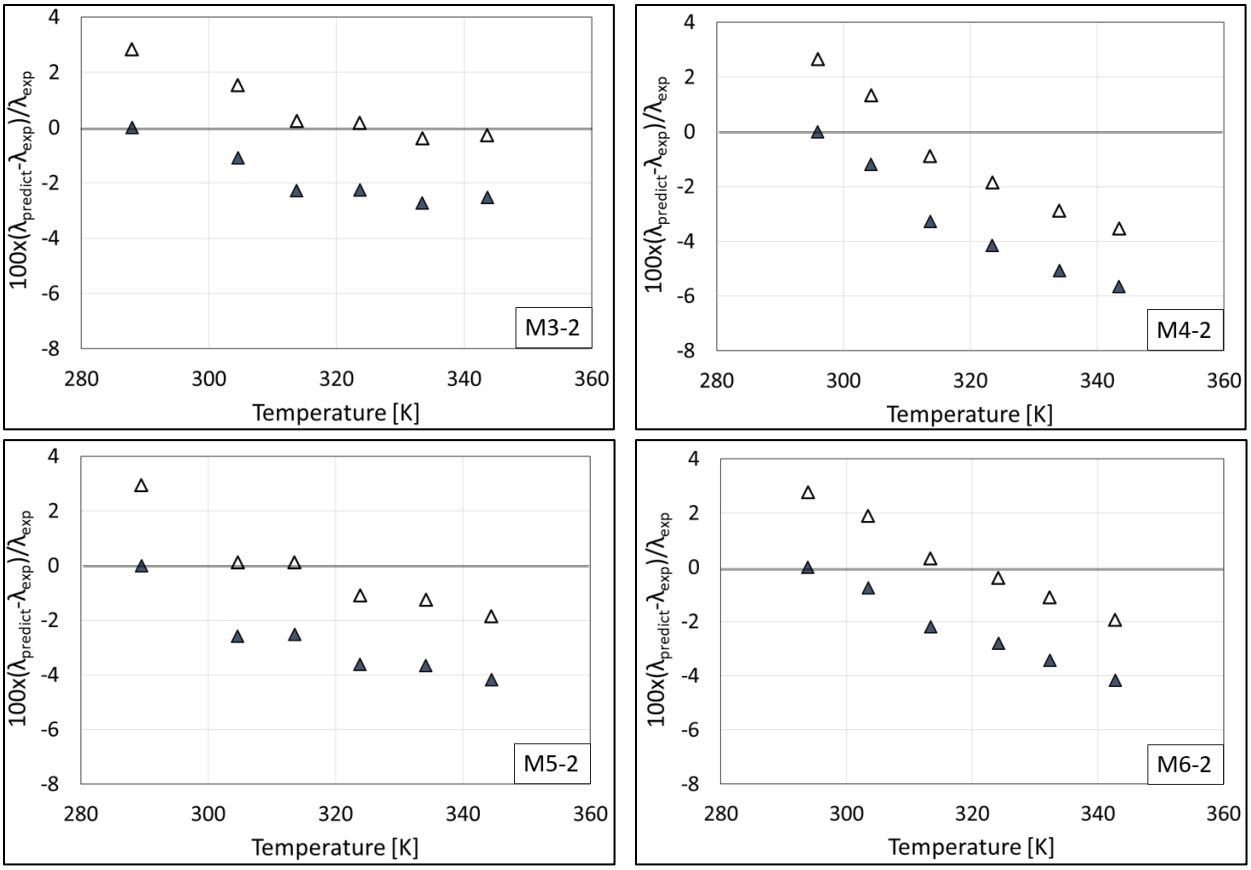

Figure 4.5. Pseudo-component thermal conductivity prediction deviations compared to experimental data [255-257] for mixtures M3-2 to M6-2 at 1 bar: two-parameter (open symbols) and three-parameter (filled symbols) models.

Table 4.4. The MAPD (%), bias (%), SD (%), and Max Deviation (%) for the pseudo-component thermal conductivity of well-characterized hydrocarbon mixtures compared to the literature [255-257].

	Two-parameter				Three-parameter			
	MAPD	Bias	SD	Max Deviation	MAPD	Bias	SD	Max Deviation
M1	20.0	20.0	7.9	45.6	3.7	2.6	3.7	15.2
M2	24.6	24.6	9.8	43.4	2.4	-1.3	1.7	5.1
M3	1.2	0.5	0.9	2.8	1.9	-1.9	1.3	4.1
M4	2.0	-0.8	1.0	3.5	2.9	-2.9	2.0	5.6
M5	1.3	0.1	0.9	2.9	2.3	-2.3	1.4	4.2
M6	1.3	0.2	0.9	2.8	2.2	-2.2	1.4	4.2

The pseudo-component technique developed in this study captures the effects of temperature and pressure for all mixtures. Figures 4.2 and 4.4 show that pseudo-component thermal conductivities are predicted for mixtures M1 and M2 with MAPDs of 20 and 25%, respectively, using the two-parameter model. The MAPDs for thermal conductivity predictions for all compositions of mixtures M1 and M2, shown in the appendix (Section 4.4), increase as the concentration of TMP, an iso-alkane, increases. Figures 4.3 and 4.5 show that more accurate thermal conductivities with MAPDs less than 2% are predicted at atmospheric pressure and a range of temperatures using the two-parameter model for mixtures M3-M6, composed of only n-alkanes. Their better predictions could be due the fact that the correlations in the technique were fit to ambient pressure data. Furthermore, since $Z = 0$ for n-alkane mixtures, the thermal conductivity coefficients in Eqs. 4.6-4.9 reduce to the correlations for n-alkanes, leading to reduced error, as there is no mixing with the PNA correlations.

It should be noted that the compounds present in mixtures M1 and M2 (nC7 with MW = 100.21 g/mol, benzene with MW = 78.11 g/mol, and TMP with MW = 114.23 g/mol) are at the

extreme lower MW bounds of the fitted PC-SAFT parameter and thermal conductivity coefficient correlations. The two-parameter pseudo-component model may not accurately represent the PC-SAFT parameters and thermal conductivity coefficients for mixtures with such low MW compounds. Note that the definition of DoU (Eq. 2.13) does not distinguish between normal and iso-alkanes, which could be an additional reason for thermal conductivity prediction deviations for mixtures containing significant amounts of iso-alkanes. Figures 4.2 and 4.3 show that inclusion of a single thermal conductivity data point at a chosen reference state to fit *B* improves the predictions for mixtures M1 and M2 containing large amounts of iso-alkanes. Thermal conductivity is predicted for hydrocarbon mixtures using the three-parameter model with an MAPD of 3.0% for all compositions of all investigated mixtures. This MAPD is comparable to thermal conductivity predictions for all 148 pure compounds studied by Hopp and Gross [227], who reported a 4.2% MAPD.

4.2.2 Fuels

Gasoline, kerosene, jet, and diesel fuel fractions distilled from crude oil are complex mixtures of hydrocarbon compounds with properties and composition that vary due to quality specifications [138, 139]. Table 4.5 lists the limited HTHP thermal conductivity literature data found only for rocket propellant (RP) and jet fuels. Akhmedova-Azizova et al. [258] measured the thermal conductivity of RP1 fuel at temperatures between 293 and 598 K and pressures up to 600 bar. Bruno [259] measured the thermal conductivity of RP2 fuel over a wide range of temperatures from 300 to 550 K and pressures up to 600 bar. Xu et al. [260] reported thermal conductivity measurements of RP3 fuel at temperatures from 285 to 513 K and pressures up to 50 bar. Jia et al. [261] reported thermal conductivity of RP3 fuel at temperatures from 311 to 399 K and a single isobar at 30 bar. Bruno [262] also measured the thermal conductivity of three different jet fuels

including S-8 4734 (referred to as S-8), JP-8 3773 (referred to as JP-8), and Jet A 4658 (referred to as Jet A) at high temperatures from 270 to 470 K and pressures up to 400 bar. Table 4.6 lists the calculated MW, the HN/CN ratio, Z parameter, thermal conductivity reference experimental data point (λ_O) at the lowest reported temperature and pressure used to fit B in the three-parameter model, the PC-SAFT parameters, and the thermal conductivity coefficients for the pseudo-components for the fuels.

Table 4.5. Summary of HTHP thermal conductivity data available in the literature for rocket propellant (RP) and jet fuels.

Reference	Fuel	T_{range}/K	P_{max}/bar	Uncertainty (%)
Akhmedova-Azizova et al. [258]	RP1 [a]	293-598	600	2
Bruno [259]	RP2 [b]	300-550	600	-
Xu et al. [260], Jia et al. [261]	RP3 [c]	285-513	50	3
Bruno [262]	S-8 [d]	304-504	700	3
Bruno [262]	JP-8 [d]	303-407	600	3
Bruno [262]	Jet A [d]	303-501	400	3

[a] The number averaged MW and the HN/CN ratio of the sample are calculated from the molecular formula of a typical RP1 fuel reported by Edwards [263].

[b] The number averaged MW and the HN/CN ratio of the sample are calculated from the molecular formula of a typical RP2 fuel reported by Xu et al. [264].

[c] The number averaged MW and the HN/CN ratio of the sample are calculated from the detailed composition of the RP3 fuel reported by Deng et al. [265]. The 30 bar thermal conductivities reported by Xu et al. [260], which are measured using a double transient hot-wire method, are on average 9% different compared to data reported by Jia et al. [261] at the single pressure of 30 bar, which are measured using a steady and kinetic method, an experimental technique proposed in the article [261]. We note that all three studies [260, 261, 265] are from the same research group.

[d] The number averaged MW and the HN/CN ratio of the mixtures are reported by Won et al. [151] and Chickos and Zhao [150].

Table 4.6. The pseudo-component properties and parameters for fuels modeled in this study [258-262]. λ_o (W/m-K) is the thermal conductivity at the lowest reported temperature and pressure used to fit B, here termed B^{fit}, in the three-parameter model. The lowest temperatures and pressures for the fuels are: RP1 at 293 K and 1 bar, RP2 at 300 K and 2 bar, RP3 at 299 K and 1 bar, S-8 at 304 K and 3 bar, JP-8 at 303 K and 8 bar, and Jet A at 302 K and 2 bar.

Fuel	MW	HN/CN	Z	λ_o	m	σ (Å)	ε/k (K)	A	B	C	D	B^{fit}
RP1	167.7	1.95	0.139	0.113	5.546	3.844	246.5	0.478	-1.041	-0.027	0.009	-0.926
RP2	177.0	2.03	0.082	0.108	5.903	3.851	242.8	0.486	-1.028	-0.016	0.010	-0.893
RP3	153.0	1.93	0.163	0.126	5.065	3.839	247.6	0.470	-1.045	-0.032	0.008	-0.989
JP-8	160.0	1.95	0.144	0.116	5.300	3.842	246.6	0.474	-1.041	-0.028	0.009	-0.948
S-8	154.5	2.14	0.028	0.117	5.241	3.851	238.7	0.483	-1.004	-0.006	0.012	-0.934
Jet A	157.5	1.96	0.140	0.112	5.227	3.842	246.2	0.474	-1.039	-0.027	0.009	-0.933

Figures 4.6 and 4.7 present the thermal conductivity predictions for the RP and jet fuels at different temperatures and pressures, respectively. Figures 4.8 and 4.9 show the thermal conductivity prediction deviations for these fuels. Table 4.7 summarizes the statistical metrics of the thermal conductivity predictions for the six fuels. The pseudo-component technique captures the effects of both temperature and pressure on thermal conductivity with an MAPD of 14.3% using the two-parameter model across all temperatures and pressures for all fuels. Two sets of experimental data are reported in the literature for the thermal conductivity of RP3 at 30 bar [260, 261]. Using the two-parameter model, thermal conductivity is predicted with 1% MAPD compared to the data reported by Jia et al. [261] and 9% MAPD compared to data reported by Xu et al. [260]. There is a 9% difference between these two sets of experimental measurements, which were obtained using two different techniques (double transient hot wire and steady and kinetic methods).

It should be noted that Jia et al. [261] proposed the steady and kinetic method in the same article as the RP3 measurements at 30 bar.

Typical RP and jet fuels contain between 10 to 40 weight percent iso-alkanes [263, 264, 266-268] and also contain amounts of alkylated compounds [260, 264, 267, 268] including alkylated cyclohexanes and alkylated benzenes. The pseudo-component technique does not distinguish the differences between normal and iso-alkanes. Since $Z = 0$ for both normal and iso-alkanes, the effect of the iso-alkanes and alkylated compounds (branching) in the fuel on the thermal conductivity may not be accurately captured using the two-parameter pseudo-component model for the fuels investigated in this study. By including a single thermal conductivity data point as a third input, predictions are significantly improved with an MAPD of 2.0%, which is within the experimental uncertainty of 3% reported in the literature [258-262]. RP3 thermal conductivities at 30 bar are predicted less accurately using the three-parameter model when comparing to the Jia et al. [261] data (8.3 % MAPD) than the Xu et al. [260] data (2.3 % MAPD) .

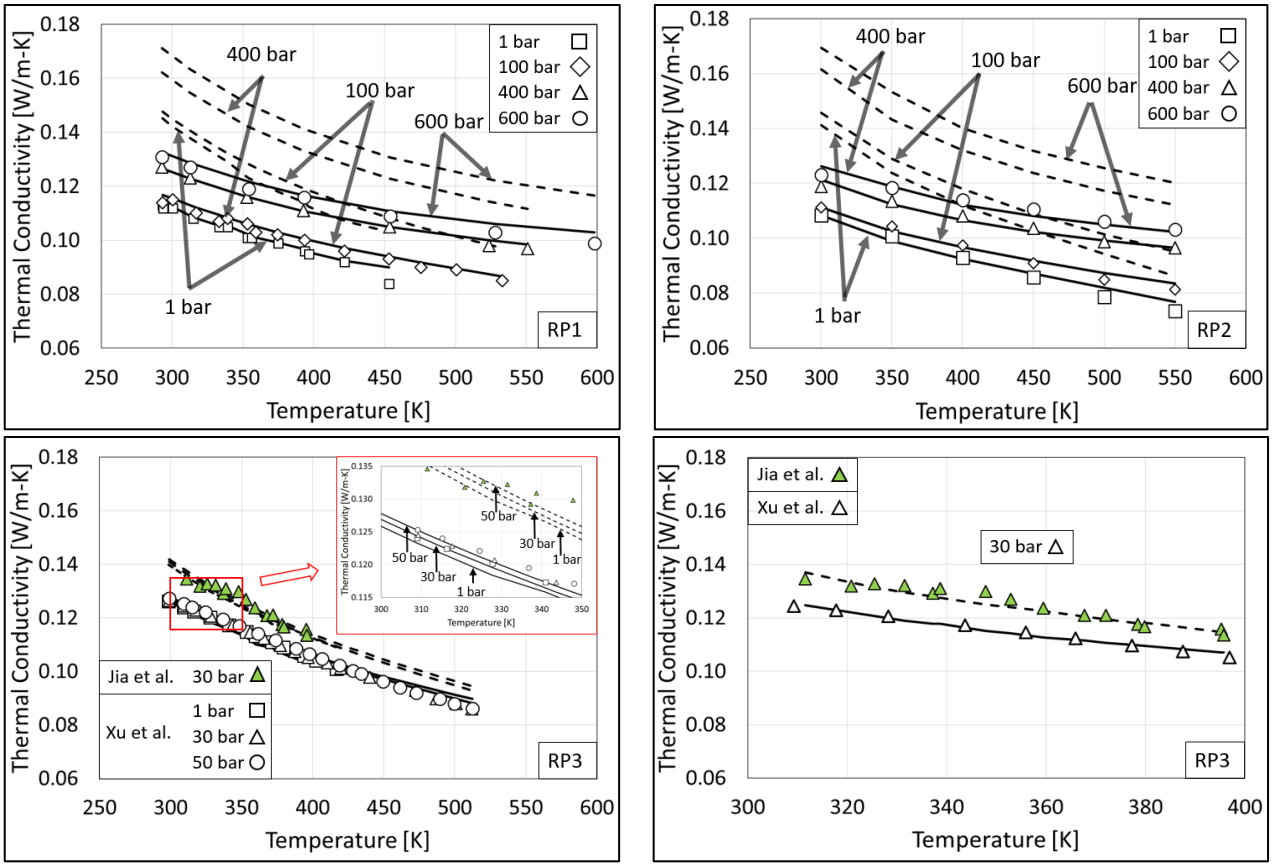

Figure 4.6. Pseudo-component thermal conductivity predictions compared to experimental data [258-261] (symbols) for rocket propellant (RP) fuels listed in Table 4.6. Dashed lines show the two-parameter predictions, and solid lines show the three-parameter predictions. A separate figure is shown for the RP3 thermal conductivities at 30 bar, since two data sets [260, 261] were reported in the literature. Note that the x-axis scale is different in the figure for RP3 at 30 bar.

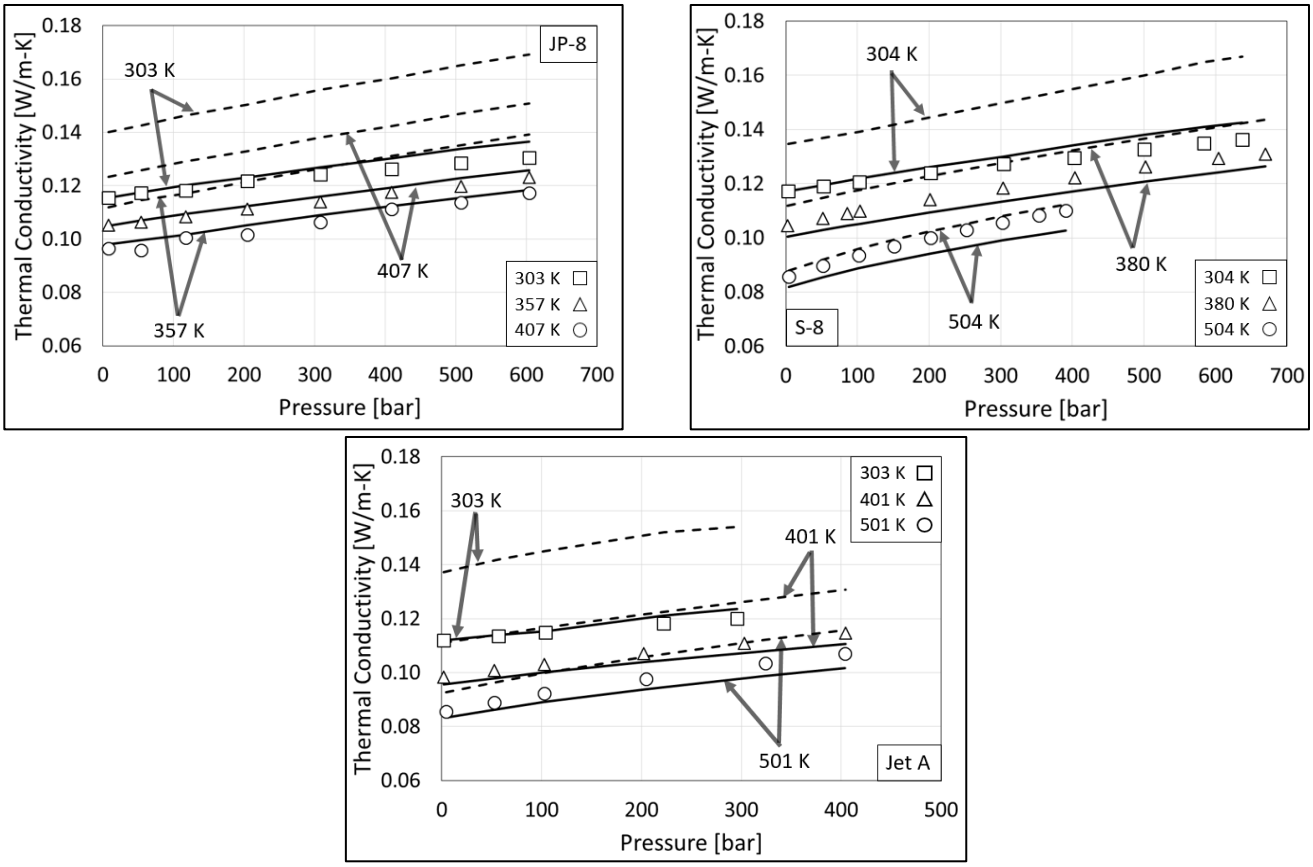

Figure 4.7. Pseudo-component thermal conductivity predictions compared to experimental data [262] (symbols) for jet fuels listed in Table 4.6. Dashed lines show the two-parameter predictions, and solid lines show the three-parameter calculations. Note that the x-axis scale is different in the figure for Jet A.

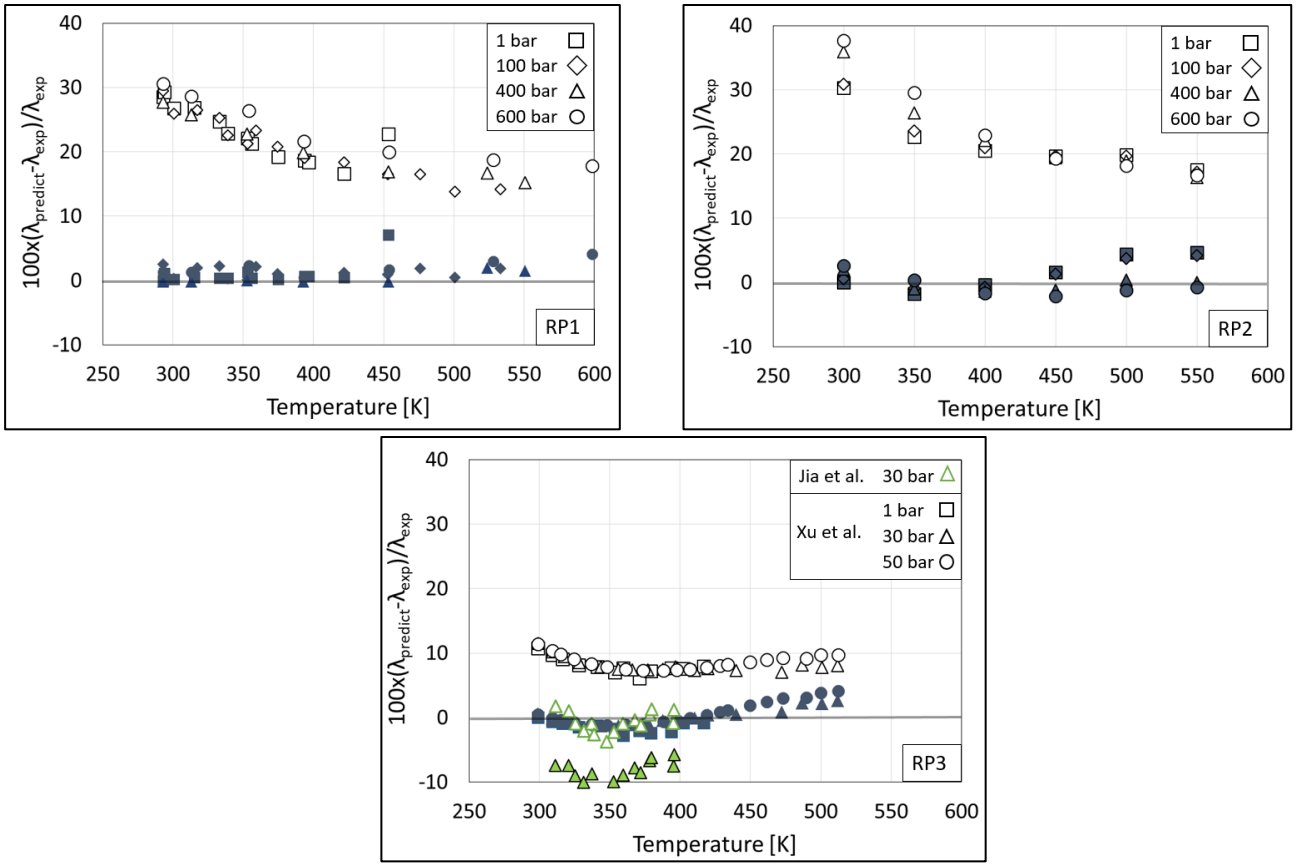

Figure 4.8. Pseudo-component thermal conductivity predictions deviations compared to experimental data [258-261] for rocket propellant (RP) fuels listed in Table 4.6: two-parameter (open symbols) and three-parameter (filled symbols) models.

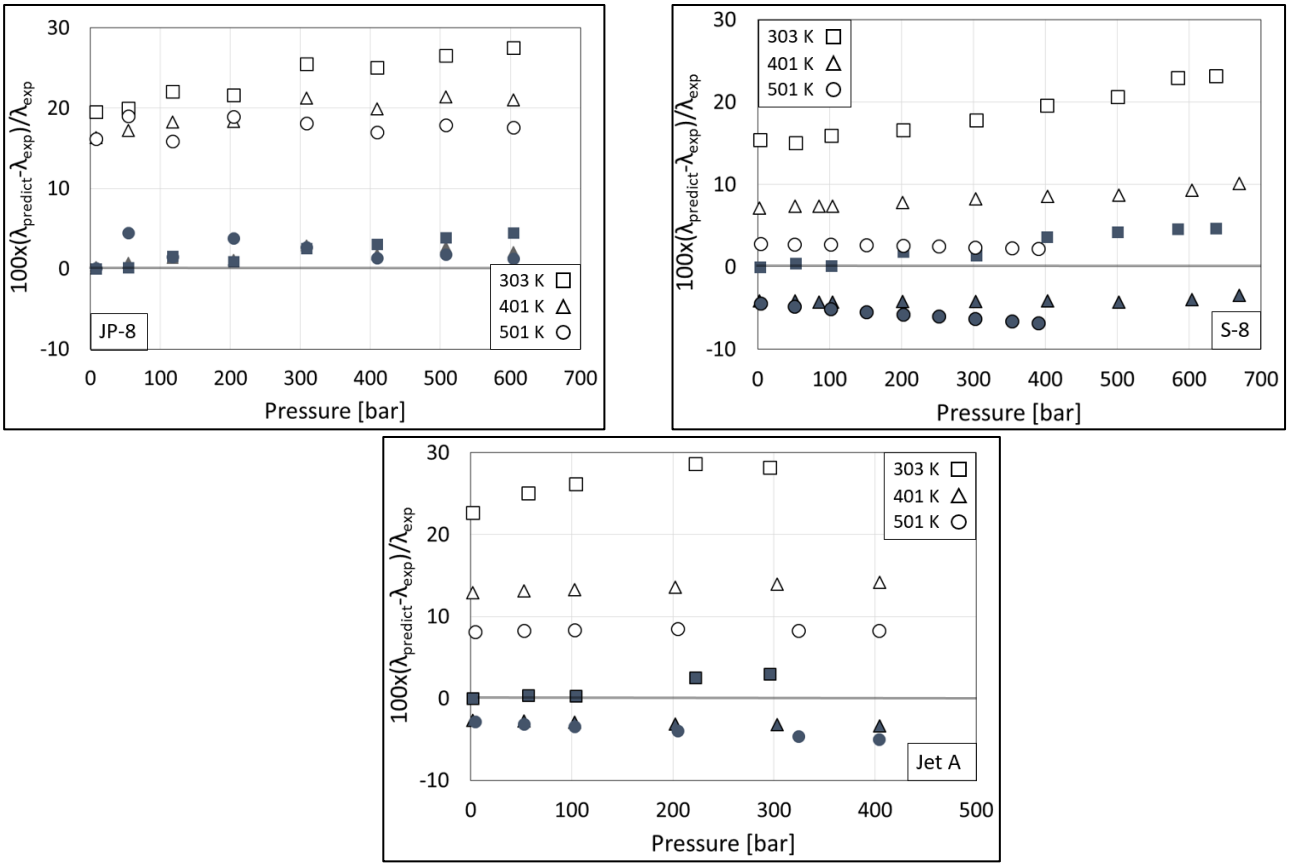

Figure 4.9. Pseudo-component thermal conductivity predictions deviations compared to experimental data [262] for jet fuels listed in Table 4.6: two-parameter (open symbols) and three-parameter (filled symbols) models. Note that the x-axis scale is different in the figure for Jet A.

Table 4.7. The MAPD (%), bias (%), SD (%), and Max Deviation (%) for pseudo-component thermal conductivity predictions of rocket propellant (RP) and jet fuels listed in Table 4.6 [258-262] at temperatures from 293 to 598 K and pressures up to 700 bar.

	Two-parameter				Three-parameter			
	MAPD	Bias	SD	Max Deviation	MAPD	Bias	SD	Max Deviation
RP1	22.3	22.3	5.4	33.8	1.1	0.5	1.2	6.2
RP2	23.6	23.6	6.7	40.1	1.4	0.0	0.9	3.5
RP3	7.3	7.0	3.5	11.6	2.3	-1.2	2.8	11.2
S-8	13.3	13.3	4.1	22.5	2.2	-0.9	1.4	4.6
JP-8	21.2	21.2	3.6	29.7	1.8	1.8	1.3	4.7
Jet A	15.4	15.4	5.9	30.3	3.1	-2.8	1.5	5.6

4.3 Conclusion

A PC-SAFT, pseudo-component technique based on entropy scaling was presented to predict the thermal conductivity of well-characterized hydrocarbon mixtures, rocket propellant fuels, and jet fuels up to high temperature and high pressure (HTHP) conditions. The two experimental mixture properties required to predict thermal conductivity were the number average molecular weight and the hydrogen-to-carbon ratio. Correlations for the model parameters were developed from pure component thermal conductivity coefficients fit at atmospheric pressure. However, the predicted thermal conductivities deviated from the experimental data for mixtures containing significant amounts of iso-alkanes. A third input, the thermal conductivity at a single low-temperature, low-pressure reference state was incorporated in the model to improve the predictions for the mixtures of interest. Although the model was developed from atmospheric pressure data, accurate predictions were obtained when the technique was applied to well-characterized hydrocarbon mixtures and fuels up to HTHP conditions. The method was predictive

and did not require measurement of or fitting to HTHP thermal conductivity data. Thermal conductivities were predicted for fuels at conditions from 285 to 598 K and up to 700 bar using the three-parameter pseudo-component technique with a mean absolute percent deviation of 2.0%, which is within 3%, the reported uncertainty of the experimental measurements.

4.4 Appendix for Chapter 4

4.4.1 Pseudo-component parameters for well-characterized hydrocarbon mixtures

Tables 4.8 and 4.9 list the calculated MW (g/mol), HN/CN ratio, Z parameter, thermal conductivity experimental data point (λ_o) at the lowest reported temperature and pressure used to fit B in the three-parameter model, the PC-SAFT parameters, and the thermal conductivity coefficients for the pseudo-components for all concentrations of all hydrocarbon mixtures [255-257] listed in Table 4.3.

Table 4.8. Pseudo-component properties (average MW, the HN/CN ratio, the PC-SAFT parameter, and the thermal conductivity coefficients) and mean absolute percent deviations (MAPDs (%)) for predictions compared to the literature. λ_o (W/m-K) is the thermal conductivity data point at the lowest reported temperature and pressure used to fit B, here termed B^{fit}, in the three-parameter model for all compositions of mixtures M1-M5 [255-257]

Mixture			MW	HN/CN	Z	λ_o	m	σ (Å)	ε/k (K)	A	B	C	D	MAPD	B^{fit}	MAPD$^{\text{fit}}$
	X_{benzene}	X_{TMP}														
M1	0.75	0.25	87.1	1.38	0.717	0.117 at 313 K and 1 bar	2.861	3.762	265.1	0.367	-1.220	-0.141	-0.004	14.6	-1.165	1.3
M1	0.25	0.75	105.2	2.00	0.178	0.098 at 313 K and 1 bar	3.557	3.821	245.3	0.449	-1.038	-0.037	0.008	33.2	-0.904	3.3
	X_{nC7}	X_{TMP}														
M2	0.489	0.511	107.4	2.27	0	0.104 at 308 K and 15 bar	3.737	3.838	236.0	0.473	-0.975	-0.001	0.013	24.5	-0.877	2.0

M2	0.744	0.256	103.8	2.28	0	0.112 at 308 K and 21 bar	3.620	3.836	235.9	0.472	-0.973	-0.001	0.013	17.4	-0.923	4.6
M2	0.751	0.249	103.7	2.28	0	0.112 at 308 K and 21 bar	3.617	3.836	235.9	0.472	-0.973	-0.001	0.013	17.8	-0.921	4.7
	X_{nC7}	X_{nC11}														
M3-1	0.75	0.25	114.2	2.26	0	0.126 at 296 K and 1 bar	3.958	3.841	236.2	0.475	-0.978	-0.001	0.013	1.3	-0.965	1.6
M3-2	0.50	0.50	128.3	2.23	0	0.130 at 288 K and 1 bar	4.416	3.847	236.5	0.479	-0.984	-0.001	0.013	0.9	-0.971	1.8
M3-3	0.25	0.75	142.3	2.21	0	0.133 at 289 K and 1 bar	4.871	3.851	236.7	0.483	-0.990	-0.001	0.013	1.4	-0.978	2.2
	X_{nC11}	X_{nC16}														
M4-1	0.75	0.25	173.8	2.17	0	0.137 at 295 K and 1 bar	5.895	3.858	237.1	0.491	-1.003	-0.001	0.013	2.0	-0.992	2.9
M4-2	0.50	0.50	191.4	2.15	0	0.139 at 296 K and 1 bar	6.467	3.861	237.3	0.496	-1.011	-0.001	0.013	2.2	-0.998	3.2
M4-3	0.25	0.75	208.9	2.14	0	0.142 at 297 K and 1 bar	7.036	3.864	237.4	0.501	-1.018	-0.001	0.013	1.8	-1.008	2.6
	X_{nC7}	X_{nC16}														
M5-1	0.75	0.25	131.8	2.25	0	0.127 at 298 K and 1 bar	4.530	3.848	236.5	0.480	-0.985	-0.001	0.013	1.2	-0.971	1.8
M5-2	0.50	0.50	163.3	2.21	0	0.136 at 290 K and 1 bar	5.554	3.856	237.0	0.488	-0.999	-0.001	0.013	1.2	-0.985	2.8
M5-3	0.25	0.75	194.9	2.17	0	0.141 at 294 K and 1 bar	6.581	3.862	237.3	0.497	-1.012	-0.001	0.013	1.5	-1.000	2.4

X is mole fraction

Table 4.9. Pseudo-component properties (Average MW, the HN/CN ratio, the PC-SAFT parameter, and the thermal conductivity coefficients) and mean absolute percent deviations (MAPDs (%)) for predictions compared to the literature. λ_o (W/m-K) is the thermal conductivity data point at the lowest reported temperature and pressure (1 bar) used to fit B, here termed B^{fit}, in the three-parameter model for all compositions of mixture M6 [255]

Mixture				MW	HN/CN	Z	λ_o	m	σ (Å)	ε/k (K)	A	B	C	D	MAPD	B^{fit}	MAPD^{fit}
	X_{nC7}	X_{nC11}	X_{nC16}														
M6-1	0.599	0.300	0.101	129.8	2.24	0	0.128 at 294 K	4.465	3.847	236.5	0.479	-0.984	-0.001	0.013	1.2	-0.970	2.0
M6-2	0.100	0.299	0.601	192.9	2.16	0	0.139 at 297 K	6.516	3.861	237.3	0.496	-1.011	-0.001	0.013	1.4	-0.999	2.4
M6-3	0.334	0.333	0.333	160.9	2.20	0	0.134 at 294 K	5.476	3.855	237.0	0.488	-0.998	-0.001	0.013	1.4	-0.985	2.2

X is mole fraction

4.4.1 Thermal conductivity of PNA derivatives

Figure 4.10 shows the calculated thermal conductivities for benzene, naphthalene, and phenanthrene using the models of Briggs [251] and Gharagheizi et al. [239] at 1 bar and a range of temperatures, which differ by up to 8, 8, and 9% for benzene, naphthalene, and phenanthrene, respectively.

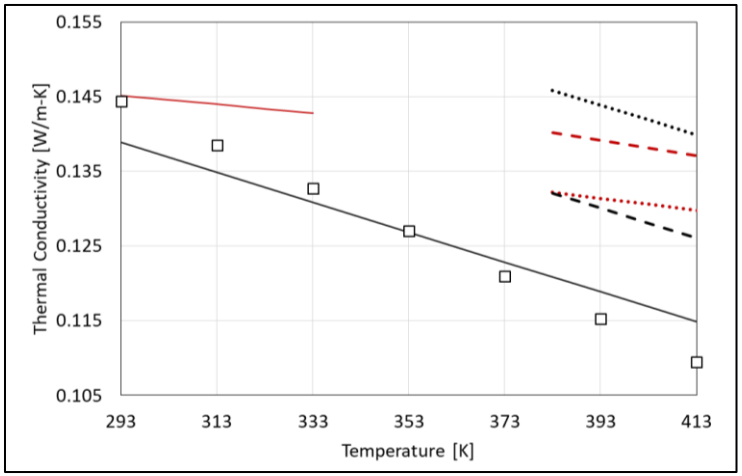

Figure 4.10. Comparison of calculated thermal conductivities at 1 bar for benzene (solid lines), naphthalene (dashed lines), and phenanthrene (dotted lines) using the correlations reported by Briggs [251] (red lines) and Gharagheizi et al. [239] (black lines). The temperature ranges of the calculated thermal conductivities shown here cover the limited range listed for the respective correlations. The open squares (□) represent experimental benzene data reported in the Dortmund Data Bank (DDB) [252]. To the best of our knowledge there are no available data for naphthalene or phenanthrene.

The thermal conductivity technique is developed to work for simple and complex hydrocarbon mixtures. However, it is interesting to compare performance for pure components such as benzene, toluene, and xylene. Figure 4.11, shows the atmospheric pressure thermal conductivities of benzene, toluene and xylene, which are predicted with MAPDs of 2.4, 9.5, and 11.5%, respectively, when using the two-parameter model, and MAPDs of 3.2, 1.6, and 1.5%, respectively, when using the three-parameter model. Because n-alkanes and PNAs are used as the two numerical bounds for the parameters and coefficients, the predictions using the two-parameter model are accurate for benzene, similar to the observation for mixtures M3 to M6. Furthermore, since both toluene and xylene are branched compounds, it is expected to observe less accurate predictions for these molecules when using the two-parameter model compared to the three-parameter model.

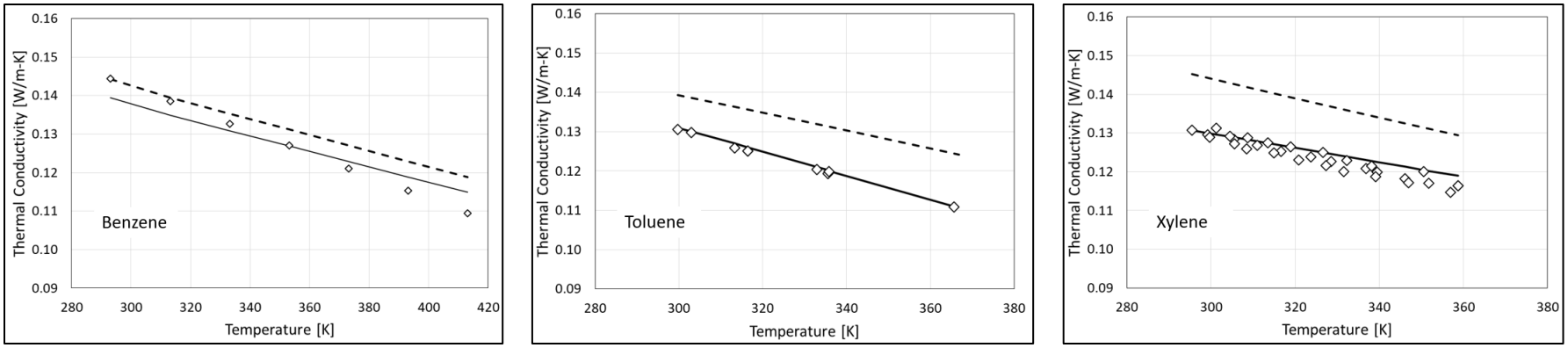

Figure 4.11. Pseudo-component thermal conductivity predictions compared to experimental data obtained from DDB [252], Assael et al. [269] and Ramires et al. [270] (symbols) for benzene, toluene, and isomers of xylene, respectively, at atmospheric pressure and a range of temperatures. Dashed lines show the two-parameter predictions, and solid lines show the three-parameter predictions. Note that the measurements for different isomers of xylene are lumped together. Note that the x-axis is different in the plot for benzene.

5. Chapter 5: Further Analysis of the Viscosity Pseudo-Component Technique

5.1 Strengths and weaknesses of the viscosity pseudo-component technique

5.1.1 Sensitivity of the entropy scaling approach to PC-SAFT parameters

Lötgering-Lin and Gross [171] calculated entropies required in the entropy scaling approach using the PC-SAFT EoS and used the GC-PC-SAFT parameters of Sauer et al. [58] to fit their GC viscosity coefficients. To investigate the sensitivity of the entropy scaling approach to GC-PC-SAFT parameters, we selected different sets of GC parameters (i.e., Tihic et al. [61], Burgess et al. [53], and Sauer et al. [58]) to calculate the viscosity for n-decane (n-$C_{10}H_{22}$) at different temperatures and pressures. Table 5.1 lists the different approaches used for calculating the PC-SAFT parameters and MAPDs of predictions achieved using these approaches compared to the measurements reported by Caudwell et al. [206] at temperatures from 298 to 373 K and pressures up to 1,917 bar. To be consistent within the entropy scaling technique, the same PC-SAFT parameters are used for calculating entropy and the viscosity coefficients.

Table 5.1. The approaches used to calculate the PC-SAFT parameters of n-$C_{10}H_{22}$ and MAPD of viscosity predictions compared to the data reported by Caudwell et al. at temperatures from 298 to 373 K and pressures up to 1,909 bar

Approach for PC-SAFT parameters	m	σ (Å)	ε/k (K)	A	B	C	D	MAPD (%)
GC parameters of Burgess et al. [53]	6.753	3.695	231.8	-0.745	-3.173	-0.586	-0.125	26.6
GC parameters of Tihic et al. [61]	4.363	3.921	246.9	-0.794	-3.130	-0.586	-0.125	5.2
GC parameters of Sauer et al. [58]	4.872	3.849	236.7	-0.773	-3.112	-0.586	-0.125	2.3

Here, as expected from [171], we noticed that the parameters used in the original fitting of Lötgering-Lin and Gross [171] (the GC-PC-SAFT parameters of Sauer et al. [58]) provided the best viscosity predictions. When using different PC-SAFT parameters (e.g., GC-PC-SAFT parameters of Tihic et al. [61]) in the entropy scaling approach, if comparable residual entropies and PC-SAFT parameters are used in the calculations, the predicted viscosities will not differ significantly compared to the predictions obtained using the original Lötgering-Lin and Gross [171] approach, which uses the GC-PC-SAFT parameters of Sauer et al. [58]. However, the GC-PC-SAFT parameters of Burgess et al. [53], fit to high pressure density data, can result in significantly different values of the calculated residual entropy compared to when using the Sauer et al. [58] or Tihic et al. [61] parameters, which will lead to greater deviation in the predicted viscosity.

5.1.2 Application of the viscosity pseudo-component technique to mixtures containing very light or heavy compounds

In section 3.2.1, the pseudo-component technique was used to study mixtures containing compounds present in typical diesel fuels as reported by Aquing et al. [25]. However, the capability of the pseudo-component technique to predict HTHP viscosity for selected mixtures, which contain very light or heavy compounds compared to the compounds found in diesel fuels [25], is further analysed in this section. Table 5.2 lists the molar compositions of selected mixtures used to evaluate the two-parameter and three-parameter viscosity pseudo-component techniques. Dymond et al. [271] measured viscosity of mixtures (referred to as M1) containing toluene (92.14 g/mol) and n-hexane (nC6) (86.18 g/mol) for three different compositions at temperatures from 298 to 373 and pressures up to 5,000 bar. Kumagai et al. [272] reported viscosity measurements of mixtures

(referred to as M2) containing n-butane (nC4) (58.12 g/mol) and squalane (iC30) (422.83 g/mol) for six different compositions up to 333 K and 300 bar.

Table 5.2. Molar composition of the mixtures studied in this work [271, 272].

	MW (g/mol)	M1	M2
n-butane	58.12	-	0.247-0.846
n-hexane	86.18	0.250-0.750	-
toluene	92.14	balance	-
squalane	422.83	-	balance

Figures 5.1 and 5.2 show the viscosity predictions using the two-parameter and three-parameter models and deviations from experiment, respectively, for the hydrocarbon mixtures reported by Dymond et al. [271] and Kumagai et al. [272]. For brevity, only one composition for each mixture is included in the figures. For mixture viscosities measured by Dymond et al. [271], only the data for mixture composition 0.5 mole fraction nC6 and 0.5 mole fraction toluene (referred to as M1-2) are shown in the figures. For mixture viscosities measured by Kumagai et al. [272], only the data for mixture composition containing 0.456 mole fraction nC4 and 0.544 mole fraction iC30 (referred to as M2-3) are shown in the figures.

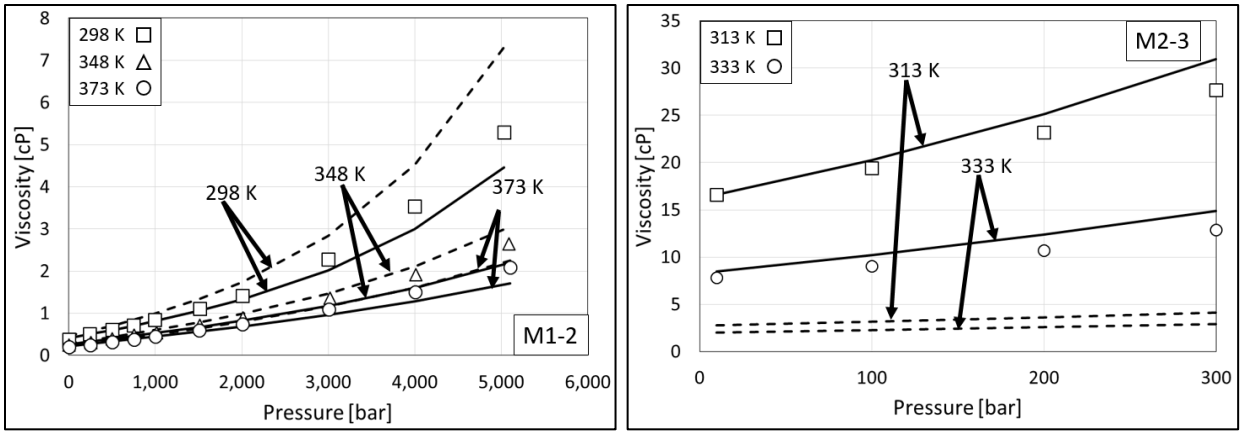

Figure 5.1. Pseudo-component viscosity predictions using the two-parameter (dashed lines) and three-parameter (solid lines) models compared to experimental data [271, 272] (symbols) for mixtures M1-2 (with 0.5 mole fraction nC6 and 0.5 mole fraction toluene) and M2-3 (with 0.456 mole fraction nC4 and 0.544 mole fraction iC30). Note that the y-axis and x-axis scales are different in each figure.

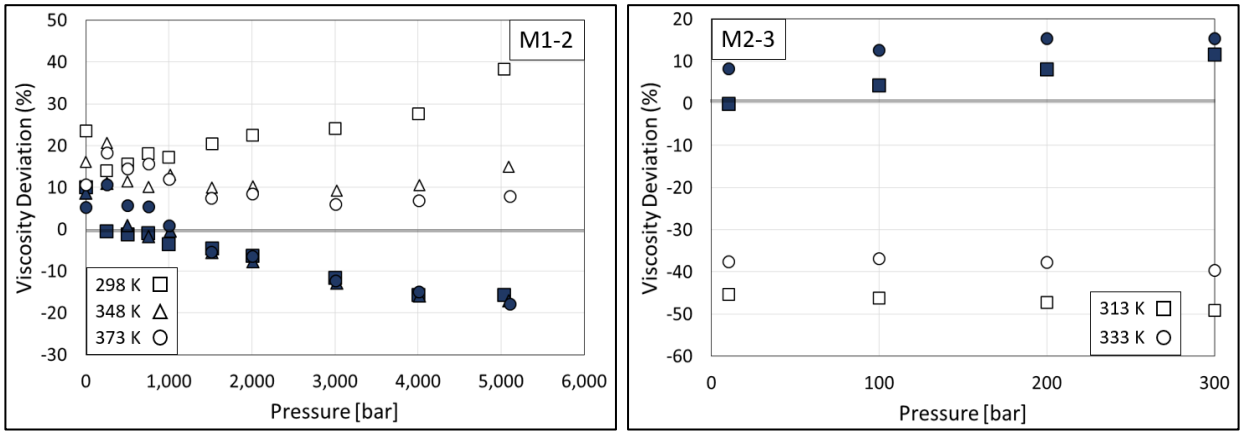

Figure 5.2. Pseudo-component viscosity deviations compared to experimental data [271, 272] for mixtures M1-2 (with 0.5 mole fraction nC6 and 0.5 mole fraction toluene) and M2-3 (with 0.456 mole fraction nC4 and 0.544 mole fraction iC30): two-parameter (open symbols) and three-parameter (filled symbols) models. Note that the y-axis and x-axis scales are different in each figure.

However, Table 5.3 lists the pseudo-component properties, the reference viscosity, the PC-SAFT parameters, the viscosity coefficients, and MAPDs for viscosity predictions of all compositions of mixtures M1 and M2. For mixture M1, the MAPD for predictions using the two-parameter model slightly decreases from 16.6 to 12.3 % when the nC6 mole fraction increases from 0.25 to 0.75. For mixture M2, which contains high concentrations of a high MW branched alkane (i.e., squalane), less accurate predictions are achieved using the two-parameter model compared to the predictions for mixture M1. The MAPD increases with mole fraction of iC30 from 0.154 to 0.482 (mixtures M2-1 to M2-3). However, the MAPD decreases with increasing concentration of squalane for mole fractions from 0.544 to 0.753 (mixtures M2-4 to M2-6). The higher MAPDs for mixtures M2-3 and M2-5 (i.e., 60.0 and 62.2 %, respectively) compared to those for mixtures M2-4 and M2-6 (i.e., 42.4 and 32.2 %, respectively) could be due to the fact that a reference point at higher reported temperature is used to fit coefficient *D* for mixtures M2-4 and M2-6. Table 5.4 summarizes the predictions using the two-parameter and three-parameter models for mixtures M1 and M2. For mixture M1, the MAPD for predictions using the two-parameter model (i.e., 14.7%) is reduced to 6.2% when using the three-parameter model, which uses a reference data point to fit the *D* viscosity coefficient. For mixture M2, which contains high concentrations of iC30, the MAPD for predictions using the two-parameter model (i.e., 47.6 %) is significantly reduced to 6.3 % when using the three-parameter model.

Although the two-parameter model yields large deviations for viscosity predictions for mixtures with lighter and heavier compounds than are present in fuels, the three-parameter model predictions show that it is possible to accurately predict viscosity up to HTHP for these mixtures when a reference data point is used to fit the *D* viscosity coefficient.

Table 5.3. Pseudo-component properties, viscosity experimental data point (η_O) at the lowest reported temperature and pressure (1 bar for M1 and 10 bar for M2), the PC-SAFT parameters, the viscosity coefficients, and MAPDs (%) of pseudo-component viscosity predictions for mixtures M1 and M2 listed in Table 5.2 [271, 272], η_O is used to fit D, now termed D^{fit}, in the three-parameter model.

Mixture			T_{range}	MW	HN/CN	Z	η_o (cP)	m	σ (Å)	ε/k (K)	A	B	C	D	MAPD	D^{fit}	MAPD
	X_{nC6}	$X_{toluene}$	(K)														
M1-1	0.250	0.750	298-373	90.6	1.4	0.6073	0.44 at 298 K	2.974	3.770	263.8	-0.631	-2.573	-0.429	-0.084	16.6	-0.073	5.1
M1-2	0.500	0.500	298-373	89.2	1.7	0.3967	0.37 at 298 K	3.007	3.790	253.6	-0.640	-2.580	-0.425	-0.080	15.0	-0.068	7.7
M1-3	0.750	0.250	298-373	87.7	2.0	0.1945	0.32 at 298 K	3.031	3.809	244.1	-0.645	-2.579	-0.421	-0.077	12.3	-0.065	7.7
	X_{nC4}	X_{iC30}															
M2-1	0.846	0.154	273-333	114.3	2.4	0	1.3 at 273 K	3.961	3.841	236.2	-0.696	-2.866	-0.501	-0.100	41.8	-0.160	6.0
M2-2	0.710	0.290	273-333	163.9	2.4	0	4.1 at 273 K	5.573	3.856	237.0	-0.784	-3.393	-0.652	-0.144	50.1	-0.223	4.4
M2-3	0.482	0.518	273-293	247.0	2.3	0	16.6 at 273 K	8.275	3.868	237.7	-0.930	-4.151	-0.905	-0.218	60.0	-0.309	9.5
M2-4	0.456	0.544	313-333	256.5	2.3	0	5.1 at 313 K	8.583	3.869	237.7	-0.947	-4.230	-0.934	-0.226	42.4	-0.308	5.1
M2-5	0.259	0.741	273-293	328.4	2.2	0	46.2 at 273 K	10.918	3.874	238.0	-1.073	-4.792	-1.153	-0.290	62.2	-0.386	11.2
M2-6	0.247	0.753	313-333	332.7	2.2	0	8.5 at 313 K	11.060	3.874	238.0	-1.081	-4.824	-1.166	-0.294	32.2	-0.351	3.7

Table 5.4. The MAPD (%), bias (%), SD (%), and Max Deviation (%) for pseudo-component viscosity predictions using the two-parameter and three-parameter models for mixtures listed in Table 5.2. Data from [271, 272].

	Two-parameter		Three-parameter	
	M1	M2	M1	M2
MAPD	14.7	47.6	6.6	6.3
Bias	14.7	-47.6	-3.6	2.9
SD	7.1	11.1	5.7	5.8
Max Deviation	44.5	72.4	21.6	26.6

5.2 Sensitivity of the pseudo-component technique to branching

As shown in Chapters 3 and 4, the viscosity and thermal conductivity techniques are not as accurate when mixtures contain high concentrations of branched alkanes. Therefore, an empirical correlation, which is a function of temperature, pressure, and three mixture properties (the number averaged MW, the HN/CN ratio, and concentration of branched alkanes), is proposed to overcome this limitation. The correlation is fit to predict the difference between the residual entropies predicted using the two-parameter model and the residual entropy fit to exactly reproduce the experimentally measured viscosity at each temperature and pressure data point. Hence, this approach improves residual entropy predictions, and it should be applicable to both the viscosity and thermal conductivity pseudo-component techniques.

5.2.1 Modifications to the viscosity pseudo-component technique

This section presents an approach to improve the viscosity predictions using corrected residual entropies. Table 5.5 lists the mixtures studied in this section. Dauge et al. [187] measured

the viscosity of binary mixtures (referred to as M3) containing 2,2,4,4,6,8,8-heptamethylnonane (i.e., iso-cetane, referred to as HMN) and n-tridecane (nC13) for seven compositions at temperatures from 293 to 353 K and pressures up to 1,000 bar. Zeberg-Mikkelsen et al. [185] measured the viscosity of ternary mixtures (referred to as M4) containing methyl-cyclohexane (MCH), decalin, and HMN for three different compositions with high concentrations of HMN at temperatures from 293 to 353 K and pressures up to 1,000 bar. Ducoulombier et al. [273] measured viscosity for a quaternary mixture (referred to as M5) containing n-decane (nC10), n-dodecane (nC12), n-tetradecane (nC14), and n-hexadecane (nC16) at temperatures from 313 to 353 K and pressures up to 1,000 bar. Zeberg-Mikkelsen et al. [188] reported the viscosity for ternary mixtures (referred to as M6) containing HMN, nC13, and methylnaphthalene (MNP) for twenty-one compositions at temperatures from 293 to 353 K and pressures up to 1,000 bar. [133, 185, 187, 188, 273]. Boned et al. [133] reported viscosity measurements for a ternary (referred to as M7) and a quinary (referred to as M8) mixture at 293 to 353 K and up to 1,000 bar.

Table 5.5. Molar composition of the mixtures considered in this study [133, 185, 187, 188, 273]

Compound	Chemical Family	M3	M4	M5	M6	M7	M8
n-heptane	n-alkanes	-	-	-	-	-	-
n-decane	n-alkanes	-	-	0.250	-	-	-
n-dodecane	n-alkanes	-	-	0.250	-	-	-
n-tridecane	n-alkanes	0.125-0.875	-	-	0.125-0.750	0.394	0.200
n-tetradecane	n-alkanes	-	-	0.250	-	-	-
n-hexadecane	n-alkanes	-	-	0.250	-	-	-
2,2,4,4,6,8,8-heptamethylnonane	iso-alkanes	balance	balance	-	0.125-0.750	-	0.162
methylcyclohexane	cyclohexanes	-	0.125-0.333	-	-	-	-
heptylcyclohexane	cyclohexanes	-	-	-	-	0.348	0.353
decalin	decalins	-	0.125-0.333	-	-	-	-
heptylbenzene	benzenes	-	-	-	-	0.258	0.156
methylnaphthalene	naphthalenes	-	-	-	balance	-	0.129

First, the residual entropies are fit to reproduce the experimentally measured viscosity using the two-parameter model for the mixtures listed in Table 5.5. Δs^*(i.e., $s^*_{\text{predicted}} - s^*_{\text{fitted}}$: the difference between the predicted (using the two-parameter model) and fitted reduced dimensionless residual entropy (see Eq. 3.4)) is calculated for the mixtures at different temperatures and pressures. For all mixtures considered in this study, Δs^* varies monotonically with temperature, pressure, and concentration of branched alkanes when the mixtures contain some concentration of branched alkane. Figure 5.3 shows that Δs^* increases with pressure and branched alkane concentration, while it decreases with increasing temperature for mixture M3. A similar dependence on temperature, pressure, and branched alkane concentration is observed for the other mixtures listed in Table 5.5. For brevity, only the mixture viscosities measured by Dauge et al. [187] at the lowest and highest temperatures are shown in Figure 5.3.

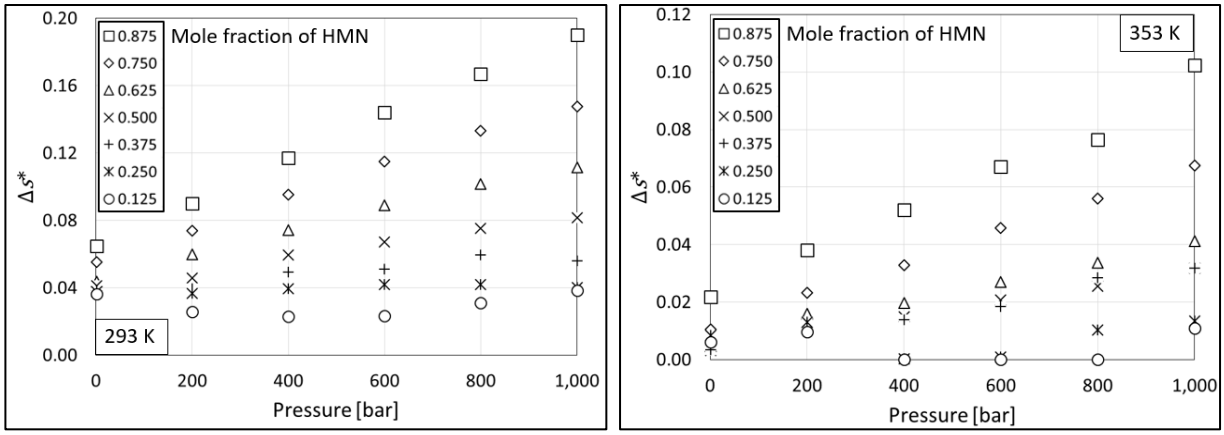

Figure 5.3. Δs^* (difference between the predicted (using the two-parameter model) and fitted reduced dimensionless residual entropy)) for different concentrations of HMN and nC13 binary mixtures at 293 and 353 K. Note that the y-axis scale is different in each figure.

Equation 5.1 is proposed to quantitatively capture the effects of temperature, pressure, and molar concentration of branched alkanes ($X_{\text{branched}-\text{alkanes}}$) on Δs^*.

$$\Delta s^* = [A_{s^*} \times (T - B_{s^*}) + C_{s^*} \times P] \times \exp(D_{s^*}/T) \quad 5.1$$

where A_{s^*}, B_{s^*}, C_{s^*}, and D_{s^*} are the coefficients needed to calculate Δs^* for mixtures and are assumed to be a linear function of the number averaged MW, the HN/CN ratio, and $X_{\text{branched alkanes}}$. It was observed that including all three mixtures properties in the correlation yielded the best predictive ability for viscosity prediction improvements for all mixtures. Table 5.6 lists the parameters in Eq. 5.1, which are fit to a training set of ~700 data points considering mixtures M3 (with HMN concentration varying from 0.875 to 0.375 mole fraction), M4, M5, M6 (M6-1 to M6-7), and M7.

Table 5.6. Parameters for Eq. 5.1 as a function of the number averaged MW, the HN/CN ratio, and $X_{b-alkanes}$: $G_{s^*} = G_{s^*_1} \times MW + G_{s^*_2} \times HN/CN + G_{s^*_3} \times X_{b-alkanes}$ when G_{s^*} is A_{s^*}, B_{s^*}, C_{s^*}, or D_{s^*} in Eq. 5.1.

G_{s^*}	$G_{s^*_1}$	$G_{s^*_2}$	$G_{s^*_3}$
A_{s^*}	-1.8163×10^{-6}	1.7068×10^{-4}	1.6145×10^{-4}
B_{s^*}	3.2832×10^{0}	-1.4095×10^{2}	-1.4018×10^{2}
C_{s^*}	2.6394×10^{-7}	-1.0013×10^{-5}	3.8451×10^{-5}
D_{s^*}	1.9597×10^{-1}	4.0696×10^{2}	-1.1123×10^{2}

Aquing et al. [25] reported the viscosity of two diesel fuels (referred to as MESR and HNA) from 323 to 423 K and up to 3,500 bar. The 12 universal parameters, listed in Table 5.6, are applied to a test set of ~800 data points considering the remaining mixtures (i.e., the mixtures not considered in fitting the parameters in Eq. 5.1) and the diesel fuels. Figures 5.4 and 5.5 show the viscosity predictions using the Δs^* correlation (referred to as correlated two-parameter) and two-parameter models and deviation plots, respectively, for selected hydrocarbon mixtures (i.e., mixtures M6-1 containing high concentration of branched alkanes (i.e., HMN) and M8) and diesel fuels (i.e., MESR and HNA). Table 5.7 lists the parameters needed in Eq. 5.1, calculated using the correlations and parameters in Table 5.6, for the hydrocarbon mixtures and diesel fuels and the MAPDs for predictions using the two-parameter, correlated two-parameter, and three-parameter models. Table 5.8 summarizes the predictions using all three models for all hydrocarbon mixtures and diesel fuels. Overall, the predictions using the correlated two-parameter model are improved compared to the predictions using the two-parameter model, whereas the predictions using the correlated two-parameter model are comparable to those achieved using the three-parameter model.

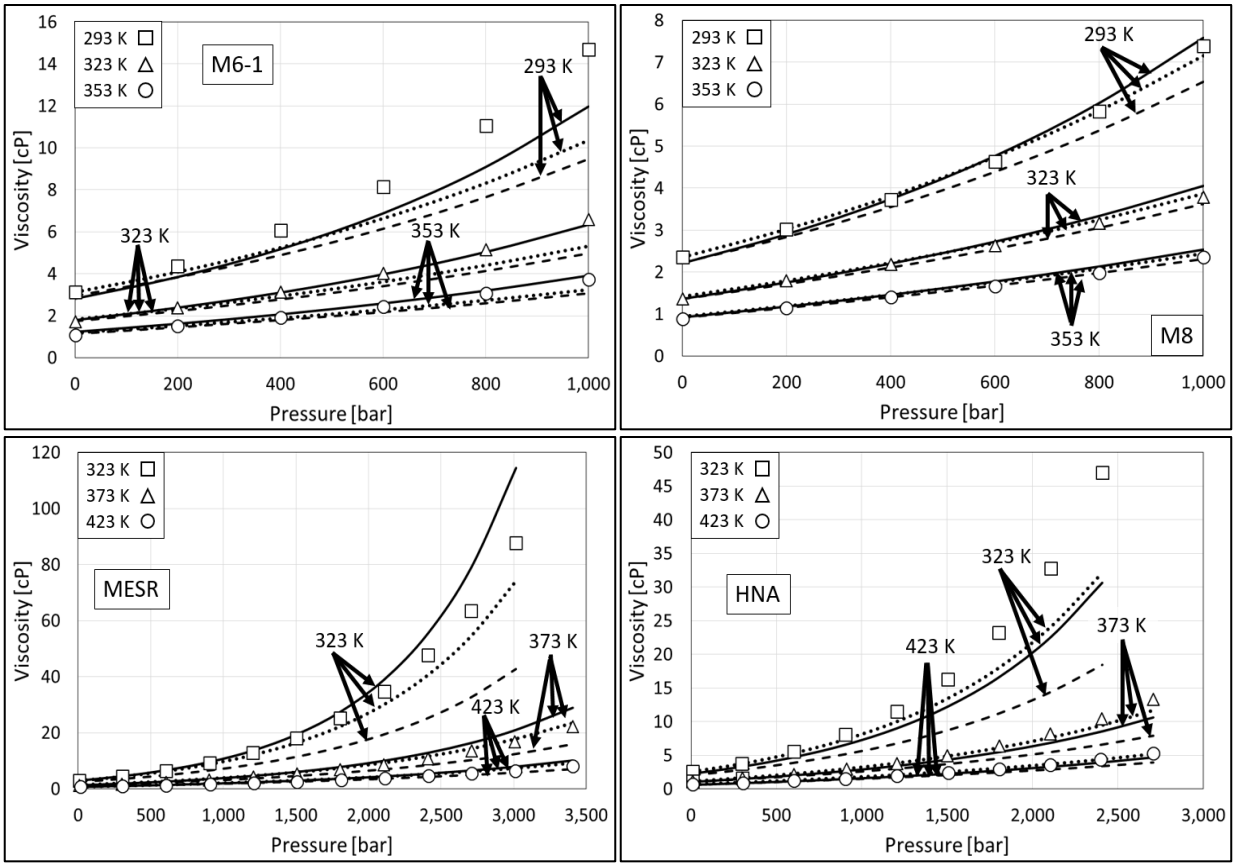

Figure 5.4. Pseudo-component viscosity predictions compared to experimental data [25, 188, 273, 274] (symbols) for selected hydrocarbon mixtures (mixtures M6-1 and M8) and diesel fuels (MESR and HNA): two-parameter (dashed lines), three-parameter (dotted lines), and correlated two-parameter (solid lines) models. Note that the y-axis and x-axis scales are different in each figure.

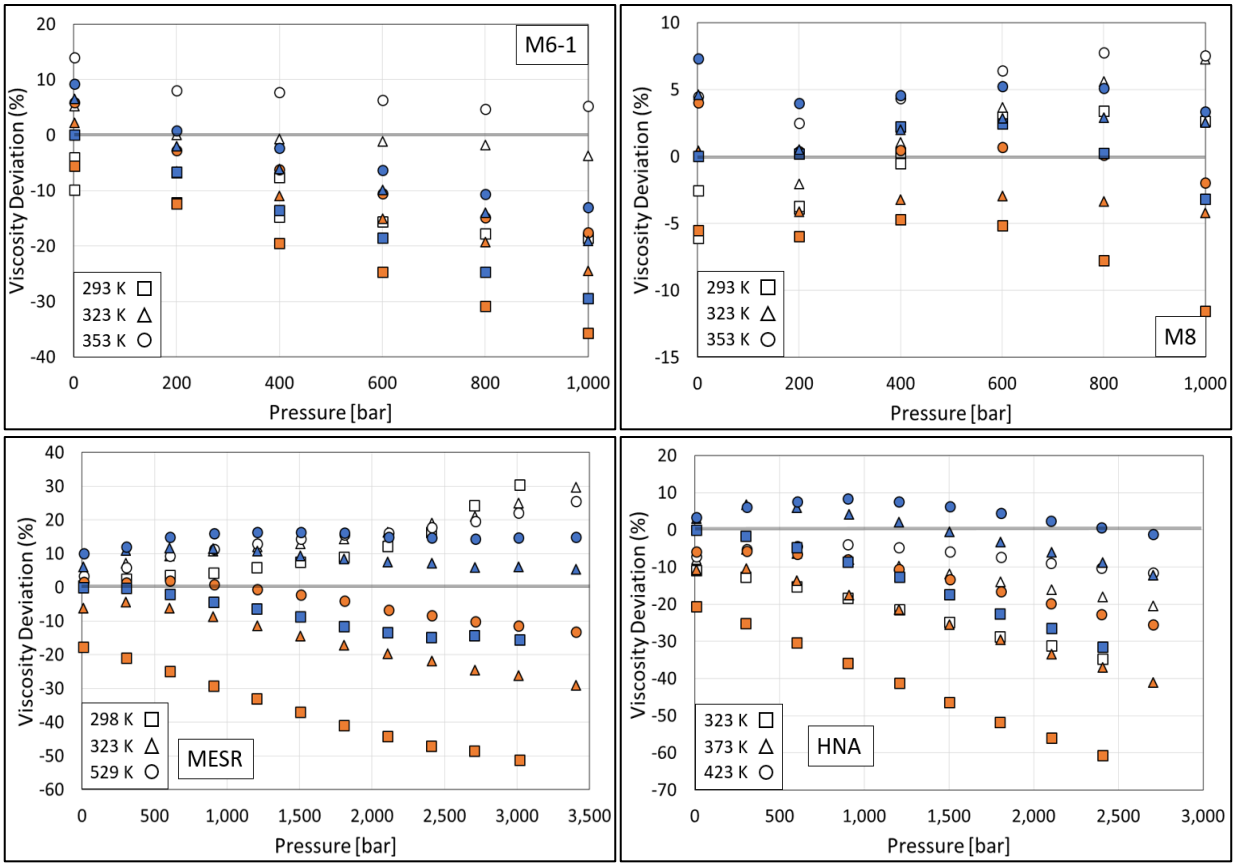

Figure 5.5. Pseudo-component viscosity deviations compared to experimental data [25, 188, 273, 274] for selected hydrocarbon mixtures (mixtures M6-1 and M8) and diesel fuels (MESR and HNA): two-parameter (orange symbols), three-parameter (blue symbols), and correlated two-parameter (open symbols) models. Note that the y-axis scale is different in each figure.

Table 5.7. The Eq. 5.1 parameters needed for hydrocarbon mixtures and diesel fuels and MAPDs for pseudo-component viscosity predictions using the two-parameter, correlated two-parameter, and three-parameter models for mixtures M3-M8 with different compositions and diesel fuels.

Sample				MW	HN/CN	$A_{s^*}\times10^4$	$B_{s^*}\times10^{-2}$	$C_{s^*}\times10^4$	$D_{s^*}\times10^{-2}$	MAPD (%)		
										Two-parameter	Correlated two-parameter	Three-parameter
		X_{nC13}	X_{HMN}									
M3-1		0.125	0.875	221	2.13	1.0285	3.0349	0.7071	8.1227	24.2	15.8	12.6
M3-2		0.250	0.750	216	2.13	0.9283	3.0324	0.6448	8.2661	18.6	9.4	9.1
M3-3		0.375	0.625	211	2.13	0.8282	3.0298	0.5825	8.4095	14.2	9.3	5.8
M3-4		0.500	0.500	205	2.14	0.7281	3.0273	0.5202	8.5529	11.1	8.7	4.2
M3-5		0.625	0.375	200	2.14	0.6280	3.0247	0.4579	8.6963	8.7	8.0	2.3
M3-6		0.750	0.250	195	2.15	0.5278	3.0221	0.3956	8.8397	6.1	7.4	1.8
M3-7		0.875	0.125	190	2.15	0.4277	3.0196	0.3333	8.9831	5.4	7.9	4.6
	X_{MCH}	X_{HMN}	$X_{decalin}$									
M4-1	0.125	0.750	0.125	199	2.07	1.1204	2.5789	0.6075	7.9754	35.0	11.0	9.8
M4-2	0.250	0.500	0.250	172	2.01	1.1121	2.1203	0.4456	7.9716	41.0	9.3	6.3
M4-3	0.333	0.334	0.333	154	1.98	1.1067	1.8148	0.3377	7.9690	45.0	4.8	4.6
			$X_{branched\ alkanes}$									
M5			0	184	1.84	0.3358	3.0103	0.2705	9.1460	3.1	5.4	2.5
	X_{MNP}	X_{nC13}	X_{HMN}									
M6-1	0.125	0.125	0.750	211	1.98	0.7303	3.0975	0.6477	7.5438	14.2	6.6	10.0
M6-2	0.125	0.250	0.625	205	1.98	0.6019	3.1137	0.5867	7.6085	10.2	6.4	9.3
M6-3	0.125	0.375	0.500	200	1.98	0.4735	3.1300	0.5256	7.6731	6.4	8.5	7.0
M6-4	0.125	0.500	0.375	195	1.99	0.3452	3.1463	0.4646	7.7378	4.2	10.3	5.3
M6-5	0.125	0.625	0.250	190	1.99	0.2168	3.1626	0.4035	7.8024	2.6	11.7	3.8
M6-6	0.125	0.750	0.125	184	1.99	0.0884	3.1789	0.3425	7.8671	2.2	12.6	2.9
M6-7	0.250	0.125	0.625	200	1.99	0.4603	3.1412	0.5871	7.0437	8.3	6.4	10.5
M6-8	0.250	0.250	0.500	195	1.83	0.3319	3.1575	0.5260	7.1083	5.7	8.7	8.2

M6-9	0.250	0.375	0.375	190	1.83	0.2036	3.1737	0.4650	7.1730	4.4	11.1	6.5
M6-10	0.250	0.500	0.250	184	1.83	0.0752	3.1900	0.4039	7.2376	4.3	12.9	4.4
M6-11	0.250	0.625	0.125	170	1.83	-0.0532	3.2063	0.3429	7.3023	5.1	13.8	2.8
M6-12	0.375	0.125	0.500	190	1.67	0.1903	3.1849	0.5264	6.5436	6.7	7.7	8.7
M6-13	0.375	0.250	0.375	184	1.67	0.0620	3.2012	0.4654	6.6082	6.0	10.9	6.6
M6-14	0.375	0.375	0.250	179	1.67	-0.0664	3.2175	0.4043	6.6729	5.6	11.2	4.6
M6-15	0.375	0.500	0.125	174	1.67	-0.1948	3.2337	0.3433	6.7375	8.1	14.6	3.0
M6-16	0.500	0.125	0.375	179	1.52	-0.0796	3.2286	0.4658	6.0434	5.8	6.3	6.6
M6-17	0.500	0.250	0.250	174	1.52	-0.2080	3.2449	0.4048	6.1081	5.7	9.2	4.9
M6-18	0.500	0.375	0.125	169	1.52	-0.3364	3.2612	0.3437	6.1727	8.6	13.1	3.1
M6-19	0.625	0.125	0.250	169	1.37	-0.3496	3.2723	0.4052	5.5433	4.8	5.2	4.5
M6-20	0.625	0.250	0.125	163	1.37	-0.4780	3.2886	0.3441	5.6080	6.1	8.9	3.3
M6-21	0.750	0.125	0.125	158	1.22	-0.6195	3.3161	0.3445	5.0432	2.7	1.4	2.8
			$X_{branched\ alkanes}$									
M7			0	184	2.15	0.0158	3.2250	0.2849	8.2571	6.8	4.6	3.3
			X_{HMN}									
M8			0.162	182	1.94	0.0613	3.2153	0.3633	7.6610	3.1	3.9	2.9
			$X_{branched\ alkanes}$									
MESR			0.258	225	1.85	-0.5159	4.4217	0.5081	7.6778	18.2	13.4	10.3
HNA			0.130	204	1.74	-0.5100	4.0435	0.4129	7.3549	25.2	13.3	7.8

Table 5.8. The MAPD (%), bias (%), SD (%), and Max Deviation (%) for pseudo-component viscosity predictions using the two-parameter, correlated two-parameter, and three-parameter models for mixtures M3-M8 and diesel fuels.

Sample	Two-parameter				Correlated two-parameter				Three-parameter			
	MAPD	Bias	SD	Max Deviation	MAPD	Bias	SD	Max Deviation	MAPD	Bias	SD	Max Deviation
M3	12.6	-12.6	9.2	48.6	8.2	0.1	5.9	29.2	5.5	1.1	4.4	28.2
M4	39.2	-39.2	8.9	57.5	9.9	-9.2	6.4	31.3	7.9	-7.2	5.3	26.2
M5	3.1	-2.2	2.0	6.7	8.4	8.2	6.1	19.3	2.5	0.5	1.5	4.7
M6	6.1	1.1	4.9	36.2	9.5	9.3	3.0	23.0	5.2	1.6	4.8	21.8
M7	2.3	0.5	1.8	8.1	4.6	-1.6	2.9	10.7	2.8	2.5	2.2	8.4
M8	3.1	-2.2	2	6.7	2.9	2.8	1.0	7.3	3.9	1.5	1.1	4.7
MESR	18.2	-17.7	15.2	51.0	13.4	13.4	8.0	30.5	10.3	4.3	5.0	17.9
HNA	25.2	-25.2	15.7	60.6	13.3	-13.3	8.4	34.8	7.8	-1.9	7.2	30.3

Equation 5.1 is also used to calculate Δs^* for mixtures M1 and M2, listed in Table 5.2. These mixtures contain compounds with molecular weight beyond the range of mixture number averaged MWs (i.e., from 154 to 221 g/mol) considered in the development of the Δs^* correlation. Table 5.9 lists the Eq. 5.1 parameters needed for different compositions of mixtures M1 and M2 and MAPDs for predictions using the two-parameter, correlated two-parameter, and three-parameter models. Table 5.10 summarizes the predictions using the three models for mixtures listed in Table 5.2. The correlated two-parameter model improved predictions for only one composition of mixture M2 (referred to as M2-2, containing 0.290 mole fraction iC30 and 0.710 mole fraction nC4), which has a number averaged MW (i.e., 163.9 g/mol) within the range of number averaged MWs varying from 154 to 221 g/mol. The correlated two-parameter provides less accurate predictions for all other compositions of mixtures M1 and M2. Thus, Eq. 5.1 appears to only improve viscosity predictions for mixtures with number averaged MWs within the range of mixture number averaged MWs (i.e., from 154 to 221 g/mol) considered when fitting the Δs^* correlation and should not be extrapolated for mixtures with MWs outside this range.

Table 5.9. The Eq. 5.1 parameters needed for mixtures listed in Table 5.2 and MAPDs for pseudo-component viscosity predictions using the two-parameter, correlated two-parameter, and three-parameter models.

Sample			MW	HN/CN	$A_{s^*}\times10^4$	$B_{s^*}\times10^{-2}$	$C_{s^*}\times10^4$	$D_{s^*}\times10^{-2}$	MAPD (%)		
									Two-parameter	Correlated two-parameter	Three-parameter
	X_{nC6}	$X_{toluene}$									
M1-1	0.250	0.750	91	1.44	0.0144	5.6770	0.6178	-0.4003	16.6	40.2	4.9
M3-2	0.500	0.500	89	1.74	0.0174	10.5423	0.0808	-1.0188	15	103.3	7.4
M1-1	0.750	0.250	88	2.04	0.0204	15.4257	-0.4594	-1.6400	12.3	376.5	7.5
	X_{nC4}	$X_{squalane}$									
M2-1	0.846	0.154	114	2.25	0.0225	15.3532	-0.2645	-0.8715	41.8	896.3	6
M2-2	0.71	0.29	164	2.17	0.0217	6.4668	1.1993	1.0109	50.1	2.8	4.4
M2-3	0.482	0.518	247	2.11	0.0211	-7.2821	3.5303	4.0217	60	29.7	9.5
M2-4	0.456	0.544	257	2.26	0.0226	-6.4436	3.5402	4.0616	42.4	30.2	5.1
M2-5	0.259	0.741	328	2.18	0.0218	-18.7738	5.6036	6.7201	62.2	23981.8	11.2
M2-6	0.247	0.753	333	2.17	0.0217	-19.5892	5.7351	6.8899	32.2	25244.0	3.7

Table 5.10. The MAPD (%), bias (%), SD (%), and Max Deviation (%) for pseudo-component viscosity predictions using the two-parameter, correlated two-parameter, and three-parameter models for mixtures listed in Table 5.2. Data from [271, 272].

	Two-parameter		Correlated two-parameter		Three-parameter	
	M1	M1	M1	M2	M1	M2
MAPD	14.7	6.6	173.3	896.3	6.6	6.3
Bias	14.7	-3.6	173.3	896.3	-3.6	2.9
SD	7.1	5.7	826.7	1965.1	5.7	5.8
Max Deviation	44.5	21.6	171.83	614.58	21.6	26.6

5.2.2 Application of the Δs^* correlation to the thermal conductivity pseudo-component technique

The correlation proposed for Δs^*, Eq. 5.1, was applied to the thermal conductivity pseudo-component technique. Table 5.11 lists the mixtures considered in this study. Wakeham et al. [256] measured thermal conductivity for binary mixtures containing benzene and 2,2,4-trimethylpentane (TMP) (referred to as M9) for two different compositions at temperatures of 313 and 345 K and pressures up to 3,500 bar. Fareleira et al. [257] reported thermal conductivity data for binary mixtures containing nC7 and TMP (referred to as M10) for two different compositions at temperatures from 308 to 337 K and pressures up to 4,440 bar. Wada et al. [255] reported thermal conductivity for ternary mixtures (referred to as M11) including nC7, n-undecane (nC11), and nC16 for three compositions at temperatures from 295 to 345 K and 1 bar. For studies which report HTHP thermal conductivity data for fuels (see Table 4.5), only Jia et al. [261] and Xu et al. [260] reported the composition of branched alkanes. Therefore, only one fuel, RP3, is considered here.

Table 5.11. Molar composition of the mixtures and mole fraction of branched alkanes in the RP3 fuel

Compound	Chemical Family	M9	M10	M11	RP3
n-heptane	n-alkanes	-	48.9 74.4	10.0 33.4 59.9	-
n-undecane	n-alkanes	-	-	29.9 33.3	-
n-hexadecane	n-alkanes	-	-	30.0 balance	-
2,2,4-trimethylpentane (TMP)	iso-alkanes	25.0 75.0	balance	-	-
benzene	benzenes	balance	-	-	-
branched alkanes	-	-	-	-	0.320

Knowing the mixture number averaged MW, the HN/CN ratio, and $X_{branched-alkanes}$, Eq. 5.1 is used to calculate Δs^* for mixtures M9-M11 and the RP3 fuel. Table 5.12 lists the parameters used in Eq. 5.1 for different compositions of mixtures M9-M11 and the RP3 fuel and MAPDs for thermal conductivity predictions using the two-parameter, correlated two-parameter, and three-parameter models. Table 5.13 summarizes the predictions compared to the data [255-257, 260, 261] using all three models for the mixtures listed in Table 5.11. Since the Δs^* correlation corrects residual entropy predictions, the parameters in Table 5.6, fit using viscosity data, should also be applicable to the thermal conductivity pseudo-component technique. However, less accurate thermal conductivity predictions are achieved using this correlation for the mixtures listed in Table 5.11, as shown in Tables 5.12 and 5.13. This deficiency could be related to the limited availability of experimental data used to fit the thermal conductivity coefficients for pure n-alkanes and PNAs, the limited number of compounds used to generate the thermal conductivity coefficient correlations, or inconsistencies in the mathematical form of the thermal conductivity coefficient correlations compared to the form of the viscosity coefficient correlations for n-alkanes and PNAs.

Table 5.12. The Eq. 5.1 parameters needed for the mixtures listed in Table 5.11 and the MAPDs for pseudo-component thermal conductivity predictions using the two-parameter, correlated two-parameter, and three-parameter models.

Sample				MW	HN/CN	$A_{s^*}\times10^4$	$B_{s^*}\times10^{-2}$	$C_{s^*}\times10^4$	$D_{s^*}\times10^{-2}$	MAPD (%)		
										Two-parameter	Correlated two-parameter	Three-parameter
		$X_{benzene}$	X_{TMP}									
M9-1		0.75	0.25	87.1	1.38	7.8761	0.0577	0.3924	5.9350	14.6	26.5	1.3
M9-2		0.25	0.75	105.2	2.00	18.1671	-1.3512	1.3220	8.7241	33.2	105.8	3.3
		X_{nC7}	X_{TMP}									
M10-1		0.489	0.511	107.4	2.27	20.4324	-1.2971	0.0110	9.7864	24.5	223.5	2.0
M10-2		0.744	0.256	103.8	2.28	18.6826	-0.8742	-0.8873	9.5500	17.4	182.3	4.6
	X_{nC7}	X_{nC11}	X_{nC16}									
M11-1	0.100	0.299	0.601	192.9	2.16	-1.8583	2.7996	0.9064	8.9857	1.4	2.0	2.4
M11-2	0.334	0.333	0.333	160.9	2.20	4.548	1.6868	-0.0128	9.0809	1.4	10.8	2.2
M11-3	0.599	0.300	0.101	129.8	2.24	10.8297	0.5978	-0.9137	9.1822	1.2	50.9	2.0
			$X_{branched\ alkanes}$									
RP3			0.340	153	1.93	5.2550	1.1256	1.3422	8.3516	7.3	19.7	2.3

Table 5.13. The MAPD (%), bias (%), SD (%), and Max Deviation (%) for pseudo-component thermal conductivity predictions using the two-parameter, correlated two-parameter, and three-parameter models for mixtures listed in Table 5.11.

Sample	Two-parameter				Correlated two-parameter				Three-parameter			
	MAPD	Bias	SD	Max Deviation	MAPD	Bias	SD	Max Deviation	MAPD	Bias	SD	Max Deviation
M9	19.4	19.4	15.2	43.4	105.8	105.8	75.6	215.1	3.7	2.6	3.7	15.2
M10	21.6	21.6	8.1	45.6	223.5	223.5	57.1	342.5	2.4	-1.3	1.7	5.1
M11	1.3	0.2	0.9	2.8	21.2	20.2	22.2	60.4	2.2	-2.2	1.4	4.2
RP3	7.3	7	3.5	11.6	19.7	19.7	4.1	27.5	2.3	-1.2	2.8	11.2

5.3 Conclusion

Sensitivity of the entropy scaling approach of Lötgering-Lin and Gross [171] was investigated using different sets of group contribution (GC) PC-SAFT parameters for n-decane at different temperatures and pressures. The GC-PC-SAFT parameters of Sauer et al. [58], which were used by Lötgering-Lin and Gross [171] in fitting their entropy scaling GC parameters, provided the best viscosity predictions with an MAPD of 2%. When using different PC-SAFT parameters in the entropy scaling approach, if comparable residual entropies and PC-SAFT parameters were used in the calculations, the predicted viscosities (e.g., with an MAPD of 5% using the GC-PC-SAFT parameters of Tihic et al. [61]) did not significantly differ compared to the predictions obtained using the original Lötgering-Lin and Gross [171] approach, who used the parameters of Sauer et al. [58]. However, greater deviations (i.e., 27% MAPD) were obtained using the GC-PC-SAFT parameters of Burgess et al. [53], fit to high pressure density data, compared to those obtained when using the parameters of Sauer et al. [58].

In Chapter 3, the viscosity pseudo-component technique was developed for mixtures containing compounds with MWs present in fuels using the two-parameter and three-parameter models. However, in Chapter 5, the capability of the viscosity pseudo-component technique was investigated for mixtures with lighter and heavier compounds compared to those compounds in fuels. Although the two-parameter model yields large deviations for viscosity predictions for mixtures with lighter and heavier compounds than are present in fuels, the three-parameter model predictions show that it is possible to accurately predict viscosity up to HTHP for these mixtures when a reference data point is used to fit the *D* viscosity coefficient.

An empirical correlation, which is a function of temperature, pressure, and mixture properties (i.e., number averaged molecular weight, hydrogen to carbon ratio, and molar concentration of branched alkanes), was proposed to improve the residual entropy calculated using the two-parameter viscosity pseudo-component model for hydrocarbon mixtures and diesel fuels which contained large concentrations of branched alkanes. A training set of ~700 data points was used to fit the correlation parameters and a test set of ~800 data points was used to validate the correlation. The correlation improved viscosity predictions (9.2% MAPD) for all hydrocarbon mixtures and diesel fuels in this study compared to when using the two-parameter (12.0% MAPD).

The residual entropy correlation (Eq. 5.1) was also applied to the thermal conductivity pseudo-component technique but did not improve predictions. This deficiency could be related to the limited availability of thermal conductivity experimental data used to fit the thermal conductivity coefficients for pure n-alkanes and PNAs in Chapter 4, the limited number of compounds used to generate the thermal conductivity coefficient correlations, or inconsistencies in the mathematical form of the thermal conductivity coefficient correlations compared to the form of the viscosity coefficient correlations for n-alkanes and PNAs. To overcome this deficiency, a different set of correlation coefficients for use in Eq. 5.1 could be fit using thermal conductivity data, repeating the exercise used with the viscosity data. However, due to the limited availability of experimental thermal conductivity data for well-characterized hydrocarbon mixtures, the fitting of different coefficients for thermal conductivity was not investigated in this study.

6. Chapter 6: Conclusions and Future Work

6.1 Conclusions

Fuel injectors are key systems that determine the performance, emissions, and fuel economy of diesel engines. Advanced computational fluid dynamics (CFD) approaches have been utilized to simulate the performance of fuel injection equipment systems and to investigate phenomena, such as cavitation and fuel atomization. The outcomes of CFD simulation at conditions up to high pressures are dependent on accurate representation of fluid physical properties. Due to the lack of experimental data for fuels up to high temperatures and high pressures (HTHP), predictive techniques are needed to model the thermophysical properties at such conditions. The goal of this study was to develop molecular-based techniques to predict transport and thermodynamic properties for well-characterized hydrocarbon mixtures and fuels up to HTHP with minimal experimental inputs.

A pseudo-component technique based upon the Perturbed-Chain Statistical Associating Fluid Theory (PC-SAFT) equation of state (EoS) was presented to predict density, isothermal compressibility, and the volumetric thermal expansion coefficient for well-characterized hydrocarbon mixtures and fuels (e.g., rocket propellant, jet, kerosene, and diesel). A pseudo-component was defined to represent mixtures and fuels through two calculated or measured mixture properties: the number averaged molecular weight (MW) and the hydrogen to carbon ratio (HN/CN). Density, isothermal compressibility, and the volumetric thermal expansion coefficient were predicted up to HTHP with mean absolute percent deviations (MAPDs) of 1, 9, and 13 %, respectively, for well-defined hydrocarbon mixtures and fuels.

The pseudo-component technique was further extended to transport properties using residual entropy scaling to predict viscosity and thermal conductivity up to HTHP with 21 and 16%

MAPDs, respectively, for mixtures and fuels when using two mixture properties as inputs. However, less accurate predictions were found for mixtures containing high concentrations of branched alkanes. Inclusion of a third input (i.e., a reference data point at a chosen state to fit a model parameter) significantly improved the viscosity and thermal conductivity predictions with MAPDs of 9 and 3%, respectively, for the well-defined hydrocarbon mixtures and fuels.

Finally, a correlation as a function of temperature, pressure, and three mixture properties (i.e., the number averaged MW, the HN/CN ratio, and mole fraction of branched alkanes in the mixture) was proposed to improve predictions for residual entropy when using the two-parameter pseudo-component technique for viscosity predictions. This correlation significantly improved viscosity predictions, reducing the MAPD to 9.2% for the well-defined hydrocarbon mixtures and fuels in this study. The correlation was also applied to the thermal conductivity pseudo-component technique but was shown not to improve predictions, which could be related to the limited availability of experimental data used to fit the thermal conductivity coefficients for pure n-alkanes and PNAs, the limited number of compounds used to generate the thermal conductivity coefficient correlations, or inconsistencies in the mathematical form of the thermal conductivity coefficient correlations compared to the form of the viscosity coefficient correlations for n-alkanes and PNAs.

The pseudo-component techniques developed in this study provide a framework for the prediction of thermodynamic and dynamic thermophysical properties for well-characterized hydrocarbon mixtures and fuels. The techniques provide simple yet accurate predictions up to HTHP without requiring expensive and time-consuming experimental measurements and can be applied to assist in the design, testing, and development of fuel injection equipment (FIE).

6.2 Future work

6.2.1 Opportunities for technique development

A pseudo-component technique based upon the PC-SAFT equation of state (EoS) was presented to predict density and derivative properties (i.e., isothermal compressibility and volumetric thermal expansion coefficient) using two inputs (i.e., the number averaged molecular weight (MW) and the hydrogen to carbon (HN/CN) ratio). Density was predicted within 1 % MAPD up to high temperatures and pressures for hydrocarbon mixtures and fuels. However, larger deviations were observed for derivative property predictions, and it was suggested that the inaccuracy in derivative property predictions was a result of the intermolecular potential used in the PC-SAFT EoS. Therefore, further work should consider extending the pseudo-component technique using more recent SAFT variants (i.e., SAFT for variable range interactions using Mie potentials (SAFT-VR Mie) and SAFT-γ-Mie) instead of PC-SAFT, which uses a square-well potential. A study would also be required to develop new SAFT parameter correlations using GC parameters for the SAFT variant used in the pseudo-component technique. The definition of the averaging parameter, *Z*, could also be improved to better account for the effects of branched alkanes.

Entropy scaling based pseudo-component techniques were developed to predict viscosity and thermal conductivity using the same two inputs, the number averaged MW and the HN/CN ratio. However, greater deviations were found when mixtures contained significant concentrations of branched-alkanes. A third input (i.e., a reference data point at a chosen state), was used to fit a model parameter, significantly improving the predictions. Furthermore, using a training set of ~700 data points, an empirical correlation was proposed to improve the residual entropy predictions used in the viscosity pseudo-component technique. The correlation was limited to the number averaged

MW for mixtures considered in the fitting. Therefore, future work should extend the correlations to a wider range of number averaged MWs to accurately predict viscosities for lighter or heavier hydrocarbon mixtures.

The proposed residual entropy correlation was also used in the thermal conductivity technique, but it did not improve predictions for thermal conductivity. A further study is required to fit the thermal conductivity coefficients for pure n-alkanes, PNAs, and other chemical families to verify that n-alkanes and PNAs numerically bound the thermal conductivity coefficient values. However, additional experimental data is required, which is not currently available in the literature. The study should also validate that the mathematical form of the third order polynomial used in the technique is appropriate to use to correlate reduced thermal conductivity to reduced dimensionless residual entropy.

6.2.2 Extension of pseudo-component technique to properties not included in this study

The pseudo-component techniques can be utilized to predict properties not considered in this study (e.g., phase equilibrium, diffusivity, heat capacity, and surface tension) for fuels and hydrocarbon mixtures. As described in Chapters 3 and 4, transport properties (i.e., viscosity, thermal conductivity, and diffusivity) scale with residual entropy. An additional investigation would be required to extend the pseudo-component technique to calculate diffusivity using entropy-scaling for fuels and hydrocarbon mixtures. To calculate heat capacity up to high temperatures and pressures, additional experimental measurements of the ideal gas heat capacity would be required for fuels. Using an EoS, heat capacity is calculated by adding contributions from an ideal gas to the residual heat capacity, which can be calculated using the pseudo-component technique. The pseudo-

component technique should also be capable of predicting surface tension for fuels and hydrocarbon mixtures, by coupling to other methods (e.g., density functional theory).

6.2.3 Calculation of properties for fuels not considered in this study

The commercial fuels considered in this study (i.e., diesel, jet, and rocket propellant fuels) are mixtures of hydrocarbons, whose properties were well predicted by the pseudo-component techniques developed in this study. The same techniques should also be capable of predicting properties of other fuels, such as gasoline, kerosene, bio-fuels (e.g., vegetable oils, liquid animal fats, and biodiesels), and their blends. However, biofuels and their blends typically contain significant amounts of compounds other than hydrocarbons (e.g., oxygenates such as esters), and the EoS used in the pseudo-component technique would need to account for association of molecules, which was neglected in this study. The association terms in the PC-SAFT EoS would need to be included in the pseudo-component technique, and the pseudo-component PC-SAFT parameter and transport property coefficient correlations would need to be modified to account for the presence of associating compounds.

Peer-Reviewed Journal Publications and Conference Proceedings and Presentations

- **Peer-Reviewed Journal Publications:**

1. **Rokni HB**, Gupta A, Moore JD, M^{c}Hugh MA, Bamgbade BA, Gavaises M. "Purely predictive method for density, compressibility, and expansivity for hydrocarbon mixtures and diesel and jet fuels up to high temperatures and pressures". *Fuel*. 2019; Vol 236: pp 1377-90: https://doi.org/10.1016/j.fuel.2018.09.041
2. **Rokni HB**, Moore JD, Gupta A, M^{c}Hugh MA, Gavaises M. "Entropy scaling based viscosity predictions for hydrocarbon mixtures and diesel fuels up to extreme conditions". *Fuel*. 2019; Vol 241: pp 1203-1213: https://doi.org/10.1016/j.fuel.2018.12.0433
3. **Rokni HB**, Moore JD, Gupta A, M^{c}Hugh MA, Mallepally R, Gavaises M. "General method for prediction of thermal conductivity for well-characterized hydrocarbon mixtures and fuels up to extreme conditions using entropy scaling". *Fuel*. 2019; Vol 245: pp 594-604: https://doi.org/10.1016/j.fuel.2019.02.0444
4. Mallepally RR, Bamgbade BA, Rowane AJ, **Rokni HB**, Newkirk MS, M^{c}Hugh MA. "Fluid properties at high pressures and temperatures: Experimental and modelling challenges". *The Journal of Supercritical Fluids.* 2018; Vol 134: pp 33-40: https://doi.org/10.1016/j.supflu.2017.12.0033
5. Rodriguez C, **Rokni HB**, Koukouvinis P, Gupta A, Gavaises M. "Simulation of pseudo-diesel injections at high-load conditions employing the Perturbed Chain Statistical Associating Fluid Theory" / Under Review as of May 14, 2019.
6. Rowane AJ, Babu VM, Mallepally RR, **Rokni HB**, Moore JD, Gupta A, Gavaises M, Wensing M, M^{c}Hugh MA. "Effect of composition on the high-temperature, high-pressure viscosities and densities of three diesel fuels" / Under Review as of July 15, 2019.
7. Rodriguez C, **Rokni HB**, Koukouvinis P, Gavaises M. "Coupling between internal nozzle flow and diesel injection under cavitation conditions employing the PC-SAFT EoS" / In Preparation.
8. **Rokni HB**, Moore JD, Gupta A, Gavaises M. "Entropy-scaling based pseudo-component viscosity predictions for hydrocarbon mixtures and diesel fuels containing branched alkanes" / In Preparation.

- **Conference Proceedings and Oral Presentations:**

1. **Rokni HB**, Gupta A, McHugh, MA. "Group Contribution SAFT-Based Prediction of Real Diesel Fuel Density at High-T, High-P". Oral presentation at International Institute for Cavitation Research (IICR) Workshop, July 2017, Chania, Greece.
2. **Rokni HB**, Moore JD, Gupta A, McHugh MA, Gavaises M. "Accurate and Efficient Thermophysical Property Models for Fuels up to High Temperatures and Pressures". Oral presentation at International Institute for Cavitation Research (IICR) Workshop, June 2019, Chania, Greece.
3. Rodriguez C, **Rokni HB**, Koukouvinis P, Gupta A, Gavaises M. "CFD simulation of pseudo-diesel injections at high-load conditions employing the PC-SAFT EoS and VLE calculations". Publication and Oral presentation to be presented at Institute for Liquid Atomization and Spray Systems (ILASS)-Europe, September 2019, Paris, France.
4. **Rokni HB**, Moore JD, Gupta A, McHugh MA, Gavaises M. "Pseudo-Component Techniques for Prediction of Thermophysical Properties of Hydrocarbon Mixtures and Fuels up to High Temperatures and Pressures". Oral presentation to be presented at American Institute of Chemical Engineers (AIChE) Annual Meeting, November 2019, Orlando, FL, USA.

- **Conference Poster Presentations:**

1. **Rokni HB**, Gupta A, McHugh, MA. "Group Contribution SAFT-Based Prediction of Real Diesel Fuel Density at High-T, High-P". International Institute for Cavitation Research (IICR) Workshop, July 2017, Chania, Greece.
2. Rodriguez C, **Rokni HB**, Koukouvinis P, Gavaises M. "Complex Multicomponent Real-Fluid Thermodynamic Model for High-Pressure Diesel Fuel Injection". City University London Poster Exhibition, April 2019, London, England.
3. Rodriguez C, **Rokni HB**, Koukouvinis P, Gavaises M. "Supercritical, transcritical and subcritical real-fluid mixing at high-pressure conditions using the PC-SAFT EoS". International Institute for Cavitation Research (IICR) Workshop, June 2019, Chania, Greece.
4. **Rokni HB**, Moore JD, Gupta A, McHugh MA, Gavaises M. "Pseudo-Component Property Predictions for Diesel Fuels up to Extreme Pressures". International Institute for Cavitation Research (IICR) Workshop, June 2019, Chania, Greece.

Literature Cited

[1] Ramanathan V, Carmichael, G. Global and regional climate changes due to black carbon. Nature Geoscience 2008;1(4):221-22.

[2] Zhao H. Advanced direct injection combustion engine technologies and development: diesel engines. Elsevier; 2009.

[3] Heywood JB. Fundamentals of internal combustion engines. Tata McGraw-Hill Education; 1988.

[4] Graham M, al. e. Soot reductions at 3000 bar injection pressure. *Proc of the IMechE*. London; 2009.

[5] European-Union. Effect of 4500bar injection pressure and super-critical phase change of surrogate and real-world fuels enriched with additives and powering Diesel engines on soot emissions reduction; 2015. Available from: https://cordis.europa.eu/project/rcn/198296_en.html. [Accessed 5 March 2018].

[6] Lee WG, Reitz, R. D. A Numerical Investigation of Transient Flow and Cavitation within Minisac and Valve-Covered Orifice Diesel Injector Nozzles. ASME J Eng Gas Turbines Power 2010;132(5):052802.

[7] Margot X, Hoyas, S., Fajardo, P., Patouna, S. A moving mesh generation strategy for solving an injector internal flow problem. Mathematical and Computer Modelling 2010;52(7):1143-50.

[8] Payri F, Margot, X., Patouna, S., Ravet, F., Funk, M. A CFD Study of the Effect of the Needle Movement on the Cavitation Pattern of Diesel Injectors. SAE Technical Paper 2009;2009-24-0025.

[9] Andriotis A, Gavaises M, Arcoumanis C. Vortex flow and cavitation in diesel injector nozzles. Journal of Fluid Mechanics 2008;610:195-215.

[10] Park SH, Suh HK, Lee CS. Effect of cavitating flow on the flow and fuel atomization characteristics of biodiesel and diesel fuels. Energy & Fuels **2008**;22(1):605-13.

[11] Salvador FJ, Martínez-López, J., Caballer, M., De Alfonso, C. Study of the influence of the needle lift on the internal flow and cavitation phenomenon in diesel injector nozzles by CFD using RANS methods. Energy conversion and management 2013;28(66):246-56.

[12] Schmidt DP, Corradini ML. The internal flow of diesel fuel injector nozzles: A review. International Journal of Engine Research **2001**;2(1):1-22.

[13] Som S, Aggarwal, S.K., El-Hannouny, E.M., Longman, D.E. Investigation of nozzle flow and cavitation characteristics in a diesel injector. Journal of Engineering for Gas Turbines and Power 2010;132(4):042802.

[14] Battistoni M, Grimaldi CN. Numerical analysis of injector flow and spray characteristics from diesel injectors using fossil and biodiesel fuels. Applied Energy **2012**;97:656-66.

[15] Battistoni M, Grimaldi CN. Analysis of transient cavitating flows in diesel injectors using diesel and biodiesel fuels. SAE International Journal of Fuels and Lubricants 2010;01(2245):879-900.

[16] Pomraning E, Richards K, Senecal PK. Modeling turbulent combustion using a RANS model, detailed chemistry, and adaptive mesh refinement. *SAE Technical Paper*. 2014-01-1116. **2014.** 2014-01-1116.

[17] Senecal PK, Pomraning E, Richards K, Som S. Grid convergent spray models for internal combustion engine CFD simulations. ASME 2012 Internal Combustion Engine Division Fall Technical Conference **2012**(55096):697-710.

[18] Arcoumanis C, Gavaises M. Linking nozzle flow with spray characteristics in a diesel fuel injection system. Atomization and Sprays **1998**;8(3):307-47.

[19] Giannadakis E, Gavaises M, Arcoumanis C. Modelling of cavitation in diesel injector nozzles. Journal of Fluid Mechanics **2008**;616:153-93.

[20] Bidabadi M, Yosefi SH, Poorfar AK, Hajilou M, Zadsirjan S. Modelling of combustion of a magnesium dust cloud in heterogeneous media. Combustion, Explosion, and Shock Waves 2014;50(6):658-63.

[21] Theodorakakos A, Strotos, G., Mitroglou, N., Atkin, C., Gavaises, M.,. Friction-induced heating in nozzle hole micro-channels under extreme fuel pressurisation. Fuel 2014;123:143-50.

[22] Strotos G, Koukouvinis, P., Theodorakakos, A., Gavaises, M., Bergeles, G. Transient heating effects in high pressure Diesel injector nozzles. International Journal of Heat and Fluid Flow 2015;51:257-67.

[23] Strotos G, Malgarinos, I., Nikolopoulos, N., Gavaises, M. Predicting the evaporation rate of stationary droplets with the VOF methodology for a wide range of ambient temperature conditions. International Journal of Thermal Sciences 2016;109:253-62.

[24] Mithun MG, Koukouvinis, P., Gavaises, M. Numerical simulation of cavitation and atomization using a fully compressible three-phase model. Physical Review Fluids 2018;3(6):064304.

[25] Aquing M, Ciotta F, Creton B, Féjean C, Pina A, Dartiguelongue C, et al. Composition analysis and viscosity prediction of complex fuel mixtures using a molecular-based approach. Energy & Fuels 2012;26(4):2220-30.

[26] Schaschke C, Fletcher, I., Glen, N.,. Density and viscosity measurement of diesel fuels at combined high pressure and elevated temperature. Processes 2013;1(2):30-48.

[27] Kwak T, Mansoori G. Van der Waals mixing rules for cubic equations of state. Applications for supercritical fluid extraction modelling. Chemical engineering science 1986;41(5):1303-9.

[28] Van der Waals JD. On the continuity of the gas and liquid state. Doctoral Dissertation, Leiden; 1873.

[29] Jamaluddin A, Kalogerakis N, Chakma A. Predictions of CO2 solubility and CO2 saturated liquid density of heavy oils and bitumens using a cubic equation of state. Fluid phase equilibria 1991;64:33-48.

[30] Nikookar M, Omidkhah M, Pazuki G. Prediction of density and solubility parameter of heavy oils and SARA fractions using cubic equations of state. Petroleum science and Technology 2008;26(16):1904-12.

[31] Peng D-Y, Robinson DB. A new two-constant equation of state. Industrial & Engineering Chemistry Fundamentals 1976;15(1):59-64.

[32] Pratas MJ, Oliveira MB, Pastoriza-Gallego MJ, Queimada AJ, Pineiro MM, Coutinho JA. High-pressure biodiesel density: experimental measurements, correlation, and cubic-plus-association equation of state (CPA EoS) modeling. Energy & Fuels 2011;25(8):3806-14.

[33] Soave G. Equilibrium constants from a modified Redlich-Kwong equation of state. Chemical engineering science 1972;27(6):1197-203.

[34] Elliott Jr JR, Suresh SJ, Donohue MD. A simple equation of state for non-spherical and associating molecules. Industrial & engineering chemistry research 1990;29(7):1476-85.

[35] Oliveira MB, Freitas SV, Llovell F, Vega LF, Coutinho JA. Development of simple and transferable molecular models for biodiesel production with the soft-SAFT equation of state. Chemical Engineering Research and Design 2014;92(12):2898-911.

[36] Rokni HB, Gupta A, Moore JD, M^{c}Hugh MA, Bamgbade BA, Gavaises M. Purely predictive method for density, compressibility, and expansivity for hydrocarbon mixtures and diesel and jet fuels up to high temperatures and pressures. Fuel **2019**;236:1377-90.

[37] Abutaqiya MI, Panuganti SR, Vargas FM. Efficient Algorithm for the Prediction of PVT Properties of Crude Oils Using the PC-SAFT EoS. Industrial & Engineering Chemistry Research 2017;56(20):6088-102.

[38] Gross J, Sadowski G. Perturbed-chain SAFT: An equation of state based on a perturbation theory for chain molecules. Industrial & Engineering Chemistry Research **2001**;40(4):1244-60.

[39] Gil-Villegas A, Galindo A, Whitehead PJ, Mills SJ, Jackson G, Burgess AN. Statistical associating fluid theory for chain molecules with attractive potentials of variable range. The Journal of chemical physics 1997;106(10):4168-86.

[40] Lymperiadis A, Adjiman CS, Galindo A, Jackson G. A group contribution method for associating chain molecules based on the statistical associating fluid theory (SAFT-γ). The Journal of chemical physics 2007;127(23):234903.

[41] Estela-Uribe J, Jaramillo J, Salazar M, Trusler J. Virial equation of state for natural gas systems. Fluid phase equilibria 2003;204(2):169-82.

[42] Onnes HK. Expression of the equation of state of gases and liquids by means of series. *KNAW, Proceedings.* 4. 1901:1901-2.

[43] Lin R, Tavlarides LL. Thermophysical properties needed for the development of the supercritical diesel combustion technology: Evaluation of diesel fuel surrogate models. The Journal of Supercritical Fluids 2012;71:136-46.

[44] Benedict M, Webb GB, Rubin LC. An empirical equation for thermodynamic properties of light hydrocarbons and their mixtures I. Methane, ethane, propane and n-butane. The Journal of Chemical Physics 1940;8(4):334-45.

[45] AlHammadi AA, Vargas FM, Chapman WG. Comparison of cubic-plus-association and perturbed-chain statistical associating fluid theory methods for modeling asphaltene phase behavior and pressure–volume–temperature properties. Energy & Fuels 2015;29(5):2864-75.

[46] de Villiers A, Schwarz, C., Burger, A., Kontogeorgis, G. Evaluation of the PC-SAFT, SAFT and CPA equations of state in predicting derivative properties of selected non-polar and hydrogen-bonding compounds. Fluid Phase Equilibria 2013;338:1-15.

[47] Hendriks E, Kontogeorgis, G.M., Dohrn, R., de Hemptinne, J.C., Economou, I.G., Zilnik, L.F., Vesovic, V. . Industrial requirements for thermodynamics and transport properties. Industrial & Engineering Chemistry Research 2010;49(22):11131-41.

[48] Leekumjorn S, Krejbjerg, K. Phase behavior of reservoir fluids: Comparisons of PC-SAFT and cubic EoS simulations. Fluid Phase Equilibria 2013;359:17-23.

[49] Perez AG, Coquelet, C., Paricaud, P., Chapoy, A. Comparative study of vapour-liquid equilibrium and density modelling of mixtures related to carbon capture and storage with the SRK, PR, PC-SAFT and SAFT-VR Mie equations of state for industrial uses. Fluid Phase Equilibria 2017;25(440):19-35.

[50] Vijande J, Pineiro M, Bessieres D, Saint-Guirons H, Legido J. Description of PVT behaviour of hydrofluoroethers using the PC-SAFT EOS. Physical Chemistry Chemical Physics 2004;6(4):766-70.

[51] Vijande J, Piñeiro, M.M., Legido, J.L., Bessières, D.,. Group-contribution method for the molecular parameters of the PC-SAFT equation of state taking into account the proximity effect. Application to nonassociated compounds. Industrial & Engineering Chemistry Research 2010;49(19):9394-406.

[52] Vijande J, Piñeiro MM, Legido JL. Group-contribution method with proximity effect for PC-SAFT molecular parameters. 2. Application to association parameters: primary alcohols and amines. Industrial & Engineering Chemistry Research 2013;53(2):909-19.

[53] Burgess WA, Tapriyal D, Gamwo IK, Wu Y, M^{c}Hugh MA, Enick RM. New group-contribution parameters for the calculation of PC-SAFT parameters for use at pressures to 276 MPa and temperatures to 533 K. Industrial & Engineering Chemistry Research **2014**;53(6):2520-8.

[54] Fu D, Li, X.S., Yan, S., Liao, T. Investigation of critical properties and surface tensions for n-alkanes by perturbed-chain statistical associating fluid theory combined with density-gradient theory and renormalization-group theory. Industrial & engineering chemistry research 2006;45(24):8199-206.

[55] NguyenHuynh D, Nguyen TTX. Application of the modified group-contribution PC-SAFT to nitrile and their mixtures. Fluid Phase Equilibria 2017;450:112-25.

[56] Papaioannou V, Lafitte, T., Avendaño, C., Adjiman, C.S., Jackson, G., Müller, E.A., Galindo, A. Group contribution methodology based on the statistical associating fluid

theory for heteronuclear molecules formed from Mie segments. The Journal of chemical physics 2014;140(5):054107.

[57] Peng Y, Goff, K.D., dos Ramos, M.C., McCabe, C. Developing a predictive group-contribution-based SAFT-VR equation of state. Fluid Phase Equilibria 2009;277(2):131-44.

[58] Sauer E, Stavrou M, Gross J. Comparison between a homo- and a heterosegmented group contribution approach based on the perturbed-chain polar statistical associating fluid theory equation of state. Industrial & Engineering Chemistry Research **2014**;53(38):14854-64.

[59] Tamouza S, Passarello JP, Tobaly P, de Hemptinne JC. Group contribution method with SAFT EOS applied to vapor liquid equilibria of various hydrocarbon series. Fluid Phase Equilibria **2004**;222:67-76.

[60] Thi TXN, Tamouza S, Tobaly P, Passarello JP, de Hemptinne JC. Application of group contribution SAFT equation of state (GC-SAFT) to model phase behaviour of light and heavy esters. Fluid phase equilibria **2005**;238(2):254-61.

[61] Tihic A, Kontogeorgis GM, von Solms N, Michelsen ML, Constantinou L. A predictive group-contribution simplified PC-SAFT equation of state: application to polymer systems. Industrial & Engineering Chemistry Research **2008**;47(15):5092-101.

[62] Anand K, Ra Y, Reitz RD, Bunting B. Surrogate model development for fuels for advanced combustion engines. Energy & Fuels 2011;25(4):1474-84.

[63] Herbinet O, Pitz, W.J., Westbrook, C.K. Detailed chemical kinetic mechanism for the oxidation of biodiesel fuels blend surrogate. Combustion and Flame 2010;157(5):893-908.

[64] Huber ML, Lemmon, E.W., Diky, V., Smith, B.L., Bruno, T.J. . Chemically authentic surrogate mixture model for the thermophysical properties of a coal-derived liquid fuel. Energy & Fuels 2008;22(5):3249-57.

[65] Mueller CJ, Cannella, W.J., Bays, J.T., Bruno, T.J., DeFabio, K., Dettman, H.D., Gieleciak, R.M., Huber, M.L., Kweon, C.B., M^{c}Connell, S.S., Pitz, W.J. . Diesel surrogate fuels for engine testing and chemical-kinetic modeling: Compositions and properties. Energy & Fuels 2016;30(2):1445-61.

[66] Pitz WJ, Mueller, C.J. Recent progress in the development of diesel surrogate fuels. Progress in Energy and Combustion Science 2011;37(3):330-50.

[67] Lin R, Tavlarides, L.L. Thermophysical properties needed for the development of the supercritical diesel combustion technology: Evaluation of diesel fuel surrogate models. The Journal of Supercritical Fluids 2012;71:136-46.

[68] Mueller CJ, Cannella, W.J., Bruno, T.J., Bunting, B., Dettman, H.D., Franz, J.A., Huber, M.L., Natarajan, M., Pitz, W.J., Ratcliff, M.A., Wright, K. Methodology for formulating diesel surrogate fuels with accurate compositional, ignition-quality, and volatility characteristics. Energy & Fuels 2012;26(6):3284-303.

[69] Vidal A, Rodriguez C, Koukouvinis P, Gavaises M, McHugh MA. Modelling of Diesel fuel properties through its surrogates using Perturbed-Chain, Statistical Associating Fluid Theory. International Journal of Engine Research 2018:1468087418801712.

[70] Kontogeorgis GM, Folas GK. Thermodynamic models for industrial applications: from classical and advanced mixing rules to association theories. John Wiley & Sons; 2009.

[71] Liang X, Yan, W., Thomsen, K., Kontogeorgis, G.M. On petroleum fluid characterization with the PC-SAFT equation of state. Fluid Phase Equilibria 2014;375:254-68.

[72] Bamgbade BA. Measurements and Modeling of Hydrocarbon Mixture Fluid Properties Under Extreme Temperature and Pressure Conditions. Ph.D.: Virginia Commonwealth University; **2015**.

[73] Gonzalez DL. Modeling of asphaltene precipitation and deposition using the PC-SAFT equation of state. PhD. Rice University; **2008**.

[74] Punnapala S, Vargas, F.M. Revisiting the PC-SAFT characterization procedure for an improved asphaltene precipitation prediction. Fuel 2013;108:417-29.

[75] Ting PL. Thermodynamic stability and phase behavior of asphaltenes in oil and of other highly asymmetric mixtures. PhD. Rice University; **2003**.

[76] Burgess WA, Bamgbade BA, Gamwo IK. Experimental and predictive PC-SAFT modeling results for density and isothermal compressibility for two crude oil samples at elevated temperatures and pressures. Fuel 2018;218:385-95.

[77] Quiñones-Cisneros SE, Zéberg-Mikkelsen, C.K., Stenby, E.H. The friction theory (f-theory) for viscosity modeling. Fluid Phase Equilibria 2000;169(2):249-76.

[78] Quiñones-Cisneros SE, Zéberg-Mikkelsen, C.K., Baylaucq, A., Boned, C. Viscosity modeling and prediction of reservoir fluids: From natural gas to heavy oils. International journal of thermophysics 2004;25(5):1353-66.

[79] Quiñones-Cisneros SE, Dalberg, A., Stenby, E.H. PVT characterization and viscosity modeling and prediction of crude oils. Petroleum science and technology 2004;22((9-10)):1309-25.

[80] Schmidt KA, Quiñones-Cisneros, S.E., Kvamme, B.,. Density and viscosity behavior of a North Sea crude oil, natural gas liquid, and their mixtures. Energy & fuels 2005;19(4):1303-13.

[81] Abutaqiya MI, Zhang J, Vargas FM. Viscosity modeling of reservoir fluids using the Friction Theory with PC-SAFT crude oil characterization. Fuel 2019;235:113-29.

[82] Yarranton HW, Satyro, M.A.,. Expanded fluid-based viscosity correlation for hydrocarbons. Industrial & Engineering Chemistry Research 2009;48(7):3640-8.

[83] Motahhari H, Satyro, M.A., Taylor, S.D., Yarranton, H.W. Extension of the expanded fluid viscosity model to characterized oils. Energy & Fuels 2013;27(4):1881-98.

[84] Motahhari H, Schoeggl, F., Satyro, M., Yarranton, H. Viscosity prediction for solvent-diluted live bitumen and heavy oil at temperatures up to 175-deg-C. Journal of Canadian Petroleum Technology 2013;52(5):376-90.

[85] Ma M, Chen, S., Abedi, J. Modeling the density, solubility and viscosity of bitumen/solvent systems using PC-SAFT. Journal of Petroleum Science and Engineering 2016;139:1-12.

[86] Assael MJ, Dymond JH, Tselekidou V. Correlation of high-pressure thermal conductivity, viscosity, and diffusion coefficients for n-alkanes. International journal of thermophysics 1990;11(5):863-73.

[87] Dymond JH, Awan, M.A. Correlation of high-pressure diffusion and viscosity coefficients for n-alkanes. International journal of Thermophysics 1989;10(5):941-51.

[88] Ijaz F. Measurement and Prediction of the Viscosity of Hydrocarbon Mixtures and Crude Oils. Imperial College, London; 2011.

[89] Redlich O, Kwong JNS. On the Thermodynamics of Solutions. V. An Equation of State. Fugacities of Gaseous Solutions. Chemical Reviews 1949;44(1):233-44.

[90] Chapman WG, Gubbins, K.E., Jackson, G., Radosz, M. New reference equation of state for associating liquids. Industrial & Engineering Chemistry Research 1990;29(8):1709-21.

[91] Chapman WG, Jackson, G., Gubbins, K.E. Phase equilibria of associating fluids: chain molecules with multiple bonding sites. Molecular Physics 1988;65(5):1057-79.

[92] Huang SH, Radosz, M. Phase behavior of reservoir fluids V: SAFT model of CO2 and bitumen systems. Fluid phase equilibria 1991;70(1):33-54.

[93] Huang SH, Radosz, M. Equation of state for small, large, polydisperse, and associating molecules. Industrial & Engineering Chemistry Research 1990;29(11):2284-94.

[94] Wertheim MS. Fluids with highly directional attractive forces. I. Statistical thermodynamics. Journal of Statistical Physics 1984;35(1):19-34.

[95] Wertheim MS. Fluids with highly directional attractive forces. II. Thermodynamic perturbation theory and integral equations. Journal of Statistical Physics 1984;35(1):35-47.

[96] Chapman WG, Gubbins KE, Jackson G, Radosz M. SAFT: Equation-of-state solution model for associating fluids. Fluid Phase Equilibria 1989;52:31-8.

[97] Carnahan NF, Starling KE. Equation of state for nonattracting rigid spheres. The Journal of Chemical Physics 1969;51(2):635-6.

[98] Huang SH, Radosz M. Equation of state for small, large, polydisperse, and associating molecules: extension to fluid mixtures. Industrial & Engineering Chemistry Research 1991;30(8):1994-2005.

[99] Beret S, Prausnitz JM. Perturbed hard-chain theory: An equation of state for fluids containing small or large molecules. AIChE Journal 1975;21(6):1123-32.

[100] Chen SS, Kreglewski, A. Applications of the Augmented van der Waals Theory of Fluids.: I. Pure Fluids. Berichte der Bunsengesellschaft für physikalische Chemie 1977;81(10):1048-52.

[101] Fu Y-H, Sandler SI. A Simplified SAFT Equation of State for Associating Compounds and Mixtures. Industrial & Engineering Chemistry Research 1995;34(5):1897-909.

[102] Rowlinson JS. The statistical mechanics of systems with steep intermolecular potentials. Molecular Physics 1964;8(2):107-15.

[103] Dufal S, Lafitte T, Galindo A, Jackson G, Haslam AJ. Developing intermolecular-potential models for use with the SAFT-VR Mie equation of state. AIChE Journal 2015;61(9):2891-912.

[104] Gubbins KE. Perturbation theories of the thermodynamics of polar and associating liquids: A historical perspective. Fluid Phase Equilibria 2016;416:3-17.

[105] Müller EA, Jackson G. Force-Field Parameters from the SAFT-γ Equation of State for Use in Coarse-Grained Molecular Simulations. Annual Review of Chemical and Biomolecular Engineering 2014;5(1):405-27.

[106] Müller EA, Gubbins KE. Molecular-Based Equations of State for Associating Fluids: A Review of SAFT and Related Approaches. Industrial & Engineering Chemistry Research 2001;40(10):2193-211.

[107] M^{c}Cabe C, Galindo A. SAFT Associating Fluids and Fluid Mixtures. Applied Thermodynamics of Fluids. Royal Society of Chemistry; 2010, p. 534.

[108] Johnson JK, Mueller EA, Gubbins KE. Equation of State for Lennard-Jones Chains. The Journal of Physical Chemistry 1994;98(25):6413-9.

[109] Johnson JK, Zollweg JA, Gubbins KE. The Lennard-Jones equation of state revisited. Molecular Physics 1993;78(3):591-618.

[110] Ghonasgi D, Chapman WG. Prediction of the properties of model polymer solutions and blends. AIChE Journal 1994;40(5):878-87.

[111] Felipe J B, Lourdes F V. Thermodynamic behaviour of homonuclear and heteronuclear Lennard-Jones chains with association sites from simulation and theory. Molecular Physics 1997;92(1):135-50.

[112] Blas FJ, Vega LF. Critical behavior and partial miscibility phenomena in binary mixtures of hydrocarbons by the statistical associating fluid theory. The Journal of Chemical Physics 1998;109(17):7405-13.

[113] Pàmies JC, Vega LF. Vapor−Liquid Equilibria and Critical Behavior of Heavy n-Alkanes Using Transferable Parameters from the Soft-SAFT Equation of State. Industrial & Engineering Chemistry Research 2001;40(11):2532-43.

[114] Lafitte T, Apostolakou, A., Avendaño, C., Galindo, A., Adjiman, C.S., Müller, E.A., Jackson, G. Accurate statistical associating fluid theory for chain molecules formed from Mie segments. The Journal of chemical physics 2013;139(15):154504.

[115] Ghosh A, Chapman WG, French RN. Gas solubility in hydrocarbons—a SAFT-based approach. Fluid Phase Equilibria 2003;209(2):229-43.

[116] García-Sánchez F, Eliosa-Jiménez G, Silva-Oliver G, Vázquez-Román R. Vapor–liquid equilibria of nitrogen–hydrocarbon systems using the PC-SAFT equation of state. Fluid phase equilibria 2004;217(2):241-53.

[117] Yarrison M, Chapman WG. A systematic study of methanol+ n-alkane vapor–liquid and liquid–liquid equilibria using the CK-SAFT and PC-SAFT equations of state. Fluid phase equilibria 2004;226:195-205.

[118] Silva-Oliver G, Eliosa-Jiménez G, García-Sánchez F, Avendaño-Gómez JR. High-pressure vapor–liquid equilibria in the nitrogen–n-pentane system. Fluid phase equilibria 2006;250(1-2):37-48.

[119] Arce P, Aznar M. Computation and modeling of tricritical phenomena in ternary and quaternary mixtures using the Perturbed Chain—Statistical Associating Fluid Theory equation of state. The Journal of Supercritical Fluids 2009;49(2):135-42.

[120] Blanco ST, Gil L, Garcia-Gimenez P, Artal M, Otín S, Velasco I. Critical properties and high-pressure volumetric behavior of the carbon dioxide+ propane system at T= 308.15 K. Krichevskii function and related thermodynamic properties. The Journal of Physical Chemistry B 2009;113(20):7243-56.

[121] Gross J. 0. Spuhl, F. Tumakaka, and G. Sadowski," Modeling copolymer systems using the Perturbed-Chain SAFT equation of state,". Industrial & Engineering Chemistry Research 2003;42:1266.

[122] Burgess WA, Tapriyal D, Morreale BD, Wu Y, M^{c}Hugh MA, Baled H, et al. Prediction of fluid density at extreme conditions using the perturbed-chain SAFT equation correlated to high temperature, high pressure density data. Fluid Phase Equilibria 2012;319:55-66.

[123] Arrhenius S. Über die innere Reibung verdünnter wässeriger Lösungen. Zeitschrift für Physikalische Chemie 1887;1(1):285-98.

[124] Novak LT. Modeling the viscosity of liquid mixtures: polymer− solvent systems. Industrial & engineering chemistry research 2003;42(9):1824-6.

[125] Novak LT, Chen, C. C., Song, Y. . Segment-based Eyring− NRTL viscosity model for mixtures containing polymers. Industrial & engineering chemistry research 2004;43(19):6231-7.

[126] Song D, Chen, J. . Density and viscosity data for mixtures of ionic liquids with a common anion. Journal of Chemical & Engineering Data 2014;59(2):257-62.

[127] Song Y, Mathias, P. M., Tremblay, D., Chen, C. C. Liquid viscosity model for polymer solutions and mixtures. Industrial & engineering chemistry research 2003;42(11):2415-22.

[128] Tihic A. Group Contribution sPC-SAFT Equation of State. 2008.

[129] Barker JA, Henderson D. Perturbation Theory and Equation of State for Fluids. II. A Successful Theory of Liquids. The Journal of Chemical Physics 1967;47(11):4714-21.

[130] Huynh DN, Benamira, M., Passarello, J.P., Tobaly, P., de Hemptinne, J.C. Application of GC-SAFT EOS to polycyclic aromatic hydrocarbons. Fluid phase equilibria 2007;254(1):60-6.

[131] Laursen T. VLXE, V. 9.3 www.vlxe.com. 2017.

[132] Baylaucq A, Boned C, Dauge P, Lagourette B. Measurements of the viscosity and density of three hydrocarbons and the three associated binary mixtures versus pressure and temperature. International journal of thermophysics 1997;18(1):3-23.

[133] Boned C, Zéberg-Mikkelsen, C.K., Baylaucq, A., Daugé, P. High-pressure dynamic viscosity and density of two synthetic hydrocarbon mixtures representative of some heavy petroleum distillation cuts. Fluid phase equilibria 2003;212(1):143-64.

[134] Gaciño FM, Regueira, T., Comuñas, M.J., Lugo, L., Fernández, J. Density and isothermal compressibility for two trialkylimidazolium-based ionic liquids at temperatures from (278 to 398) K and up to 120MPa. The Journal of Chemical Thermodynamics 2015;81:124-30.

[135] Navia P, Troncoso, J., Romaní, L. Isobaric thermal expansivity for nonpolar compounds. Journal of Chemical & Engineering Data 2009;55(6):2173-9.

[136] Taravillo M, Baonza, V.G., Cáceres, M., Núñez, J. Thermodynamic regularities in compressed liquids: I. The thermal expansion coefficient. Journal of Physics: Condensed Matter 2003;15(19):2979-89.

[137] Dzida M, Prusakiewicz, P. The effect of temperature and pressure on the physicochemical properties of petroleum diesel oil and biodiesel fuel. Fuel 2008;87(10-11):1941-8.

[138] ASTM International. ASTM D975-18 Standard Specification for Diesel Fuel Oils. West Conshohocken, PA; **2018**.

[139] ASTM International. ASTM D1655-18a Standard Specification for Aviation Turbine Fuels. West Conshohocken, PA; **2018**.

[140] Outcalt S, Laesecke, A., Freund, M.B. Density and speed of sound measurements of Jet A and S-8 aviation turbine fuels. Energy & Fuels 2009;23(3):1626-33.

[141] Outcalt SL, Laesecke, A., Brumback, K.J. Comparison of jet fuels by measurements of density and speed of sound of a flightline JP-8. Energy & Fuels 2010;24(10):5573-8.

[142] Safarov J, Ashurova, U., Ahmadov, B., Abdullayev, E., Shahverdiyev, A., Hassel, E. Thermophysical properties of Diesel fuel over a wide range of temperatures and pressures. Fuel 2018;216:870-89.

[143] Peters EJ, Chenevert, M.E., Zhang, C. A model for predicting the density of oil-base muds at high pressures and temperatures. SPE drilling engineering 1990;5(2):141-8.

[144] Payri R, Salvador, F.J., Gimeno, J., Bracho, G. The effect of temperature and pressure on thermodynamic properties of diesel and biodiesel fuels. Fuel 2011;90(3):1172-80.

[145] Bazile JP, Nasri D, Boned C, Daridon JL. High pressure thermophysical characterization of fuel used for testing and calibrating diesel injection systems. Fuel 2012;98:288-94.

[146] Desantes JM, Salvador, F.J., Carreres, M., Jaramillo, D. Experimental characterization of the thermodynamic properties of diesel fuels over a wide range of pressures and temperatures. SAE International Journal of Fuels and Lubricants 2015;8(1):190-9.

[147] Ivaniš GR, Radović, I.R., Veljković, V.B., Kijevčanin, M.L. Thermodynamic properties of biodiesel and petro-diesel blends at high pressures and temperatures. Experimental and modeling. Fuel 2016;184:277-88.

[148] Communication with the corresponding author of Ref. [142]. **2018**.

[149] Abdulagatov IM, Azizov ND. Density of rocket propellant (RP-1 fuel) at high temperatures and high pressures. Fuel 2010;89(7):1731-5.

[150] Chickos JS, Zhao H. Measurement of the vaporization enthalpy of complex mixtures by correlation-gas chromatography. The vaporization enthalpy of RP-1, JP-7, and JP-8 rocket and jet fuels at T= 298.15 K. Energy & fuels **2005**;19(5):2064-73.

[151] Won SH, Dooley S, Veloo P, Santner JS, Ju Y, Dryer FL. Characterization of global combustion properties with simple fuel property measurements for alternative jet fuels. *50th ASME/SAE/ASEE Joint Propulsion Conference*. Cleveland, OH; **2014,** AIAA 2014-3469.

[152] van der Westhuizen R, Ajam, M., De Coning, P., Beens, J., de Villiers, A., Sandra, P. Comprehensive two-dimensional gas chromatography for the analysis of synthetic and crude-derived jet fuels. Journal of Chromatography A 2011;1218(28):4478-86.

[153] Solash J, Hazlett, R.N., Hall, J.M., Nowack, C.J. Relation between fuel properties and chemical composition. 1. Jet fuels from coal, oil shale and tar sands. Fuel 1978;57(9):521-8.

[154] Lafitte T, Bessieres, D., Piñeiro, M.M., Daridon, J.L. Simultaneous estimation of phase behavior and second-derivative properties using the statistical associating fluid theory with variable range approach. The Journal of chemical physics 2006;124(2):024509.

[155] Baylaucq A BC, Dauge P, Lagourette B. . Measurements of the viscosity and density of three hydrocarbons and the three associated binary mixtures versus pressure and temperature. International journal of thermophysics 1997;18(1):3-23.

[156] Rokni HB, Moore JD, Gupta A, M^{c}Hugh MA, Gavaises M. Entropy scaling based viscosity predictions for hydrocarbon mixtures and diesel fuels up to extreme conditions. Fuel **2019**;241:1203-13.

[157] Baled H, Gamwo IK, Enick RM, M^{c}Hugh MA. Viscosity models for pure hydrocarbons at extreme conditions: A review and comparative study. Fuel 2018;218:89-111.

[158] Alade OS, Ademodi B, Sasaki K, Sugai Y, Kumasaka J, Ogunlaja AS. Development of models to predict the viscosity of a compressed Nigerian bitumen and rheological property of its emulsions. Journal of Petroleum Science and Engineering 2016;145:711-22.

[159] Eghbali S, Dehghanpour, H., Dragani, J., Zhang, X., . Phase Behaviour and Viscosity of Bitumen-CO 2/Light Hydrocarbon Mixtures at Elevated Temperatures: A Cold Lake Case Study. *SPE Canada Heavy Oil Technical Conference.* Calgary, Alberta, Canada: Society of Petroleum Engineers; 2018.

[160] Gülüm M, Bilgin, A. Measurements and empirical correlations in predicting biodiesel-diesel blends' viscosity and density. Fuel 2017;199(567-77).

[161] Bair S. The pressure and temperature dependence of volume and viscosity of four Diesel fuels. Fuel 2014;135:112-9.

[162] Ilyin SO, Strelets, L.A. Basic Fundamentals of Petroleum Rheology and Their Application for the Investigation of Crude Oils of Different Natures. Energy & Fuels 2018;32(1):268-78.

[163] Kanaveli IP, Atzemi, M., Lois, E. Predicting the viscosity of diesel/biodiesel blends. Fuel 2017;199:248-63.

[164] Lapuerta M, Rodríguez-Fernández, J., Fernández-Rodríguez, D., Patiño-Camino, R. Modeling viscosity of butanol and ethanol blends with diesel and biodiesel fuels. Fuel 2017;199:332-8.

[165] Nguyen T-B, Vesovic V. Predicting the viscosity of liquid mixtures consisting of n-alkane, alkylbenzene and cycloalkane species based on molecular description. Fluid Phase Equilibria 2019.

[166] Khoshnamvand Y, Assareh, M. Viscosity Prediction for Petroleum Fluids Using Free Volume Theory and PC-SAFT. International Journal of Thermophysics 2018;39(4):54.

[167] Sun Y, Shen, G., Held, C., Lu, X., Ji, X.,. Modeling Viscosity of Ionic Liquids with Electrolyte Perturbed-Chain Statistical Associating Fluid Theory and Free Volume Theory. Industrial & Engineering Chemistry Research 2018;57(26):8784-801.

[168] Macias-Salinas R, Durán-Valencia, C., López-Ramírez, S., Bouchot, C. Eyring-theory-based model to estimate crude oil viscosity at reservoir conditions. Energy & Fuels 2008;23(1):464-70.

[169] Eyring H. Viscosity, plasticity, and diffusion as examples of absolute reaction rates. The Journal of chemical physics 1936;4(4):283-91.

[170] Rosenfeld Y. Relation between the transport coefficients and the internal entropy of simple systems. Physical Review A **1977**;15(6).

[171] Lötgering-Lin O, Gross J. Group contribution method for viscosities based on entropy scaling using the perturbed-chain polar statistical associating fluid theory. Industrial & Engineering Chemistry Research **2015**;54(32):7942-52.

[172] Lötgering-Lin O, Fischer, M., Hopp, M., Gross, J. Pure Substance and Mixture Viscosities Based on Entropy Scaling and an Analytic Equation of State. Industrial & Engineering Chemistry Research 2018;57(11):4095-114.

[173] Fouad WA, Vega, L.F. On the anomalous composition dependence of viscosity and surface tension in refrigerant blends. Journal of Molecular Liquids 2018;268:190-200.

[174] Fouad WA, Vega, L.F. Transport properties of HFC and HFO based refrigerants using an excess entropy scaling approach. The Journal of Supercritical Fluids 2018;131:106-16.

[175] Rosenfeld Y. A quasi-universal scaling law for atomic transport in simple fluids. Journal of Physics: Condensed Matter 1999;11(28):5415.

[176] Chopra R, Truskett TM, Errington JR. On the use of excess entropy scaling to describe the dynamic properties of water. The Journal of Physical Chemistry B 2010;114(32):10558-66.

[177] Goel T, Patra CN, Mukherjee T, Chakravarty C. Excess entropy scaling of transport properties of Lennard-Jones chains. The Journal of chemical physics 2008;129(16):164904.

[178] Galliero G, Boned C, Fernández J. Scaling of the viscosity of the Lennard-Jones chain fluid model, argon, and some normal alkanes. The Journal of chemical physics 2011;134(6):064505.

[179] Novak L. Self-diffusion coefficient and viscosity in fluids. Journal of Chemical Reactor Engineering 2011;9(1).

[180] Novak L. Fluid viscosity-residual entropy correlation. International Journal of Chemical Reactor Engineering 2011;9(1).

[181] Novak LT. Predictive corresponding-states viscosity model for the entire fluid region: n-Alkanes. Industrial & Engineering Chemistry Research 2013;52(20):6841-7.

[182] Novak LT. Predicting fluid viscosity of nonassociating molecules. Industrial & Engineering Chemistry Research 2015;54(21):5830-5.

[183] Neufeld PD, Janzen, A.R., Aziz, R.A. Empirical equations to calculate 16 of the transport collision integrals Ω (l, s)* for the Lennard-Jones (12–6) potential. The Journal of Chemical Physics 1972;57(3):1100-2.

[184] International A. ASTM D445-12 Standard Test Method for Kinematic Viscosity of Transparent and Opaque Liquids (and Calculation of Dynamic Viscosity). West Conshohocken, PA; 2012.

[185] Zéberg-Mikkelsen CK, Barrouhou, M., Baylaucq, A., Boned, C. High-pressure viscosity and density measurements of the ternary system methylcyclohexane+ cis-decalin+ 2, 2, 4, 4, 6, 8, 8-heptamethylnonane. Journal of Chemical & Engineering Data 2003;48(6):1387-92.

[186] Baylaucq A, Dauge P, Boned C. Viscosity and density of the ternary mixture heptane+ methylcyclohexane+ 1-methylnaphthalene. International journal of thermophysics 1997;18(5):1089-107.

[187] Dauge P, Canet, X., Baylaucq, A., Boned, C. Measurements of the density and viscosity of the tridecane+ 2, 2, 4, 4, 6, 8, 8-heptamethylnonane mixtures in the temperature range 293.15-353.15 K at pressures up to 100 MPa. High Temerpatures High Pressures 2001;33(2):213-30.

[188] Zeberg-Mikkelsen CK, Canet, X., Baylaucq, A., Quiñones-Cisneros, S.E., Boned, C., Stenby, E.H. High-pressure viscosity and density behavior of ternary mixtures: 1-methylnaphthalene+ n-tridecane+ 2, 2, 4, 4, 6, 8, 8-heptamethylnonane. International journal of thermophysics 2001;22(6):1691-726.

[189] Baylaucq A, Zeberg-Mikkelsen CK, Daugé P, Boned C. Dynamic viscosity and density of heptylbenzene and heptylcyclohexane up to 100 MPa. Journal of Chemical & Engineering Data 2002;47(4):997-1002.

[190] Caudwell DR, Trusler, J.M., Vesovic, V., Wakeham, W.A. Viscosity and Density of Five Hydrocarbon Liquids at Pressures up to 200 MPa and Temperatures up to 473 K. Journal of Chemical & Engineering Data 2008;54(2):359-66.

[191] Haynes WM. CRC handbook of chemistry and physics. CRC press; 2014.

[192] Michailidou EK, Assael, M.J., Huber, M.L., Abdulagatov, I.M., Perkins, R.A. Reference Correlation of the Viscosity of n-Heptane from the Triple Point to 600 K and up to 248 MPa. Journal of Physical and Chemical Reference Data 2014;43(2):1-13.

[193] Oshmyansky Y, Hanley, H.J.M., Ely, J.F., Kidnay, A.J. The viscosities and densities of selected organic compounds and mixtures of interest in coal liquefaction studies. International Journal of Thermophysics 1986;7(3):599-608.

[194] Pereiro AB, Rodríguez, A., Canosa, J., Tojo, J. Density, viscosity, and speed of sound of dialkyl carbonates with cyclopentane and methyl cyclohexane at several temperatures. Journal of Chemical & Engineering Data 2004;49(5):1392-9.

[195] Rafiee HR, Ranjbar, S., Poursalman, F. Densities and viscosities of binary and ternary mixtures of cyclohexanone, 1, 4-dioxane and isooctane from T=(288.15 to 313.15) K. The Journal of Chemical Thermodynamics 2012;54:266-71.

[196] Van Velzen D, Lopes Cardozo, R., Langenkamp, H. Liquid Viscosity and Chemical Constitution of Organic Compounds: A New Correlation and a Compilation of Literature Data. Joint Nuclear Research Centre - Ispra Establishment (Italy): Commission of the European Communities; 1972.

[197] Krahn UG, Luft, G. Viscosity of several liquid hydrocarbons in the temperature range 298-453 K at pressures up to 200 MPa. Journal of Chemical and Engineering Data 1994;39(4):670-2.

[198] Politte MD. Invert oil mud rheology as a function of temperature and pressure. *SPE/IADC Drilling Conference* Society of Petroleum Engineers.; 1985.

[199] Duncan AM, Pavlicek, N., Depcik, C.D., Scurto, A.M., Stagg-Williams, S.M. High-pressure viscosity of soybean-oil-based biodiesel blends with ultra-low-sulfur diesel fuel. Energy & Fuels 2012;26(11):7023-36.

[200] Duncan AM, Ahosseini, A., M^{c}Henry, R., Depcik, C.D., Stagg-Williams, S.M., Scurto, A.M. High-pressure viscosity of biodiesel from soybean, canola, and coconut oils. Energy & Fuels 2010;24(10):5708-16.

[201] Robertson LX, Schaschke, C.J.,. Combined high pressure and low temperature viscosity measurement of biodiesel. Energy & Fuels 2009;24(2):1293-7.

[202] Allal A, Boned C, Baylaucq A. Free-volume viscosity model for fluids in the dense and gaseous states. Physical Review E 2001;64(1):011203.

[203] Baled HO, Koronaios P, Xing D, Miles R, Tapriyal D, Gamwo IK, et al. High-temperature, high-pressure viscosity of n-octane and isooctane. Fuel 2016;164:199-205.

[204] Caudwell D, Trusler J, Vesovic V, Wakeham W. The viscosity and density of n-dodecane and n-octadecane at pressures up to 200 MPa and temperatures up to 473 K. International Journal of Thermophysics 2004;25(5):1339-52.

[205] Baled HO, Xing D, Katz H, Tapriyal D, Gamwo IK, Soong Y, et al. Viscosity of n-hexadecane, n-octadecane and n-eicosane at pressures up to 243 MPa and temperatures up to 534 K. The Journal of Chemical Thermodynamics 2014;72:108-16.

[206] Caudwell DR, Trusler JM, Vesovic V, Wakeham WA. Viscosity and Density of Five Hydrocarbon Liquids at Pressures up to 200 MPa and Temperatures up to 473 K. Journal of Chemical & Engineering Data 2008;54(2):359-66.

[207] Rowane AJ, Mallepally RR, Bamgbade BA, Newkirk MS, Baled HO, Burgess WA, et al. High-temperature, high-pressure viscosities and densities of toluene. The Journal of Chemical Thermodynamics 2017;115:34-46.

[208] Rokni HB, Moore JD, Gupta A, M^{c}Hugh MA, Mallepally RR, Gavaises M. General method for prediction of thermal conductivity for well-characterized hydrocarbon mixtures and fuels up to extreme conditions using entropy scaling. Fuel **2019**;245:594-604.

[209] Baroncini C, di Filippo P, Latini G, Pacetti M. An improved correlation for the calculation of liquid thermal conductivity. International Journal of Thermophysics **1980**;1(2):159-75.

[210] Baroncini C, di Filippo P, Latini G, Pacetti M. Organic liquid thermal conductivity: A prediction method in the reduced temperature range 0.3 to 0.8. International Journal of Thermophysics **1981**;2(1):21-38.

[211] Baroncini C, di Filippo P, Latini G. Thermal conductivity estimation of the organic and inorganic refrigerants in the saturated liquid state. International Journal of Refrigeration **1983**;6(1):60-2.

[212] Latini G. Thermophysical properties of fluids: dynamic viscosity and thermal conductivity. Journal of Physics: Conference Series **2017**;923-012001:1-12.

[213] Latini G, di Nicola G, Pierantozzi M. Liquid thermal conductivity prediction for alkanes, ketones and silanes. Physics and Chemistry of Liquids **2017**;55(6):747-65.

[214] Baroncini C, Latini G, Pierpaoli P. Thermal conductivity of organic liquid binary mixtures: measurements and prediction method. International Journal of Thermophysics **1984**;5(4):387-401.

[215] Sastri SRS, Rao KK. A new temperature–thermal conductivity relationship for predicting saturated liquid thermal conductivity. Chemical Engineering Journal **1999**;74(3):161-9.

[216] Chung TH, Ajlan M, Lee LL, Starling KE. Generalized multiparameter correlation for nonpolar and polar fluid transport properties. Industrial & Engineering Chemistry Research **1988**;27(4):671-9.

[217] Chung TH, Lee LL, Starling KE. Applications of kinetic gas theories and multiparameter correlation for prediction of dilute gas viscosity and thermal conductivity. Industrial & Engineering Chemistry Fundamentals **1984**;23(1):8-13.

[218] Huber ML, Hanley HJM, Millat J, Dymond JH, de Castro CN. Transport properties of fluids: Their correlation, prediction and estimation. Cambridge: Cambridge Univ. Press; **1996**.

[219] Huber ML, Laesecke A, Perkins RA. Model for the viscosity and thermal conductivity of refrigerants, including a new correlation for the viscosity of R134a. Industrial & Engineering Chemistry Research **2003**;42(13):3163-78.

[220] Roy D, Thodos G. Thermal conductivity of gases. Hydrocarbons at normal pressures. Industrial & Engineering Chemistry Fundamentals **1968**;7(4):529-34.

[221] Teja AS, Rice P. A generalized corresponding states method for the prediction of the thermal conductivity of liquids and liquid mixtures. Chemical Engineering Science **1981**;36(2):417-22.

[222] Teja AS, Tarlneu G. Prediction of the thermal conductivity of liquids and liquid mixtures including crude oil fractions. The Canadian Journal of Chemical Engineering **1988**;66(6):980-6.

[223] Arikol M, Gürbüz H. A new method for predicting thermal conductivity of pure organic liquids and their mixtures. The Canadian Journal of Chemical Engineering **1992**;70(6):1157-63.

[224] Mathias PM, Parekh VS, Miller EJ. Prediction and correlation of the thermal conductivity of pure fluids and mixtures, including the critical region. Industrial & Engineering Chemistry Research **2002**;41(5):989-99.

[225] Lashkarbolooki M, Hezave AZ, Bayat M. Correlating thermal conductivity of pure hydrocarbons and aromatics via perceptron artificial neural network (PANN) method. Chinese Journal of Chemical Engineering **2017**;25(5):547-54.

[226] Gharagheizi F, Ilani-Kashkouli P, Sattari M, Mohammadi AH, Ramjugernath D, Richon D. Development of a general model for determination of thermal conductivity of liquid chemical compounds at atmospheric pressure. AIChE Journal **2013**;59(5):1702-8.

[227] Hopp M, Gross J. Thermal conductivity of real substances from excess entropy scaling using PCP-SAFT. Industrial & Engineering Chemistry Research **2017**;56(15):4527-38.

[228] Assael MJ, Dymond JH, Papadaki M, Patterson PM. Correlation and prediction of dense fluid transport coefficients: II. Simple molecular fluids. Fluid Phase Equilibria **1992**;75:245-55.

[229] Assael MJ, Dymond JH, Papadaki M, Patterson PM. Correlation and prediction of dense fluid transport coefficients. I. n-alkanes. International Journal of Thermophysics **1992**;13(2):269-81.

[230] Assael MJ, Dymond JH, Patterson PM. Correlation and prediction of dense fluid transport coefficients. V. Aromatic hydrocarbons. International Journal of Thermophysics **1992**;13(5):895-905.

[231] Guo XQ, Sun CY, Rong SX, Chen GJ, Guo TM. Equation of state analog correlations for the viscosity and thermal conductivity of hydrocarbons and reservoir fluids. Journal of Petroleum Science and Engineering **2001**;30(1):15-27.

[232] Fouad WA, Vega LF. Transport properties of HFC and HFO based refrigerants using an excess entropy scaling approach. The Journal of Supercritical Fluids 2018;131:106-16.

[233] Schilling J, Tillmanns D, Lampe M, Hopp M, Gross J, Bardow A. From molecules to dollars: integrating molecular design into thermo-economic process design using consistent thermodynamic modeling. Molecular Systems Design & Engineering 2017;2(3):301-20.

[234] Assael MJ, Dymond JH, Papadaki M, Patterson PM. Correlation and prediction of dense fluid transport coefficients. III. n-Alkane mixtures. International Journal of Thermophysics **1992**;13(4):659-69.

[235] Assael MJ, Kalyva AE, Kakosimos KE, Antoniadis KD. Correlation and prediction of dense fluid transport coefficients. VIII. Mixtures of alkyl benzenes with other hydrocarbons. International Journal of Thermophysics **2009**;30(6):1733-47.

[236] Fareleira JMNA, Nieto de Castro CA, Pádua AAH. Prediction of the thermal conductivity of liquid alkane mixtures. Berichte der Bunsengesellschaft für Physikalische Chemie **1990**;94(5):553-9.

[237] Huber ML. Preliminary models for viscosity, thermal conductivity, and surface tension of pure fluid constituents of selected diesel surrogate fuels. US Department of Commerce, National Institute of Standards and Technology; **2017**.

[238] Ramos-Pallares F, Schoeggl FF, Taylor SD, Yarranton HW. Expanded fluid-based thermal conductivity model for hydrocarbons and crude oils. Fuel **2018**;224:68-84.

[239] Gharagheizi F, Ilani-Kashkouli P, Sattari M, Mohammadi AH, Ramjugernath D, Richon D. Development of a quantitative structure–liquid thermal conductivity relationship for pure chemical compounds. Fluid Phase Equilibria **2013**;355:52-80.

[240] Gharagheizi F, Ilani-Kashkouli P, Sattari M, Mohammadi AH, Ramjugernath D. A group contribution method for determination of thermal conductivity of liquid chemicals at atmospheric pressure. Journal of Molecular Liquids **2014**;190:223-30.

[241] Govender O, Rarey J, Moller BC, Ramjugernath D. A new group contribution method for the estimation of thermal conductivity for non-electrolyte organic compounds; **2016**. Available from: http://www.ddbst.com/files/files/Durban/SACEC2009-TCN-Manuscript.pdf. [Accessed 4 November 2018].

[242] Nagvekar M, Daubert TE. A group contribution method for liquid thermal conductivity. Industrial & engineering chemistry research **1987**;26(7):1362-5.

[243] Wu KJ, Zhao CX, He CH. Development of a group contribution method for determination of thermal conductivity of ionic. Fluid Phase Equilibria **2013**;339:10-4.

[244] Rodenbush CM, Viswanath DS, Hsieh FH. A group contribution method for the prediction of thermal conductivity of liquids and its application to the Prandtl number for vegetable oils. Industrial & Engineering Chemistry Research **1999**;38(11):4513-9.

[245] Lazzús JA. A group contribution method to predict the thermal conductivity λ (T, P) of ionic liquids. Fluid Phase Equilibria **2015**;405:141-9.

[246] Ramos-Pallares F, Schoeggl FF, Taylor SD, Yarranton HW. Prediction of thermal conductivity for characterized oils and their fractions using an expanded fluid based model. Fuel **2018**;234:66-80.

[247] University OS. Fluid Properties Research Report LV **1983**:25-32.

[248] Kesler MG, Lee BI. Improve prediction of enthalpy of fractions. Hydrocarbon process **1976**;55:153-8.

[249] Liang Z, Tsai HL. The vibrational contribution to the thermal conductivity of a polyatomic fluid. Molecular Physics **2010**;108(13):1707-14.

[250] Stiel LI, Thodos G. The self-diffusivity of dilute and dense gases. The Canadian Journal of Chemical Engineering **1965**;43(4):186-90.

[251] Briggs DKH. Thermal conductivity of liquids. Industrial & Engineering Chemistry **1975**;49(3):418-21.

[252] Dortmund Data Bank (DDB), 2018, www.ddbst.com.

[253] Rastorguev YL, Pugach VV. Untersuchung der wärmeleitfähigkeit von aromatischen kohlenwasserstoffen bei hohem druck. Izv.Vyssh.Uchebn. Zaved, Neft'i Gaz **1970**;13(8):69-72.

[254] Kashiwagi H, Oishi M, Tanaka Y, Kubota H, Makita T. Thermal conductivity of fourteen liquids in the temperature range 298–373 K. International Journal of Thermophysics **1982**;3(2):101-16.

[255] Wada Y, Nagasaka Y, Nagashima A. Measurements and correlation of the thermal conductivity of liquid n-paraffin hydrocarbons and their binary and ternary mixtures. International Journal of Thermophysics **1985**;6(3):251-65.

[256] Wakeham WA, Yu HR, Zalaf M. The thermal conductivity of the mixtures of liquid hydrocarbons at pressures up to 400 MPa. International Journal of Thermophysics **1990**;11(6):987-1000.

[257] Fareleira JMNA, Li SFY, Wakeham WA. The thermal conductivity of liquid mixtures at elevated pressures. International Journal of Thermophysics **1989**;10(5):1041-51.

[258] Akhmedova-Azizova LA, Abdulagatov IM, Bruno TJ. Effect of RP-1 compositional variability on thermal conductivity at high temperatures and high pressures. Energy & Fuels **2009**;23(9):4522-8.

[259] Bruno TJ. The Properties of RP-1 and RP-2 MIPR F1SBAA8022G001. **2008**.

[260] Xu GQ, Jia ZX, Wen J, Deng HW, Fu YC. Thermal-conductivity measurements of aviation kerosene RP-3 from (285 to 513) K at sub-and supercritical pressures. International Journal of Thermophysics **2015**;36(4):620-32.

[261] Jia Z, Xu G, Deng H, Jie W, Fu Y. Experimental measurements of thermal conductivity of hydrocarbon fuels by a steady and kinetic method. Journal of Thermal Analysis and Calorimetry **2016**;123(1):891-8.

[262] Bruno TJ. Thermodynamic, Transport and Chemical Properties of Reference JP-8. NIST; **2006**.

[263] Edwards T. "Kerosene" Fuels for Aerospace Propulsion-Composition and Properties. *38th AIAA/ASME/SAE/ASEE Joint Propulsion Conference & Exhibit* Indianapolis, Indiana; **2002**.

[264] Xu R, Wang H, Billingsley M. Thermochemical properties of rocket fuels; **2015**. Available from:

https://web.stanford.edu/group/haiwanglab/HyChem/approach/Report_RP2_Fuel_Thermochemical_Properties_v2.pdf. [Accessed 1 November 2018].

[265] Deng HW, Zhang CB, Xu GQ, Tao Z, Zhang B, Liu GZ. Density measurements of endothermic hydrocarbon fuel at sub-and supercritical conditions. Journal of Chemical & Engineering Data **2011**;56(6):2980-6.

[266] Shafer L, Striebich R, Gomach J, Edwards T. Chemical class composition of commercial jet fuels and other specialty kerosene fuels. *14th AIAA/AHI Space Planes and Hypersonic Systems and Technologies Conference* Canberra, Australia; **2006,** AIAA 2006-7972.

[267] Balagurunathan J. Investigation of ignition delay times of conventional (Jp-8) and synthetic (S-8) jet fuels: A shock tube study Ph.D.: University of Dayton; **2012**.

[268] Davidson DF, Zhu Y, Wang S, Parise T, Sur R, Hanson RK. Tube Measurements of Jet and Rocket Fuels. *54th AIAA Aerospace Sciences Meeting.* San Diego, CA; **2016,** AIAA 2016-0178.

[269] Assael MJ, Charitidou E, Avgoustiniatos S. The thermal conductivity of xylene isomers in the temperature range 290–360 K. International Journal of Thermophysics 1988;9(4):501-10.

[270] Ramires MLV, dos Santos FV, Mardolcar UV, de Castro CN. The thermal conductivity of benzene and toluene. International Journal of Thermophysics 1989;10(5):1005-11.

[271] Dymond J, Awan M, Glen N, Isdale J. Transport properties of nonelectrolyte liquid mixtures. VIII. Viscosity coefficients for toluene and for three mixtures of toluene+ hexane from 25 to 100 C at pressures up to 500 MPa. International journal of thermophysics 1991;12(2):275-87.

[272] Kumagai A, Tomida D, Yokoyama C. Measurements of the Liquid Viscosities of Mixtures of n-Butane, n-Hexane, and n-Octane with Squalane to 30 MPa. International journal of thermophysics 2006;27(2):376-93.

[273] Ducoulombier D, Zhou H, Boned C, Peyrelasse J, Saint-Guirons H, Xans P. Pressure (1-1000 bars) and temperature (20-100. degree. C) dependence of the viscosity of liquid hydrocarbons. The Journal of Physical Chemistry 1986;90(8):1692-700.

[274] Rowane AJ, Babu VM, Mallepally RR, Rokni HB, Moore JD, Gupta A, et al. Effect of composition on the high-temperature, high-pressure viscosities and densities of three diesel fuels. Submitted to Energy and Fuels 2019.